NASA CR- 66585

PEPP REPORT
PR25-37
SPED - 2

GOODYEAR AEROSPACE
CORPORATION

AKRON, OHIO 44315

PEPP BALLUTE

DESIGN AND DEVELOPMENT

FINAL REPORT NAS1-6703

GER-13368 **22 September 1967**

FOREWORD

This final report was prepared by Goodyear Aerospace Corporation, (GAC), Akron, Ohio, for Martin Marietta Corporation, Denver Division, Denver, Colorado, under Contract MC 7-709030.

The purpose of this report is to summarize the design and analysis performed by Goodyear Aerospace for the PEPP BALLUTE. The program was a group effort headed by Mr. F. R. Nebiker, manager, Recovery Systems Engineering. Mr. Nebiker was assisted by Mr. A. C. Aebisher, section head, Mr. W. H. Glidden, project engineer, Mr. W. A. Barr, configuration analysis, Mr. K. Birklein, trajectory analysis, Mr. D. B. Block, mass properties, Mr. R. Nissel, materials and fabrication techniques, Mr. J. E. Houmard, structural analysis, Mr. I. M. Jaremenko, aerodynamic analysis, Mr. W. W. Sowa, thermal analysis, and Mr. D. L. Mansfield, development tests.

Goodyear Aerospace gratefully acknowledges the assistance of NASA personnel at Wallops Island, Virginia, and Langley Research Center, Hampton, Virginia, in conducting the developmental testing.

TABLE OF CONTENTS

LIST OF ILLUSTRATIONS

LIST OF TABLES

SECTION I - INTRODUCTION AND SUMMARY

Goodyear Aerospace Corporation designed and tested lightweight BALLUTEs[a] from March, 1967 through September, 1967, for flight testing under the Planetary Entry Parachute Program (PEPP). The BALLUTE described in this report is designed to meet the test conditions in Contract MC 7-709030 from the Martin Marietta Corporation. Because the design conditions cannot be met by the launch vehicle, the BALLUTE design also was verified for the anticipated deployment window.

The two main phases of the program were Phase I (design analysis) and Phase II (preliminary testing for design validation prior to the rocket-launched flight test). The design constraints were established by the requirement to package the BALLUTE in the existing PEPP parachute mortar for deployment at Mach = 4; flight path angle, γ = 63.6 deg; and dynamic pressure, q = 40 psf.

Nomex was selected for the BALLUTE envelope because of the sterilization temperature regime. The strength of dacron deteriorates at a point near the sterilization temperature. The size and placement of the burble fence were determined from previous designs in which a similar flight regime was encountered. The test objective was to determine the validity of the design analysis.

The developmental testing series consisted of two aerial drops from a helicopter at NASA Wallops Station, Wallops Island, Virginia and two vacuum-sphere mortar-deployment tests at NASA Langley Research Center, Hampton, Virginia. The rocket-launched flight test will not be reported in this document.

After the BALLUTE design was finalized, Goodyear Aerospace fabricated the following items for the PEPP flight-test program:

1. One developmental BALLUTE with riser and bridle
2. One flight-test BALLUTE with riser and bridle
3. One spare flight-test BALLUTE with riser and bridle
4. One spare riser and bridle assembly

[a] TM, Goodyear Aerospace Corporation, Akron, Ohio.

The design analysis included a statement of design conditions (Section II); the design requirements (Section III); and aerodynamic (Section IV), structural (Section V), and thermal (Section VI) analyses. In-plant testing (Section VII) was conducted for design validation prior to the developmental testing (Section VIII).

SECTION II - DESIGN CONDITIONS

The test conditions that dictated the design of the PEPP BALLUTE were specified in the work statement of Contract MC 7-709030. The following parameters express the test conditions for which the BALLUTE deployment point was established.

Parameter	Value
Mach number	4.0
Altitude	145,000 ft
Dynamic pressure, q	40 psf
Flight path angle, γ	63.6- deg ascent
Total weight at deployment	240 lb

The changes in the values of these parameters with time indicate the influence of the forces acting on the BALLUTE and payload during the deceleration period. The values versus time of five major parameters are presented in Figures 1 through 3. Figure 1 presents Mach number and altitude versus time. Figure 2 presents dynamic pressure, $1/2\ \rho V^2$, and deceleration in g's versus time. Figure 3 presents flight path angle and drag force versus time.

The calculated decelerations are based on trajectory calculations where the ballistic coefficient is varied linearly for a 0.5-sec deployment period and varied as a function of Mach number for the balance of the deceleration period. The 2-sec deployment was examined and determined to be less severe for design and consequently is not reported here.

Figure 4 shows the characteristic curve[1, a] for the drag coefficient, C_D, variation as a function of Mach number, exclusive of the linearly variable ballistic coefficient. The characteristic drag curve is pertinent to a BALLUTE located in the wake of a forebody and indicates somewhat lower drag coefficients than were expected in the PEPP configuration where the BALLUTE diameter is nine times as large as the forebody diameter. Figures 5 through 9 show scalar expansions of some of the trajectory parameters. Figure 10 shows the iterative process employed in the design of this BALLUTE system.

[a]Superior numbers in the text refer to items in the List of References

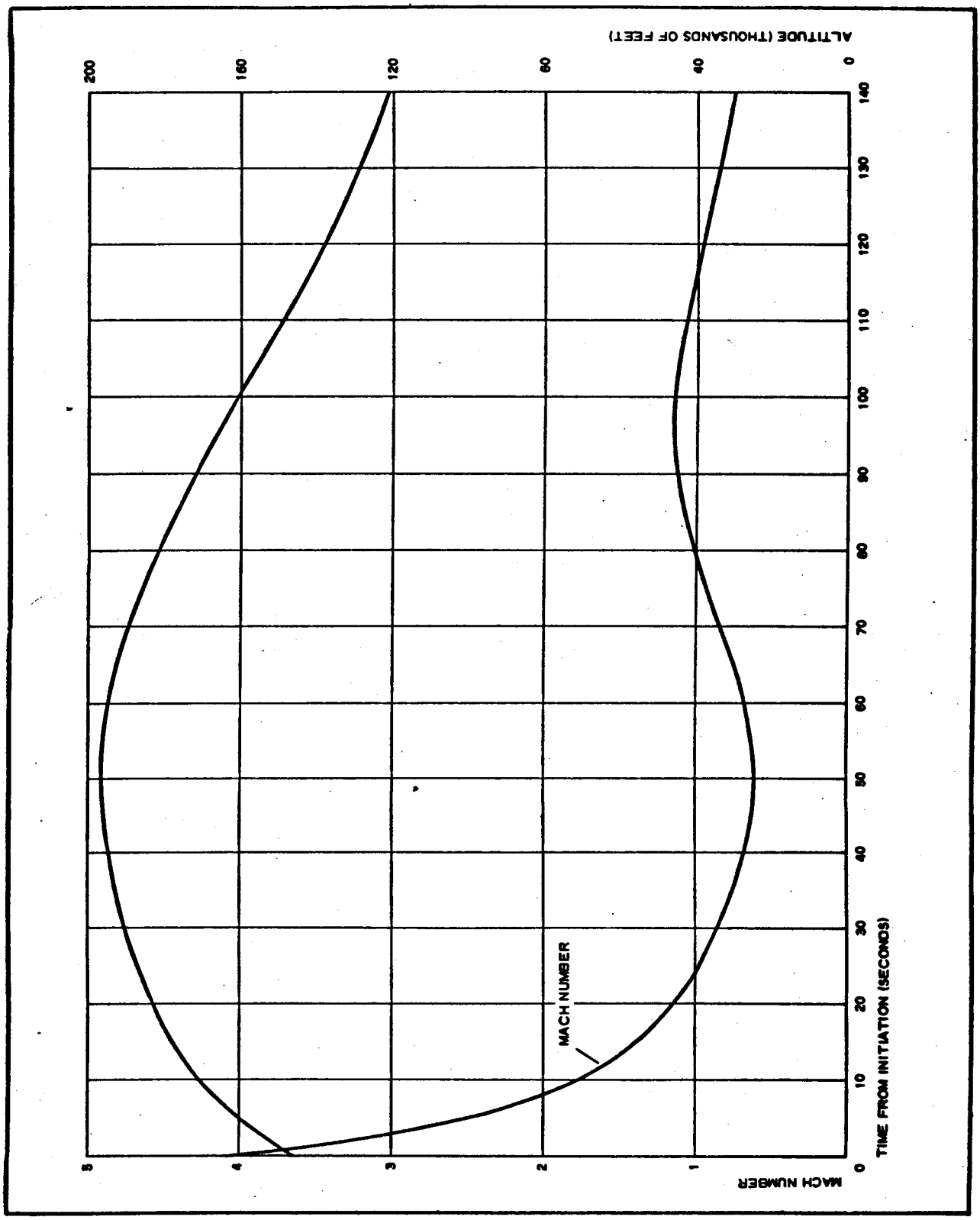

Figure 1 - Mach Number and Altitude versus Time

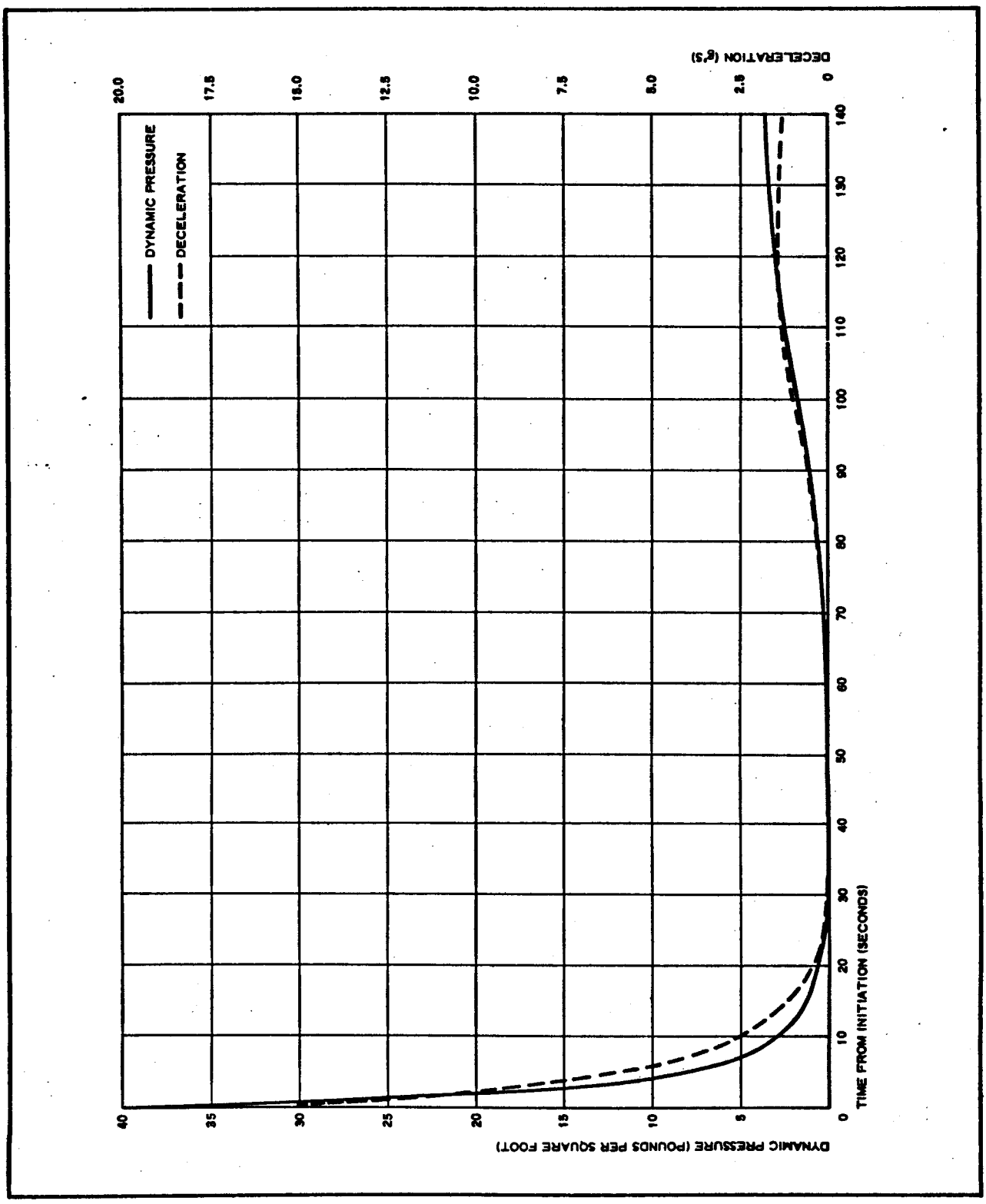

Figure 2 - Dynamic Pressure and Deceleration versus Time

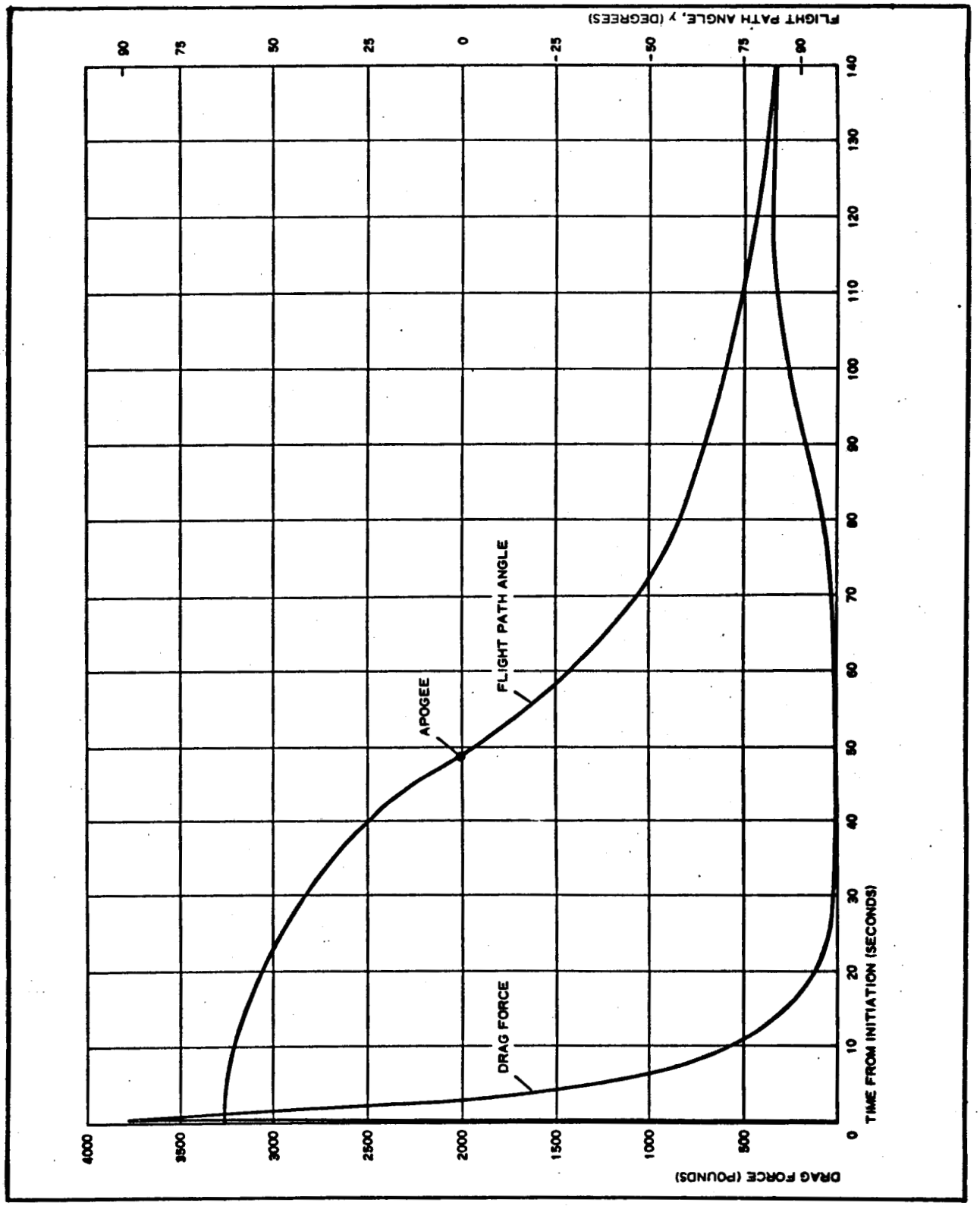

Figure 3 - Flight Path Angle and Drag Force versus Time

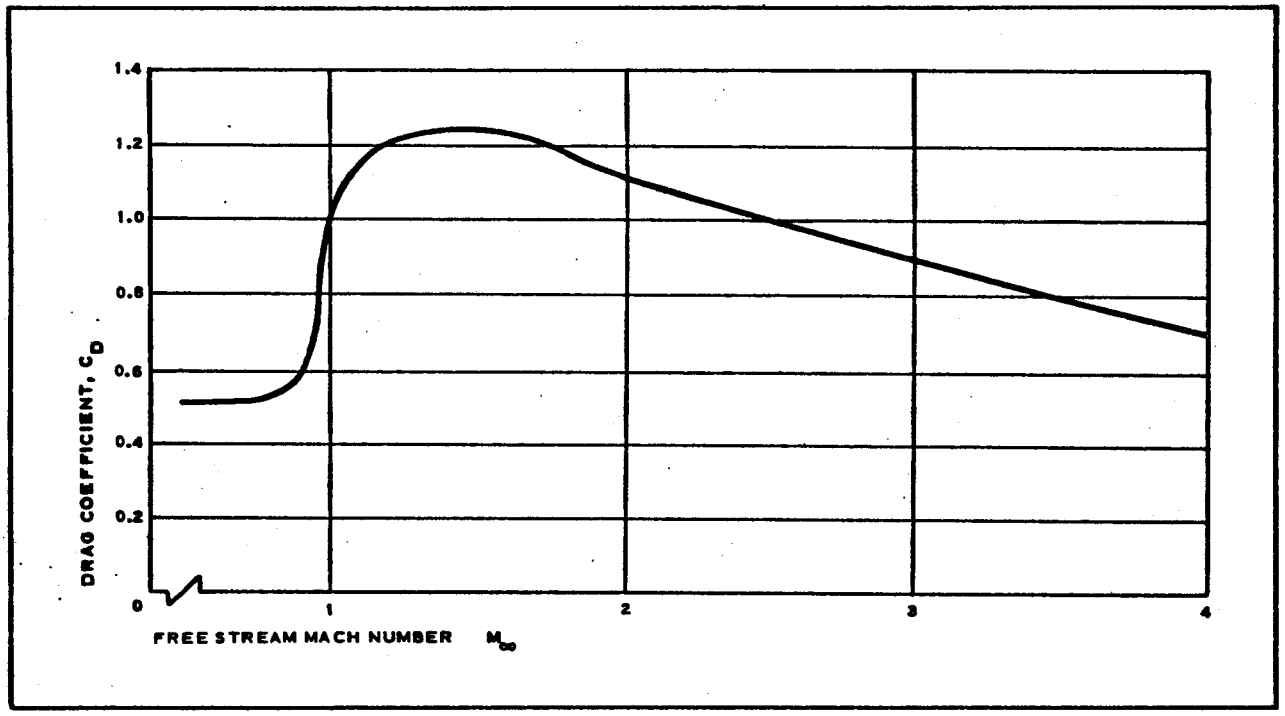

Figure 4 - Characteristic Drag Curve for BALLUTE

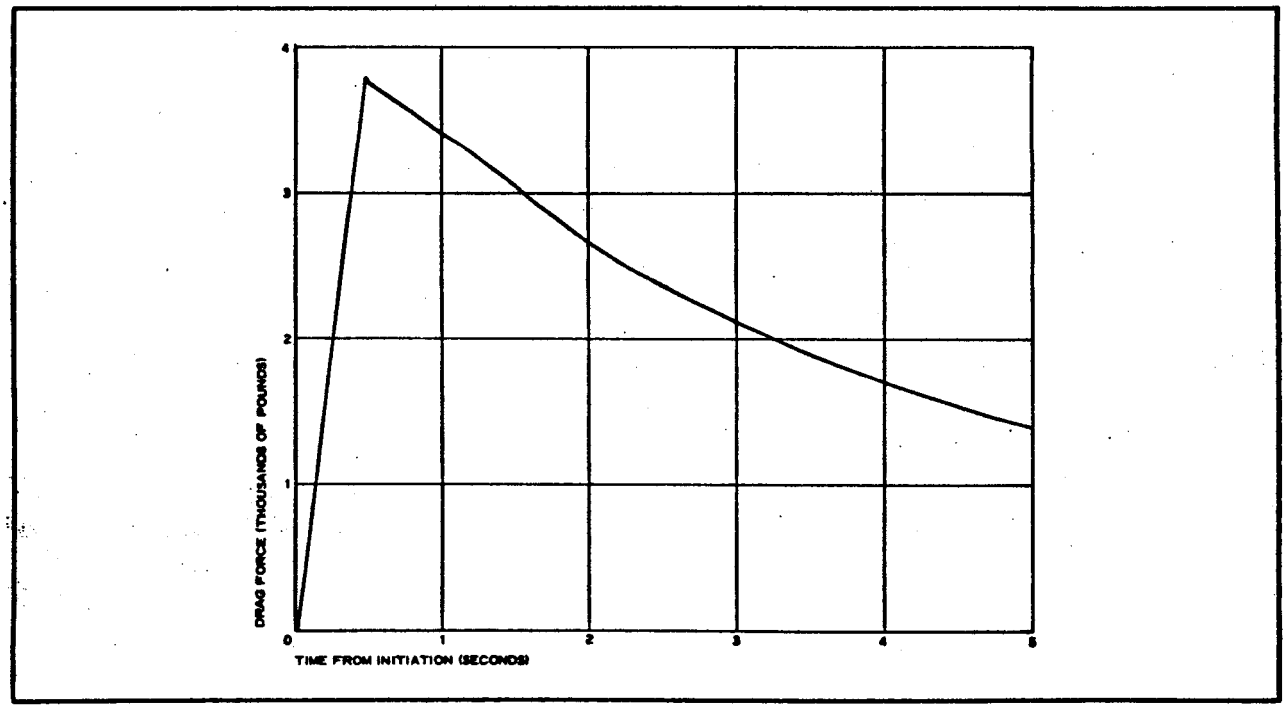

Figure 5 - Drag Force on BALLUTE versus Time

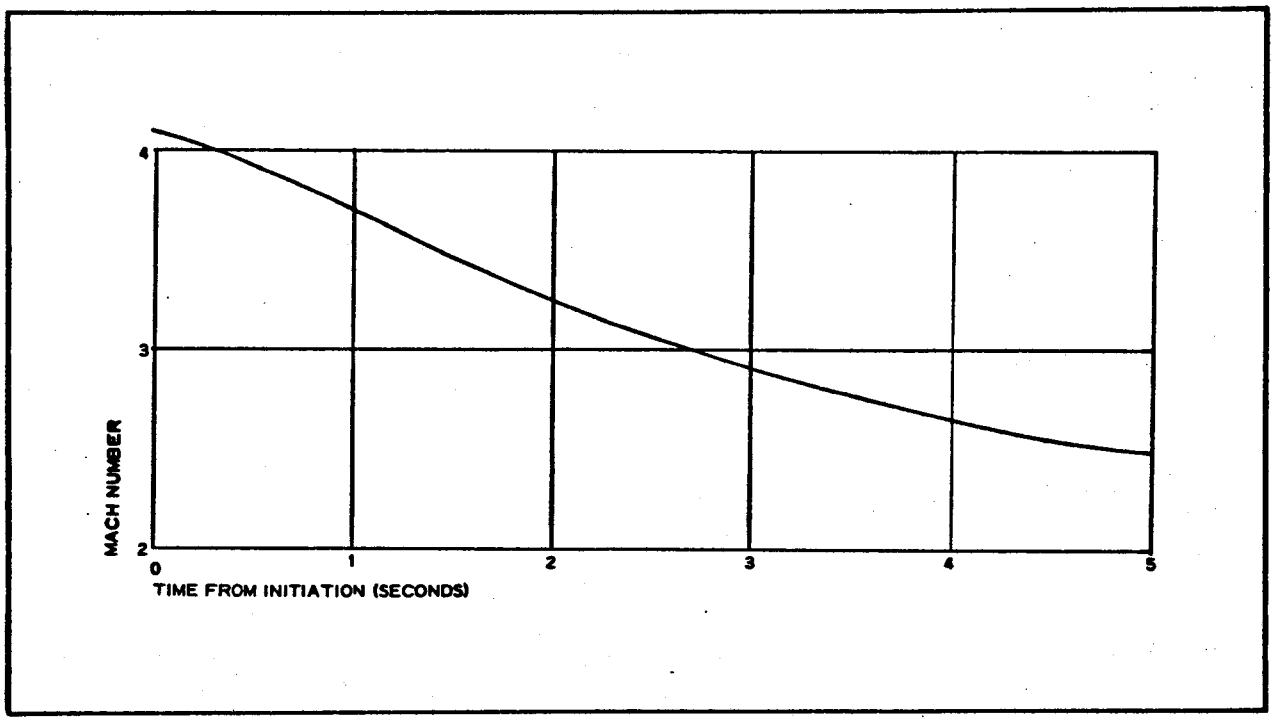

Figure 6 - Mach Number versus Time

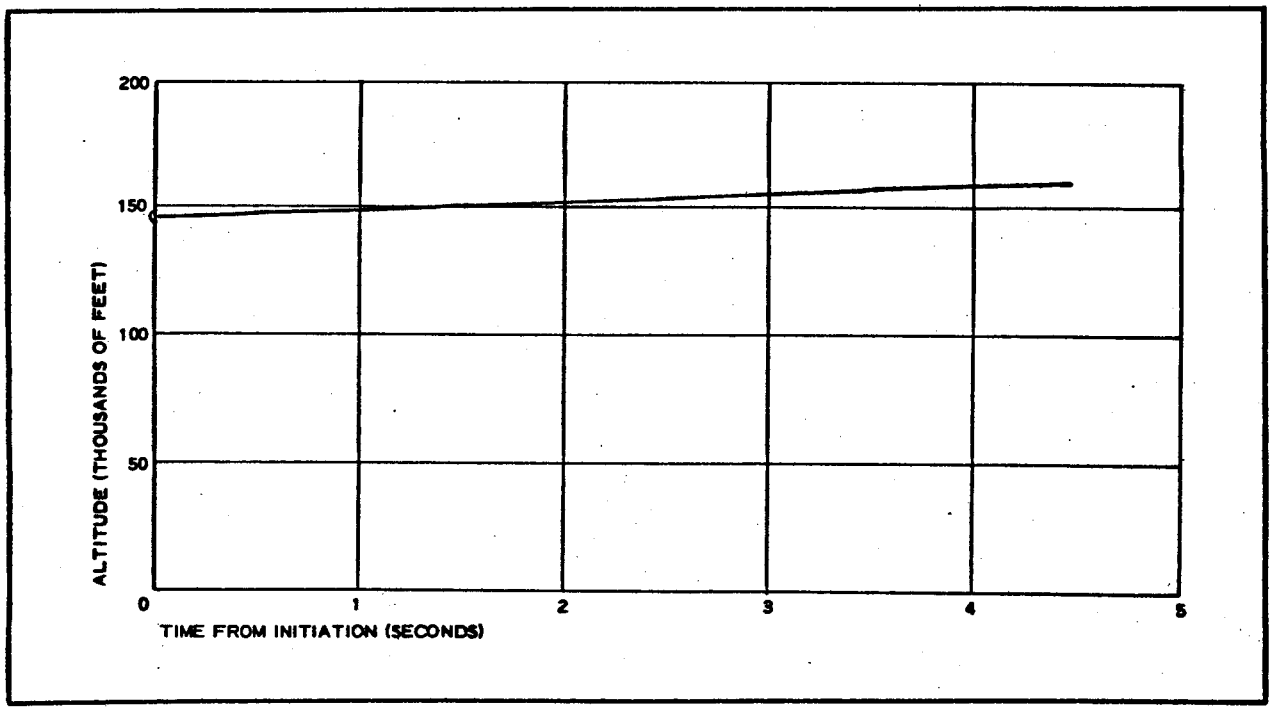

Figure 7 - Altitude versus Time

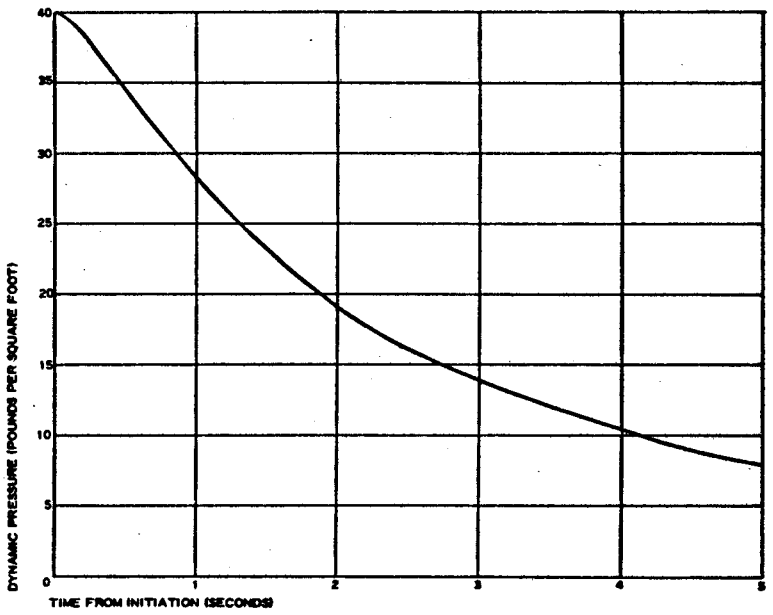

Figure 8 - Dynamic Pressure versus Time

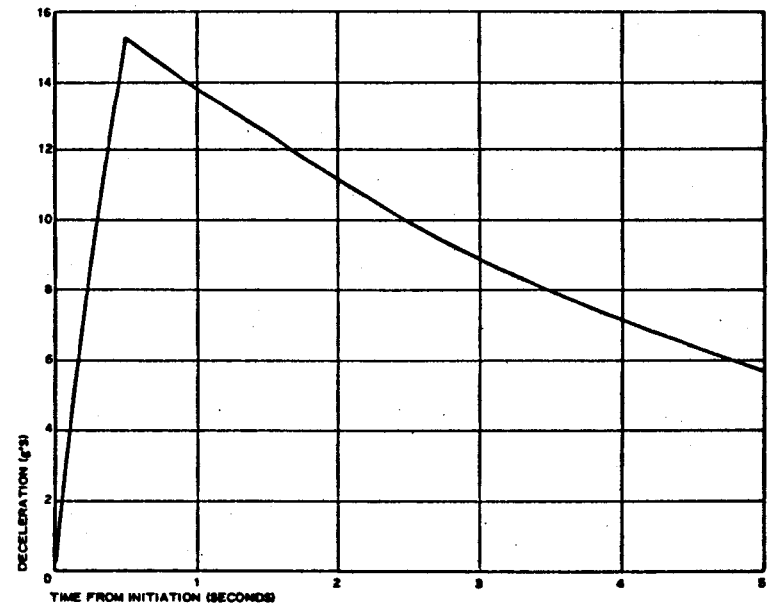

Figure 9 - Deceleration versus Time

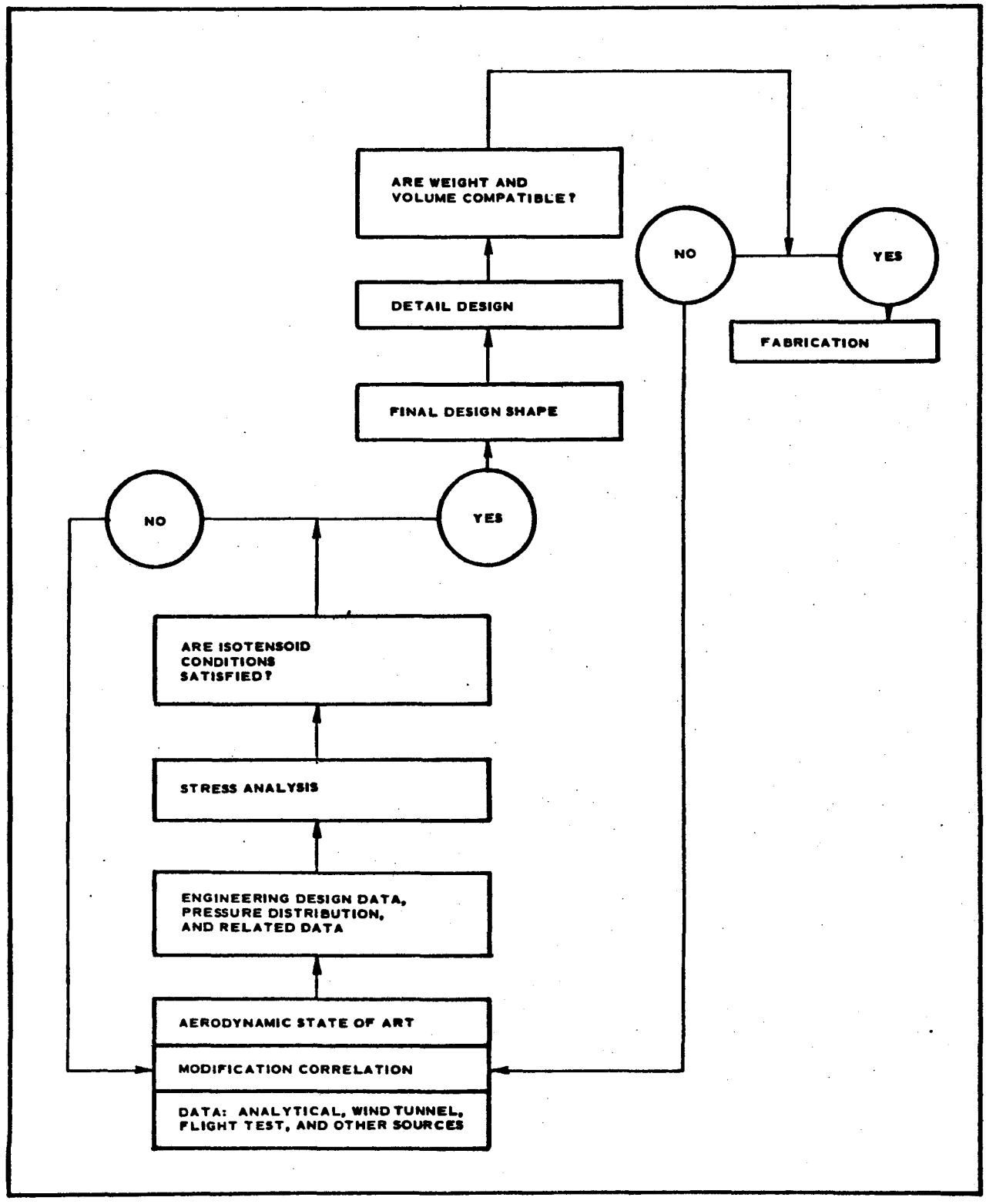

Figure 10 - Iterative Design Procedure

SECTION III - DESIGN REQUIREMENTS

The design of the PEPP BALLUTE was initiated by defining the purpose of the BALLUTE and the deployment conditions. By itself, a BALLUTE has two basic requirements to fulfill: (1) generation of a constant, high-rate drag force and (2) stabilization by application of this force in the force-vector diagram of a system. In meeting these requirements, the BALLUTE should preserve its structural integrity and thermal and shape stability within the constraints of 0.97-cu-ft packaging volume and a total weight of 35 ± 4 lb. These conditions set the limits of the configuration, which is defined here by the set of values describing the coordinates in terms of dimensionless ratios (X/R and Y/R), maximum radius, R, surface inclination angle, θ, and location and size of a burble fence. All these values and their interrelationships were selected to conform with the flow environment specified by the Mach number, altitude, and dynamic pressure. These defining principles and approaches as well as supporting experimental data are given in References 1 and 2.

The resultant profile for the PEPP BALLUTE is shown in Section IV and the design details are given in Section V. The aerodynamic evaluation is given in Section IV, while the structural analysis and thermal calculations can be found in Sections V and VI, respectively.

In conclusion, the selected configuration, incorporating a 10-percent burble fence based on the maximum BALLUTE diameter, is capable of deployment in the Mach number-3 to -4 regime and of retention of the desired characteristics throughout the deceleration flight regime.

SECTION IV - AERODYNAMIC ANALYSIS

1. INITIAL CONDITIONS

The aerodynamic requirements for determining the BALLUTE shape and loading included the examination of the payload/BALLUTE flow field, pressure distribution, inlet and fence considerations, inflation, and drag coefficient. The data were obtained for a PEPP BALLUTE within limits set by the complexity of each problem and the time allowed for solution. The following initial conditions[a] were assumed for this investigation:

$M_\infty = 4.0$ $\quad V_\infty = 4256$ fps

$h_\infty = 145 \times 10^3$ ft $\quad c_\infty = 1064$ fps

$P_\infty = 3.4$ psf $\quad T_t = 471.5$ deg R

$q_\infty = 40$ psf $\quad \rho_\infty = 0.1431 \times 10^{-3}$ pcf

$Re_\infty/ft = 0.65 \times 10^5$

2. ANALYSIS

a. Payload-BALLUTE Flow Field

Because the PEPP BALLUTE trails the payload, it is influenced by the wake flow field of the payload. The payload is a blunted cone-cylinder with about a six-degree flare around which three pods are attached. Pods complicate the boundary layer separation at the base and the wake formation behind, but a detailed analysis was not the purpose of this consideration. The estimated flow structure for the decelerator test vehicle and trailing BALLUTE is based on the principles outlined in NASA CR-748[b, 3] and empirical analytical data available, where the following constraints are assumed: $d_{base\ (hydraulic)} = 28$ in., $x/d_{base} = 5.14$, $d_{b(tot)}/d_{base} = 7.7$, and $l_{riser} = 12$ ft.

---

[a] See the List of Symbols at the end of Section IV for a definition of each symbol.

[b] Superior numbers in the text refer to items in the List of References

The estimated flow field is given in Figure 11, keeping the geometric proportions and the physical nature of the flow. The nature of the flow (in the lateral coordinate system of a BALLUTE) can be outlined as follows:

Location	Description
$0 \leq X/R_B \leq 0.34$	Viscous inner and inviscid outer (supersonic) wake
$0.21 \leq X/R_B \leq 0.48$	Region of shock-on-shock, shock-intersection interactions, and inviscid wake boundary
$X/R_B > 0.48$	Region influenced by main bow shock of BALLUTE where $\theta_c = 40$ deg
$0.8 \leq X/R_B \leq 1.0$	Region where flow approaches free stream conditions

From Figure 11, it is apparent that for this system the wake flow field of a payload influences a distance of only about $Y/R = 0.4$ of the longitudinal length of a BALLUTE. The downstream location of a BALLUTE makes the divergence of the payload wake less probable; therefore, only the forward

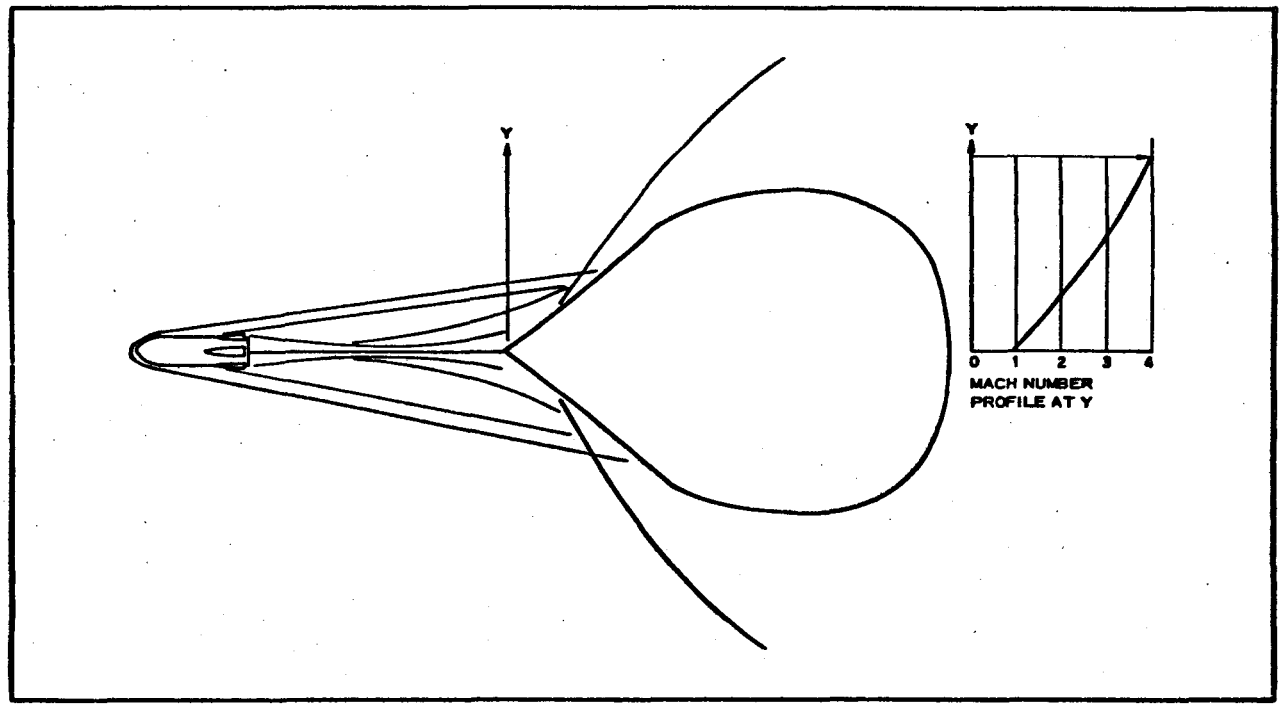

Figure 11 - Estimated Flow Field Structure about Payload and BALLUTE

part of a BALLUTE flow is modified by the decelerator test vehicle wake.

b. BALLUTE Flow and Pressure Field

The flow field of the PEPP BALLUTE was considered to be similar to the flow field described in TR-65-27.[2] The initial attachment point was assumed to be at $X/R_B = 0.34$ (attached shock condition). The resultant Mach lines at the selected stations of the profile indicated the local flow conditions as the guidance for a positioning of the inlets and the burble fence. The flow field is shown schematically in Figure 12. The last two Mach lines (M = 3.3 and 4.1) are shown for a configuration without the burble fence. The values reflect the changing slope of the local surface favorable for the flow expansion. The pressure distribution given in Figure 13 for $M_\infty = 4$ is based on the wind tunnel data modified in accordance with the structure of the payload decelerator flow field and location of the burble fence. The shape of the distribution is valid for the configuration and flow conditions shown, the local loading being dependent on the free stream static pressure, i.e., the deployment altitude.

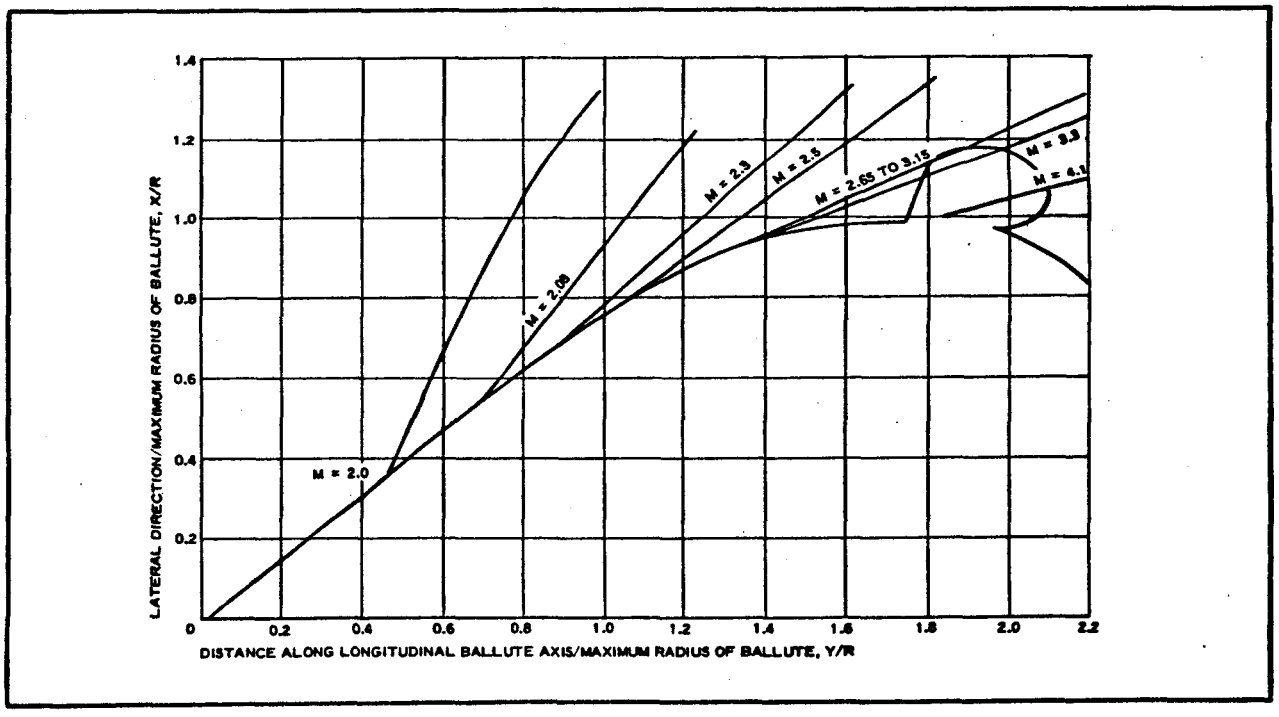

Figure 12 - BALLUTE Pressure Distribution

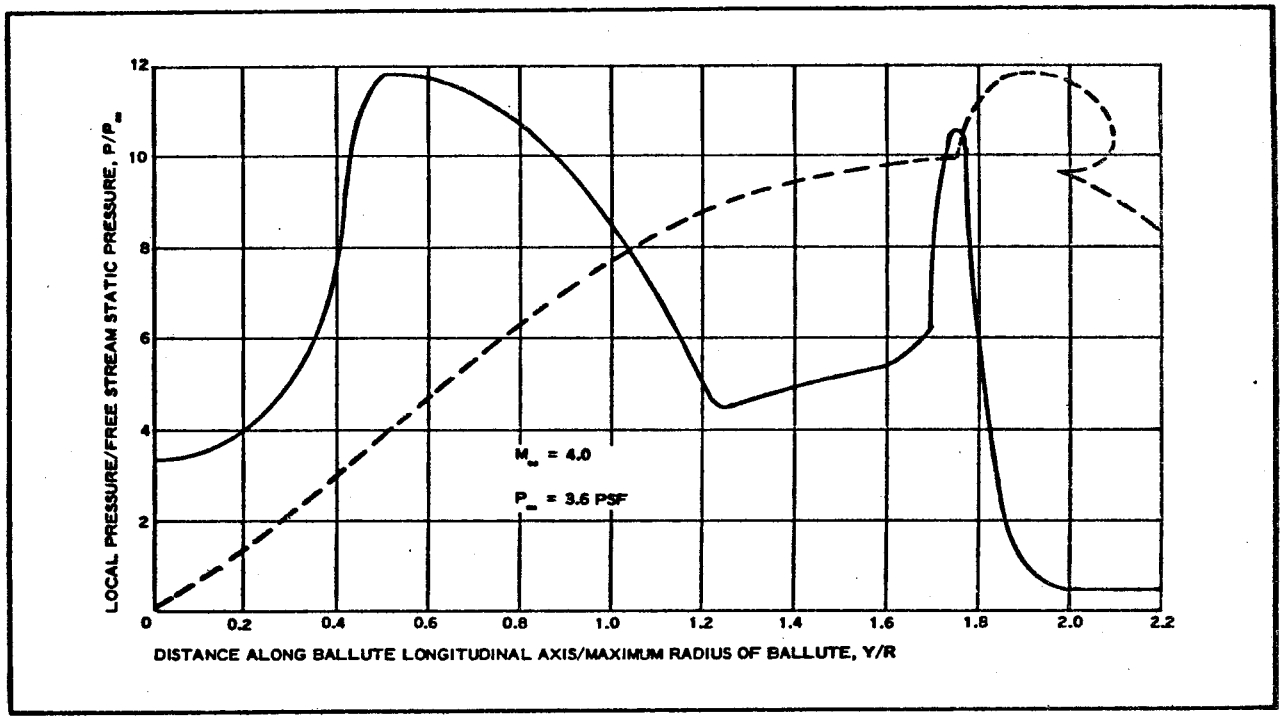

Figure 13 - BALLUTE Pressure Distribution

The height of a burble fence on this BALLUTE is equal to 10 percent of the maximum diameter above the projection of a half profile or h_{bf} = 1.5 ft. The total diameter of the PEPP BALLUTE with the burble fence then is 18 ft. The coordinates for the fence location are:

Y/R_B = 1.75 at leading edge,
Y/R_B = 2.00 at trailing edge, and
Y/R_B = 1.96 at maximum height.

The Mach line tangent to the burble fence is:

M_{bf} = 2.65, originating at Y/R_B = 1.2

or

M_{bf} = 3.15, originating at Y/R_B = 0.91.

c. BALLUTE Inflation Considerations

At high velocities the pressure can be obtained if velocity is reduced efficiently. The highest possible pressure at a duct exit can be achieved when the flow density is the largest possible with smallest possible decrease in the total pressure at an inlet. If an inlet is located in a stagnation area or interference area, the ram-air inflation will be reduced.

An inlet is assumed to be a diffuser. If the diffuser is subsonic, it provides a pressure rise by converting the kinetic energy of the subsonic flow. The flow compression is obtained most effectively by the external compression. If the flow ahead of an inlet is supersonic, the diffusion takes place by an increase in the entropy with a corresponding decrease in the free stream total pressure because of shock phenomena. The design that keeps the exit-to-inlet ratio of total pressure high is associated with increase of the external drag of a diffuser. It is logical to assume that an erected inlet can be simulated by the normal shock supersonic diffuser. With this type of diffuser, the external flow at $M > 1$ is decelerated to a subsonic flow by a normal shock occurring:

1. At an inlet opening (optimum design point - see sketch) with $M_\infty > 1$; then, the weight rate of flow is maximum:

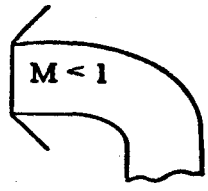

$$\dot{W}_{max} = M_\infty A \sqrt{\frac{\gamma P_\infty W}{g}} \text{ (lb/sec)}, \quad (1)$$

where

$$W = \rho g \text{ (lb/cu ft)}, \quad (2)$$

2. Inside an inlet (see sketch) with $M_\infty > 1$; $\dot{W} = \rho AV$ (lb/sec) and pressure at the exit is less than at the inlet,

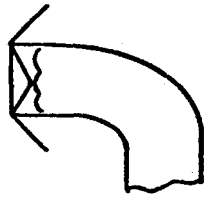

(3)

3. In front of an inlet (see sketch) with $M_\infty > 1$; $\dot{W} > \rho AV$ and properties downstream of a shock are determined from the normal shock relations.

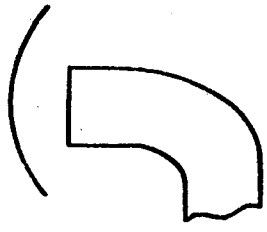

(4)

There are several criteria for diffuser performance. The two most useful criteria are diffuser efficiency and ram recovery pressure ratio. The diffuser isentropic efficiency is the stagnation enthalpy of the diffused air from the free stream static pressure to final total pressure. Figure 14 shows the efficiency and ram pressure recovery for a normal shock diffuser in the Mach number range of interest here.

The inlet considered for the PEPP BALLUTE has the following configurational characteristics: constant diameter, circular cross section, duct bend of 67 to 72 deg, nonrigid structure, and plane of the inlet normal to the BALLUTE surface.

There is no reliable data for the inlet configuration described above, but the following trends might be indicated.

The flow through a constant diameter duct is affected by the friction. Hence, if the initial velocity is subsonic, the friction accelerates the flow to local sonic velocity as a limit (choked orifice). If initial flow is supersonic, the friction decelerates the flow to the local sonic velocity as a limit (supersonic diffusion). Since these effects are confined to the boundary layer, the flow in a core is essentially isentropic with a thick boundary layer.

The performance of an inlet can be indicated by the flow parameters in the vicinity of a hypothetical location. Figure 15 gives such indications in terms of the expected dynamic pressure ratios at an altitude of 145×10^3 ft and back pressure ratios above which the normal shock will detach from the inlet.

When the leading edge of an inlet is skewed, then (according to the limited data[4] available) the flow is first spilled over the most rearward part of the edge and then over the entire periphery of the inlet. Thus an oblique shock is attached to skewed lip of an inlet and, when the back pressure is increased, the shock detaches and moves forward into a detached position. Also, if the leading edge is skewed at 45 deg and the inlet is long, there is a 10-percent reduction in the total diffuser loss at $M = 1.4$. The velocity distribution at the exit is not changed radically by skewing the leading edge.

Changing the angle of the flow in an inlet produces certain effects on velocity

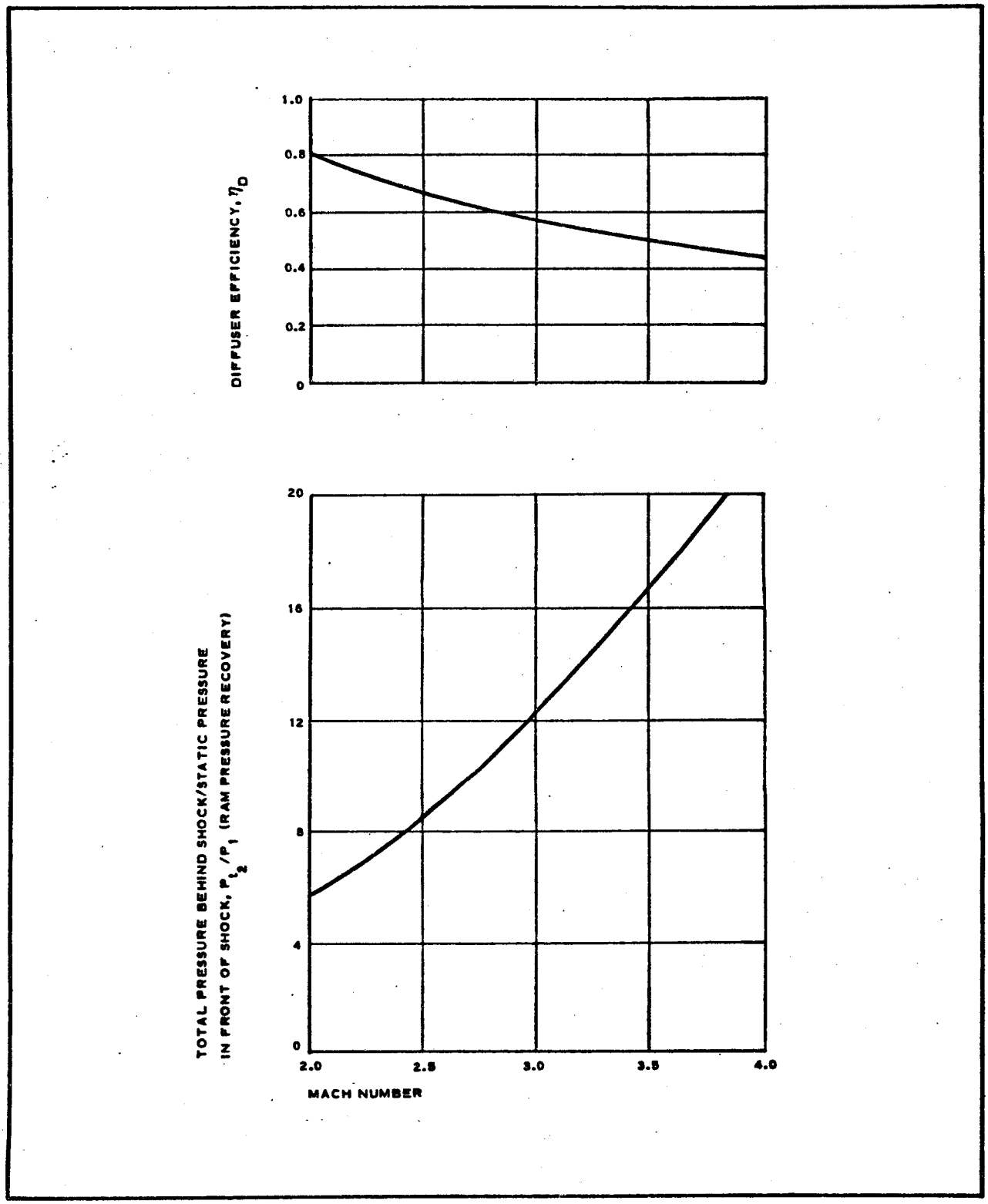

Figure 14 - Efficiency and Ram Pressure Recovery for Normal Shock Diffuser

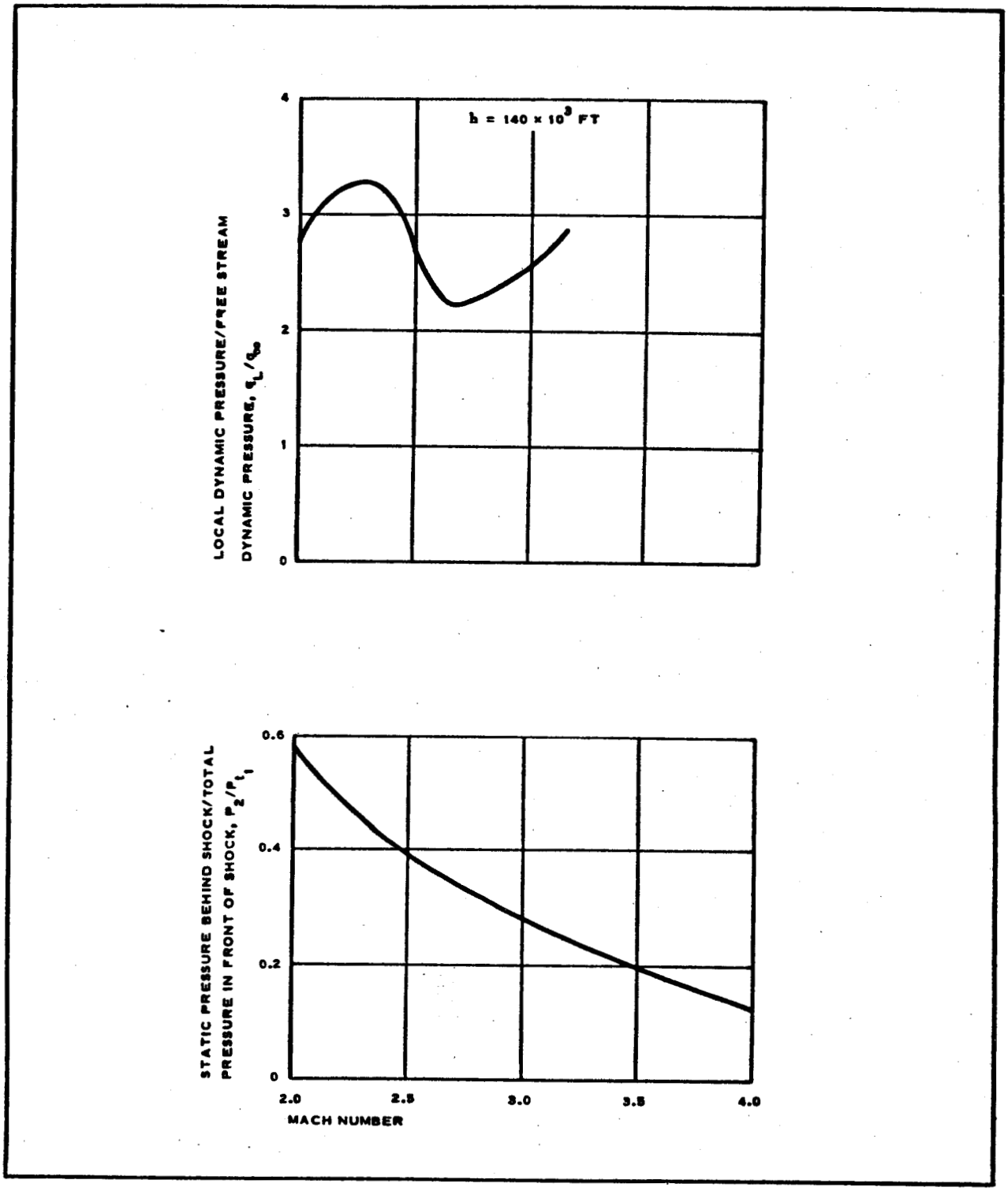

Figure 15 - Dynamic Pressure and Normal Shock Attachment Parameters for Diffuser-Inlet

distributions downstream. A brief review[5] of the phenomena indicates the presence of three flow regions: the core, layer of peripheral flow, and eddying flow. If elbows are present in an inlet, the resulting flow separation will cause a double-spiralling motion that persists over a great distance. The inference is that if the bend is located in a large-aspect-ratio duct, there is a flow instability due to a mixing of flow elements possessing different kinetic energies.

Although the inlet under consideration has the elbows at the seams, the fabric stretch smooths them out under the full deployment, yet a certain amount of instability will be present. Velocity distributions are indicated for circular ducts in Table I. The last entry is for the PEPP BALLUTE inlet, where no velocity measurements are available but can be inferred from the representative values above.

The estimated total volume of a PEPP BALLUTE is $\forall_{tot} \approx 2220$ cu ft. The volume to be ram-inflated also is approximately equal to 2220 cu ft and the flow rate into a BALLUTE is:

$$\dot{W}_{in} = 28.3\, C_W A_i\, \rho\sqrt{T}\,, \tag{5}$$

at

$$h_\infty = 145 \times 10^3 \text{ ft},$$

$$\rho_\infty = 0.1431 \times 10^{-3} \text{ pcf},$$

$$T_\infty = 471.5 \text{ R},$$

$$C_W = 0.9, \text{ and}$$

$$A_{i_{tot}} = 4.36 \text{ sq ft}.$$

If the density and temperature at the inlet are assumed as those existing behind the normal shock located at or near the inlet, the rates of flow for total inlet area at Mach numbers representative for the flow around the inlet are given in Figure 16 and are valid at $h = 145 \times 10^3$ ft. The representative time to fill the volume when the flow is incompressible or compressible is

TABLE I - VELOCITY DISTRIBUTIONS FOR VARIOUS CIRCULAR DUCTS

d_i (in.)	A (sq in.)	λ (deg)	r_m (in.)	r_m/d	Re_D	V_1/V_m	V_2/V_n	V_3/V_m
6	28.2	90	9	1.5	$0.15 - 0.01 \times 10^6$	1.21	-0.23	0.14
6	28.2	60	9	1.5	$0.15 - 0.01 \times 10^6$	1.20	. . .	. . .
6	28.2	90	24	4.0	0.53×10^6	0.90	-0.43	-0.06
6	28.2	60	24	4.0	0.53×10^6	1.03	-0.43	0
10	78.5	67	13.5	1.35	$0.10 - 0.15 \times 10^5$	. . .	. . .	. . .

estimated by the simplified approach and given in Figure 16 for the same altitude condition.

d. BALLUTE Inflation Aid Analysis

Although mutual agreement between NASA, Martin Marietta Corporation, and Goodyear Aerospace eliminated the preinflation aid from the first flight test BALLUTE, a typical analysis is included here.

Preinflation systems are helpful for initiating BALLUTE inlet deployment and increasing the effectiveness of ram-air inflation. For the PEPP BALLUTE, a mechanical mixture of 75 percent methanol and 25 percent water by weight was chosen because of its low freezing point and availability of sensible and latent heats for the process desired. The volume of one pound of the mixture will be:

$$\frac{12}{16}\left(\frac{1}{50}\right) + \frac{4}{16}\left(\frac{1}{62.4}\right) = 0.019 \text{ cu ft}$$

$$= 32.8 \text{ cu in.}$$

$$= 18.2 \text{ fl oz}$$

Since the actual dynamics for the evaporation from this mixture when subjected to rapidly reduced vapor pressure are difficult to predict, a quasi-steady state analysis is used.

Assuming that only the methanol vaporizes and that lowering the temperature of the water below the freezing point leads to subsequent ice crystal

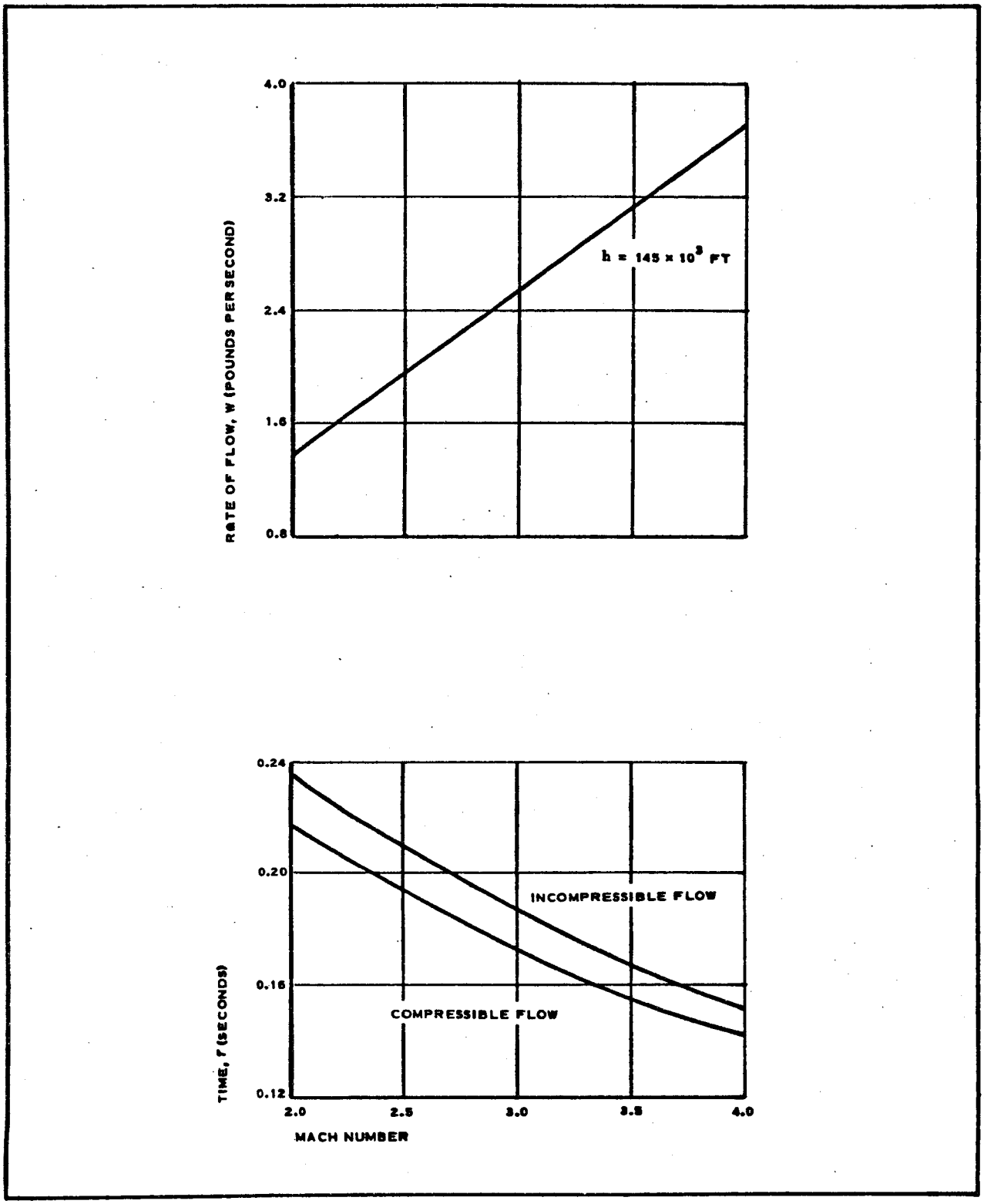

Figure 16 - Flow Parameters for Diffuser-Inlet

formation, there will be 12 oz of methanol changing state. The heat energy available to produce this change of state is found in the sensible heat of the mixture:

$$Q_m = W_m C_{p_m} (535 \text{ R} - T_2), \tag{6}$$

where the initial mixture temperature is 75 F and T_2 is the boiling point temperature of the methanol corresponding to the deployment static pressure. The specific heat of the mixture, C_{p_m}, is found by:

$$C_{p_m} = \frac{(W_1 C_{p1} + W_2 C_{p2})}{W_1 + W_2}$$

$$= \frac{(0.75 \times 0.57 + 0.25 \times 1)}{0.75 + 0.25}$$

$$= 0.677 \text{ Btu/lb/F.} \tag{7}$$

The energy required to vaporize the methanol is W_m(482 Btu/lb):

$$Q_V = 0.75(482)$$

$$= 362 \text{ Btu} \tag{8}$$

From the vapor pressure charts, the evaporation temperature limit for methanol at 145,000 ft MSL (3.45 psfa) is -44 F, which becomes T_2 in the energy equation (Equation 6) or $Q_m = (1)(0.677)(535 - 416) = 80.5$ Btu sensible heat in fluid.

Assuming the water freezes, its heat of fusion also will be available to raise the temperature of the methanol:

$$Q_{w_L} = (0.25)(144)$$

$$Q_{w_L} = 36 \text{ Btu} \tag{9}$$

By summing the available heat energy (Q_m = 80.5 Btu and $Q_w L$ = 36.0 Btu), 116.5 Btu are available. Since vaporization of the methanol requires 362 Btu and there is only 116.5 Btu available from the fluid, additional heat would be required. With 35 lb of BALLUTE envelope fabric in contact with

portions of the mixture, it is reasonable to assume that the additional 194.5 Btu will be available for the vaporization process. With the assumption that all of the methanol vaporizes, the gas volume created may be determined from the equation of state for a perfect gas:

$$V = \frac{W_a RT}{P}$$

$$V = \frac{(0.75)(48.4)(416)}{3.45}$$

$$V = 4380 \text{ cu ft} \qquad (10)$$

As the BALLUTE temperature increases to maximum operating temperature, the gas volume will increase linearly to a value of 8590 cu ft. If the actual test point does not meet the 145,000-ft altitude design point, but rather the 134,000- to 136,000-ft altitude as noted in the Nike-Nike-Honest John preliminary trajectory data, the inflation system must be re-examined.

For the worst case, 134,000 ft provides an ambient static pressure of 5.35 psfa. The boiling point temperature corresponding to this pressure is approximately -36 F. The heat available from one pound of the mixture is: $Q_m = (1)(0.677)(535 - 424) = 75.2$ Btu sensible heat in fluid. The latent heat of the ice will be the same as in the initial case. The sum of the available heat energy ($Q_m = 75.2$ Btu and $Q_{w_L} = 36.0$ Btu), is 111.2 Btu. This is not a significant change. The volume of gas created at 134,000 ft will be:

$$V = \frac{(0.75)(48.4)(424)}{5.35}$$

$$= 2880 \text{ cu ft.}$$

This volume still will be acceptable for preinflation of the BALLUTE envelope.

e. Conclusion

The aerodynamic information presented includes the set of the assumed initial deployment conditions for the PEPP BALLUTE of the TB-1 type, corresponding estimated flow field for a system and BALLUTE, pressure distribution, and data that should be useful for inflation considerations and comparison with the results of future developments.

The drag coefficient of the BALLUTE for the conditions assumed is estimated to be about one. The inside pressure, although defined by the equation of state, cannot be solved directly because of the transient conditions existing during the inflation.

f. List of Aerodynamic Symbols

A = reference area of inlet, sq in.

A_i = area of inlet, sq in.

$A_{i_{tot}}$ = total area of inlets, sq in.

C_{p_m} = specific heat at constant pressure of a mixture, Btu/lb/F

C_{p_1} = specific heat of one constituent, Btu/lb/F

C_{p_2} = specific heat of second constituent, Btu/lb/F

C_w = orifice coefficient

c = sonic velocity, fps

d_{base} = base diameter, in.

$d_{base\ (hydraulic)}$ = hydraulic base diameter, in.

$d_{b\ (tot)}$ = total diameter of BALLUTE with burble fence, in.

d_i = diameter of inlet, in.

g = gravity constant

h = altitude, ft

h_{bf} = height at burble fence, in.

l_{riser} = length of BALLUTE riser, in.

M = Mach number

M_{bf} = Mach line tangent to burble fence

MSL = mean sea level

P = static pressure, psf

P_t = total pressure, psf

Q_m = sensible heat of mixture, Btu

Q_V = energy required to vaporize 0.75 lb of methanol, Btu

Q_{w_L} = heat of fusion of the water in mixture, Btu

q = dynamic pressure, psf

R = gas constant = 1545/molecular weight, ft-lb/lb/R

R_B = radius of BALLUTE, in.

Re = Reynolds number

Re_D = Reynolds number based on equivalent diameter

r_m = radius of mean curvature, in.

T = absolute temperature, Rankine

T_t = total temperature, Rankine

V = velocity, fps

V_m = mean velocity, fps

V_1 = axial velocity on centerline, fps

V_2 = maximum velocity directed inward, fps

V_3 = radial velocity, fps

$\forall_{tot}$ = total volume of BALLUTE

W = specific weight of gas

W_a = weight of gas, lb

$\dot{W}_{in}$ = flow rate of gas into BALLUTE, lb/sec

W_m = weight of methanol, lb

$\dot{W}_{max}$ = weight rate of flow, lb/sec

W_1 = weight of one constituent, lb

W_2 = weight of second constituent, lb

X = axial distance between payload and BALLUTE, in.

Y = distance along longitudinal axis of BALLUTE, in.

θ_c = cone angle of BALLUTE, deg

λ = angle of bend, deg

ρ = density, pcf

Subscripts

bf = burble fence

∞ = initial condition

SECTION V - STRUCTURAL ANALYSIS

1. FULFILLMENT OF REQUIREMENTS

This section fulfills the requirements of Sections B.I.1.b, B.I.2.a and B.I.2.c of the Program Work Statement. Trajectory analyses indicated that the combination of maximum heating with the corresponding dynamic pressure yielded less severe stresses than the deployment dynamic pressure of 40 psf at room temperature. However, Nomex fabric and meridians were used to provide negligible strength reduction due to the sterilization environment. Flag-snapping effects, opening forces, and minimum gages were considered. Margins of safety between the ultimate component strengths as derived from appropriate test data and the calculated ultimate component stresses are presented.

2. SUMMARY

The calculations for the minimum margins of safety of the various components of the PEPP BALLUTE system are shown in Table II, along with the reference from this section where each calculation was derived. The loading conditions and design factors of safety upon which these margins were based are given in the body of this section.

TABLE II - MINIMUM MARGINS OF SAFETY

Component	Margin of safety	Reference page
BALLUTE fabric (seam)	+0.06	48
BALLUTE fabric (meridian shear stitching)	+2.6	49
Meridian straps	+0.00	49
Burble fence fabric (seam)	+1.92	57
Inlet fabric (seam)	+5.65	61
Riser and bridle	+0.74	72

3. DISCUSSION

A complete BALLUTE profile is defined by joining two isotensoid curves (front- and back-half curves) having common boundary conditions at their juncture, which is the BALLUTE's maximum diameter. The fabric and meridian stresses of the BALLUTE shape are constant for the design pressure distribution.

The theoretical stresses in the back half generally are close to those of the derived shape. The stresses in the front half vary more than the back-half stresses. In general, the maximum stresses for conditions differing from those used to derive the BALLUTE shape, occur in the front half of the BALLUTE.

All stress calculations were made using the dynamic pressure existing at the time the BALLUTE deployment was initiated. No attenuation of the dynamic pressure during the time for BALLUTE deployment was considered; this is a conservative approach to the problem. The temperature of deployment was taken as the prelaunch vehicle soak temperature (approximately 75 F).

The strengths of the fabric components are based on a combination of specified minimum strengths and measured material strengths. These data were used to provide a conservative estimate of the ultimate strength of the components made of these materials. Allowance was made for assembly and plying effects on the strength of these components.

4. ANALYSIS

a. BALLUTE

(1) General

The shape of the TB-1 BALLUTE[2] was selected for this experiment to provide a stable pressure vessel under a rather wide range of external pressure distributions. Of course, the isotensoid condition, i.e., constant fabric stress and constant meridian tension, exists only for the particular pressure distribution for which the shape was derived. The method for deriving the BALLUTE's design shape was developed by Goodyear Aerospace.[6]

The approach taken in this structural analysis is to first determine stress and strength requirements along with the corresponding weights for the BALLUTE by considering each of the two loading conditions and assuming that the isotensoid design shape requirements are satisfied. A more detailed stress analysis then is made using the pressure distribution for the critical loading condition as determined by aerodynamic analysis. Structural stability is verified, because tensile stresses and tensile forces exist everywhere. The variations of fabric stresses, meridian tension, and shear stresses along the meridian profile are determined. The maximum values then are compared to the allowable strengths to yield the minimum margins of safety.

(2) Design Shape and Stresses

(a) Derivation of Profile

The BALLUTE profile is divided into two parts at the equator and is described by the cartesian coordinates indicated in Figure 17. The back-half profile was selected from the data.[6] The pressure distribution over the

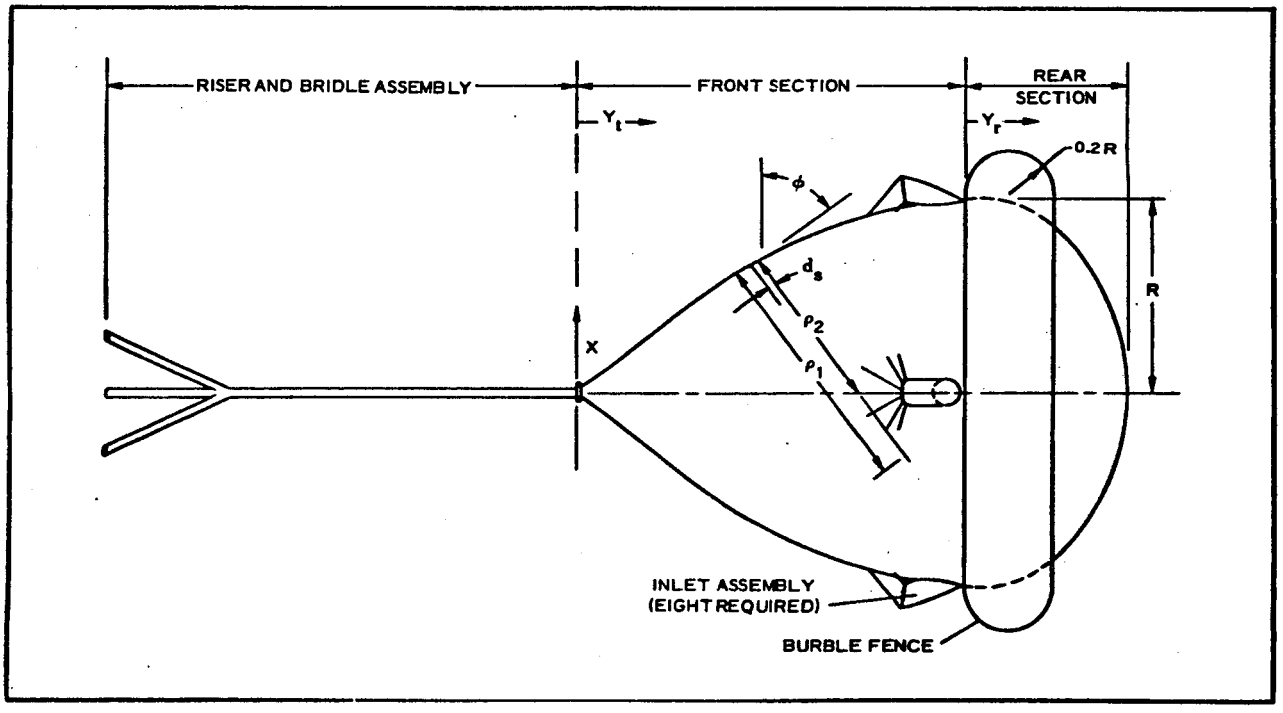

Figure 17 - Configuration of Deployed BALLUTE

back half is practically constant. In particular, the back-half profile corresponding to a K value of 0.6 is used.

The coordinates of the front-half profile are tabulated in Table III, along with the slope angles of the meridian, the incremental arc lengths, and the two principal radii of curvature.

The meridian profile of the burble fence of the TB-1 BALLUTE was determined by a method developed by Goodyear Aerospace.[6] The burble fence is a tucked-back type with no meridians, where K = 0 and $\rho \approx 0.8$. The shape thus derived was approximated by a combination of three circular arcs as shown in Figure 18. The dimensions of this figure are for a TB-1 BALLUTE that had a five-foot equatorial diameter and therefore had to be multiplied by the scale factor of three for the PEPP BALLUTE.

The work in this section provides the basis for material selection and first generation weight estimation. In general, fabric and meridian strength values should be conservative because of the 20-percent seaming reduction and the material strength variation factor of 1.25. These factors later are

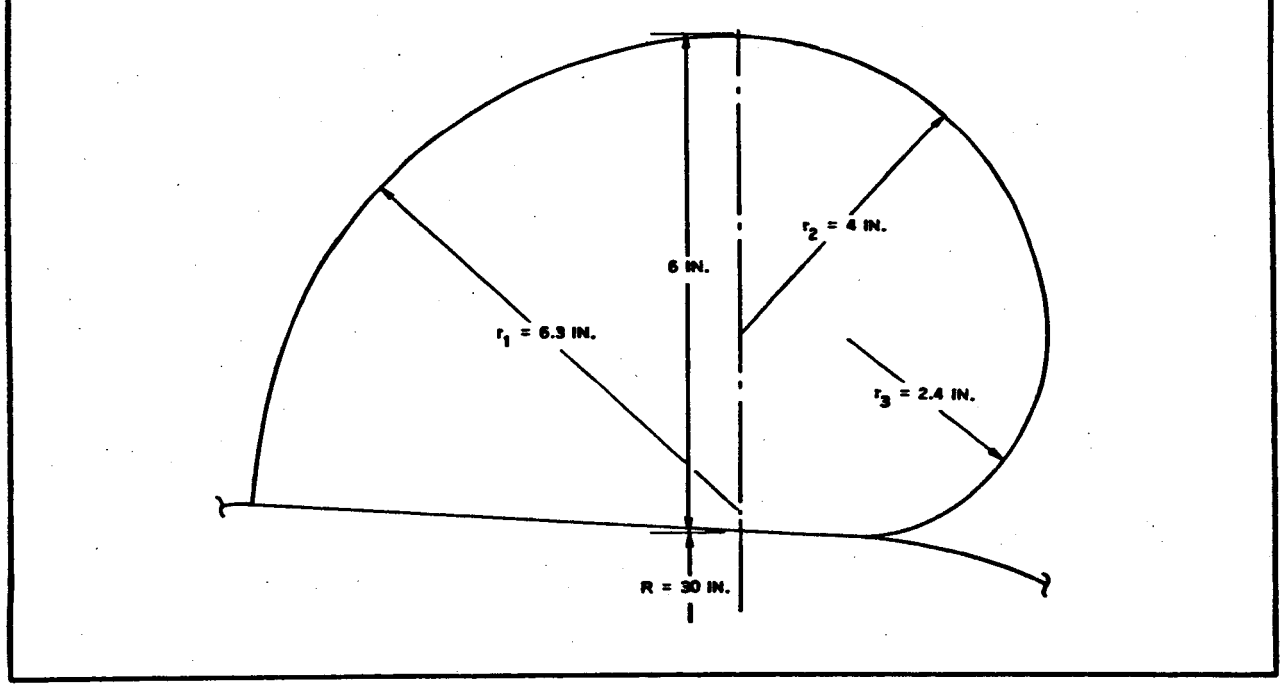

Figure 18 - Cross Section of Burble Fence

TABLE III - PROPERTIES OF THE FRONT-HALF PROFILE

X/R	Y/R	$\tan\phi = \Delta Y/\Delta X$	ϕ (deg)	ϕ (min)	Sin ϕ	(X/R) sin ϕ	$\rho_2/R = X/R \sin\phi$	$\Delta^2 Y/\Delta X^2$	$1 + (\Delta Y/\Delta X)^2$	$\Delta S/R = \frac{\Delta X}{R}\sqrt{1+\left(\frac{\Delta Y}{\Delta X}\right)^2}$	$\left[1+\left(\frac{\Delta Y}{\Delta X}\right)^2\right]^{2/3}$	ρ_1/R
0.0	0.0		58	30	0.8526							-2.0
0.05	0.08207	1.5640	57	24	0.8425	0.04213	0.05935		3.4461	0.1855	6.4	-2.22
0.1	0.15640	1.434	55	7	0.8203	0.08203	0.12190	-2.195	3.0564	0.175	5.34	-2.43
0.15	0.22547	1.3445	53	22	0.8025	0.12038	0.18691	-1.526	2.8077	0.1675	4.7	-3.08
0.2	0.29085	1.2814	52	2	0.7884	0.15768	0.25368	-1.078	2.6420	0.1623	4.29	-3.98
0.25	0.35361	1.2367	51	2	0.7775	0.19438	0.32154	-0.751	2.5294	0.159	4.02	-5.35
0.3	0.41452	1.2063	50	21	0.7700	0.231	0.38961	-0.489	2.4552	0.1568	3.85	-7.87
0.35	0.47424	1.1878	49	54	0.7649	0.26772	0.45758	-0.269	2.4109	0.1552	3.745	-13.9
0.4	0.53230	1.1794	49	42	0.7627	0.30508	0.52445	-0.066	2.3910	0.1547	3.95	-59.9
0.45	0.59218	1.1812	49	45	0.7632	0.34344	0.58962	0.16	2.3952	0.1549	3.7	23.15
0.5	0.65142	1.1954	50	5	0.7670	0.3835	0.65189	0.433	2.4290	0.1558	3.78	8.74
0.55	0.71172	1.2245	50	46	0.7746	0.4260	0.71004	0.755	2.4994	0.158	3.955	5.25
0.6	0.77387	1.2709	51	48	0.7859	0.47154	0.76346	1.141	2.6152	0.1618	4.23	3.71
0.65	0.83881	1.3386	43	14	0.8011	0.52072	0.81138	1.633	2.7918	0.167	4.66	2.85
0.7	0.90773	1.4342	55	7	0.8203	0.57421	0.85335	2.322	3.0569	0.175	5.35	2.3
0.75	0.98223	1.5708	57	31	0.8435	0.63263	0.88915	3.391	3.4674	0.1862	6.46	1.905
0.8	1.06481	1.7733	60	35	0.8711	0.69688	0.91878	5.216	4.1446	0.2035	8.44	1.62
0.85	1.15956	2.0924	64	27	0.9022	0.76687	0.94214	9.152	5.3781	0.2315	12.46	1.36
0.9	1.27405	2.6835	69	36	0.9373	0.84357	0.96020	18.726	8.2280	0.287	23.6	1.26
0.95	1.42841	3.965	75	51	0.9700	0.9215	0.97938	40.769	16.7212	0.327	68.4	1.13
0.98	1.56979	5.95	80	28	0.9862	0.96648	0.99371	270.0	36.4025	0.271	219.5	1.05
0.995	1.70005	10	84	18	0.9951	0.99012	0.9999	∞	101.0000	0.201	∞	1.01
1.0	1.75	∞	90	0	1.0	1.0	1.0	∞	∞	∞	∞	1.0

refined in Item (c), "Off-Design Stresses," from results of the tests of the selected materials.

The steady-state ultimate stress equations (Equations 11 and 13) and the definition of K are taken from Equation 7 of Reference 6. Here, $\rho = 0$ and $p = C_{pi}q$ The design factor N is also introduced to convert from limit to ultimate stresses.

An empirical formula was developed at Goodyear Aerospace to provide adequate strength in the BALLUTE fabric for flag-snapping effects on partially inflated BALLUTES during deployment. The formula for the ultimate strength of the fabric is given in Equation 12.

The meridians also were checked with a factor of safety of two for the peak deceleration, which is an indication of the deployment shock. The opening shock forces on the fabric are accounted for by using a dynamic factor of 1.5 applied to the steady-state stresses.

(b) Stresses and Weights for Isotensoid Conditions

Summary - The stresses, loads, and weights of fabric for certain conditions are given in Table IV.

TABLE IV - STRENGTH AND WEIGHT REQUIREMENTS

Condition	F_u (lb/in.)	γ_f (oz/sq yd)	T_u (lb)	γ_m (oz/yd)
A - deployment	58.5	2.24	755	0.3
B - q and T combination	30.2	1.46	535	0.27
C - minimum gage	64.0*	3.08	800+	0.32

*With 20-percent seaming reduction.

+Estimated value.

Condition C governs the design of the BALLUTE. The corresponding margins of safety are:

1. Fabric M.S. = 64/58.5 - 1 = +0.09
2. Meridians M.S. = 800/755 - 1 = +0.06

The volume of the BALLUTE, V_B, is about 2065 cu ft, while the volume of the burble fence, V_b, is about 175 cu ft. The total volume is about 2240 cu ft. The areas, lengths, and weights of BALLUTE components are given in Table V. The volumes are considered approximate and check closely with the 2220 cu ft given earlier.

TABLE V - AREAS, LENGTHS, AND WEIGHTS

Item	Fabric area (sq yd)	Length (ft)	Weight (lb)
Basic BALLUTE	85.5		16.5
Gore meridian seams	3.87	418	0.75
Cross gore seams	2.68	290	0.52
Meridians		1254	8.36
Basic burble fence	26.9		5.2
Meridian seams	0.7	75.5	0.14
Circumferential seams	4.0	91	0.77
Totals	123.65	. . .	32.24

The weights of the following items were estimated:

Item	Weight (lb)
8 Inlets (8 at 0.5 lb each)	4
Riser line	1
Packaging bag	1
Grand total	38.24

General Equations - The general equations for the ultimate strength requirements and the amounts of material are listed below. The equations for the ultimate strength requirements are:

1. Fabric

(a) Steady state - $F_u = \frac{1}{2}\left[NC_{pi}qR(1 - k)\right]$ (11)

(b) Flag snapping - $F'_u = \frac{7}{3}(qR)$ (12)

2. Meridians

a. Steady state - $T_u = \frac{1}{n} NC_{pi} q \pi R^2 k$ (13)

b. Deployment shock - $T'_u = \frac{F.S.}{n} gW_p$ (14)

To determine the proper amounts of materials, the values are substituted in the equations from Appendix A:

1. Fabric

a. Basic BALLUTE surface area

$$A_{f_B} = 4(1.085)\pi R^2 = 4.35\pi R^2 \quad (15)$$

b. Ten-percent burble fence

$$A_{f_b} = 0.315 A_{f_B} = 1.37\pi R^2 \quad (16)$$

2. Seams

a. Meridian gore seams

$$\ell_m = 3.48\, n_g R \quad (17)$$

$$A_{f_{gm}} = 3.48\, m_g R m w_m \quad (18)$$

b. Cross-splice seams

$$\ell_s = 2n_g \sqrt{2}\left(j_o m w_m + \frac{1.085\pi}{n_g} \sum_1^{j_o} X_j\right), \quad (19)$$

where

$$j_o = \frac{3.48\, R}{A\sqrt{2}}, \quad (20)$$

$$X_j = 1.11R \sin \phi_j, \quad (21)$$

$$\phi_j = \frac{C_j}{1.11R} \quad (22)$$

$$C_j = jA\sqrt{2}, \text{ and} \quad (23)$$

$$A_{f_s} = m w_m \ell_s. \quad (24)$$

c. Burble fence seams (meridional)

$$\ell_{bm} = n_{bm}\, 0.2\pi R \tag{25}$$

$$A_{f_{bm}} = m w_m \ell_{bm} = 0.2\pi n_{bm} R m w_m \tag{26}$$

d. Burble fence seams (circumferential)

$$\ell_{bc} = 4\pi R \cos\theta_b \tag{27}$$

$$A_{f_{bc}} = m_c w_c \ell_{b_c} = 4\pi R m_c w_c \cos\theta_b \tag{28}$$

$m_c = 4.75$

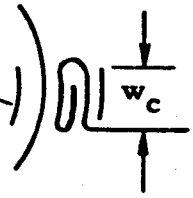

3. Meridians

$$\ell_c = 3.48\, n\, R \tag{29}$$

Design Factors - The design factors for the BALLUTE are tabulated below.

Factor	Value
Overload	1.0
Dynamic (opening shock)	1.5
Seam efficiency	Curves of Reference 7
Temperature	Curves of Reference 7
Material strength variation	1.25
Raking	1.0
Basic safety factor	1.5
Total design factor, N	2.84

Numerical Results - The numerical values given for Nomex cloth and meridians are: $n = 48$, $N = 2.84$, $K = 0.6$, $W_p = 204$ lb, $n_g = 16$, $C_{pi} = 3$, $R = 7.5$ ft, and F.S. = 2. The dynamic pressure and maximum acceleration at deployment (Condition A) are: $q = 40$ psf and $g = 16.5$ g's. The critical pressure and temperature condition (Condition B) have values of $q = 28.35$ psf and $T = 307$ F.

The strength-to-weight ratios and the unit weights for both fabric and meridians are listed below for the three conditions:

1. Condition A[7]
   a. k_f = 45,000 ft at room temperature
   b. k_m = 120,000 ft at room temperature
2. Condition B
   a. k_f = 35,700 ft at T = 307 F
   b. k_m = 95,000 ft at T = 307 F
3. Condition C (minimum gage) - the unit weights of calendered Nomex cloth, γ = 2.08 oz/sq yd and of the coating, γ = 1 sq yd. The total fabric unit weight, γ_f = 3.08 oz/sq yd. The minimum ultimate strength, $F_{u_{min}}$ = 80 lb/in. The unit weight and the minimum ultimate strength of the Nomex meridians are, respectively, γ_m = 0.32 oz/sq yd and $F_{u_{min}}$ = 800 lb.

Stress Conditions - The values of the ultimate stresses and unit weights are determined below:

1. Condition A
   a. $F_u = \frac{1}{2}(2.84)(3)(40)(7.5)(0.4) = 512$ lb/ft = 42.6 lb/in.
   b. $F'_u = \frac{7}{3}(40)(7.5) = 700$ lb/ft = 58.5 lb/in.
   c. Therefore, $\gamma_{f_{req'd}} = \frac{F'_u}{K_f} = \left(\frac{700}{45,000}\right)(144) =$ 2.24 oz/ sq yd
   d. $T_u = \frac{2.84}{48}(3)(40)\pi(7.5)^2(0.6) = 755$ lb
   e. $T'_u = 2\,\frac{16.5}{48}(204) = 140$ lb
   f. Therefore, $\gamma_{m_{req'd}} = \left(\frac{755}{120,000}\right)(48) = 0.3$ oz/yd

2. Condition B

a. $\gamma_{f_{req'd}} = \left(\frac{28.35}{40}\right)\left(\frac{42.6}{58.5}\right)\left(\frac{45,000}{35,700}\right)(2.24) =$ 1.46 oz/sq yd

b. $\gamma_{m_{req'd}} = \left(\frac{28.35}{40}\right)\left(\frac{120,000}{95,000}\right)(0.3) = 0.268$ oz/yd

3. Condition C

a. $\gamma_f = 3.08$ oz/sq yd

b. $\gamma_m = 0.32$ oz/yd

A comparison of the three conditions above shows the minimum gage condition (Condition C) governs.

Weight Breakdown - The values of the various amounts of materials are determined below:

1. $A_{fB} = 4.35\pi(7.5)^2 = 770$ sq ft = 85.5 sq yd
2. $W_{fB} = \gamma_f A_{fB} = \left(\frac{3.08}{16}\right)(85.5) = 16.5$ lb
3. $A_{fb} = (0.315)(770) = 242$ sq ft = 26.9 sq yd
4. $W_{fb} = (0.315)(16.5) = 5.2$ lb
5. $\ell_m = (3.48)(16)(7.5) = 418$ ft = 139 yd
6. $A_{f_{gm}} = (418)(2)(1/2)(1/12) = 34.8$ sq ft = 3.87 sq yd
7. $W_{f_{gm}} = \left(\frac{3.08}{16}\right)(3.87) = 0.745$ lb
8. $\ell_s = 290$ ft = 96.7 yd
9. $A_{fs} = (290)(2)(1/2)(1/12) = 24.2$ sq ft = 2.68 sq yd
10. $W_{fs} = \left(\frac{3.08}{16}\right)(2.68) = 0.515$ lb
11. $\ell_{bm} = (16)(0.2)\pi(7.5) = 75.5$ ft = 25.15 yd
12. $A_{f_{bm}} = (75.5)(2)(1/2)(1/12) = 6.3$ sq ft = 0.7 sq yd

13. $W_{f_{bm}} = \left(\frac{3.08}{16}\right)(0.7) = 0.135$ lb

14. $\ell_{bc} = 4\pi(7.5)(0.965) = 91$ ft $= 30.3$ yd

15. $A_{f_{bc}} = (91)(4.75)(1)(1/12) = 36$ sq ft $= 4$ sq yd

16. $W_{f_{bc}} = \frac{3.08}{16}(4) = 0.77$ lb

17. $\ell_c = (3.48)(48)(7.5) = 1254$ ft $= 418$ yd

18. $W_c = \left(\frac{0.32}{16}\right)(418) = 8.36$ lb

(c) Off-Design Stresses

General - The external pressure distribution was determined by aerodynamic analysis and is shown in Figure 19. Since the pressure on the rear half of the BALLUTE is seen to be essentially constant as was used for the design shape, the stresses remain unchanged. However, the stresses in the front half must be investigated since they will vary from those of the design shape due to the given pressure distribution and the additional drag on the burble fence.

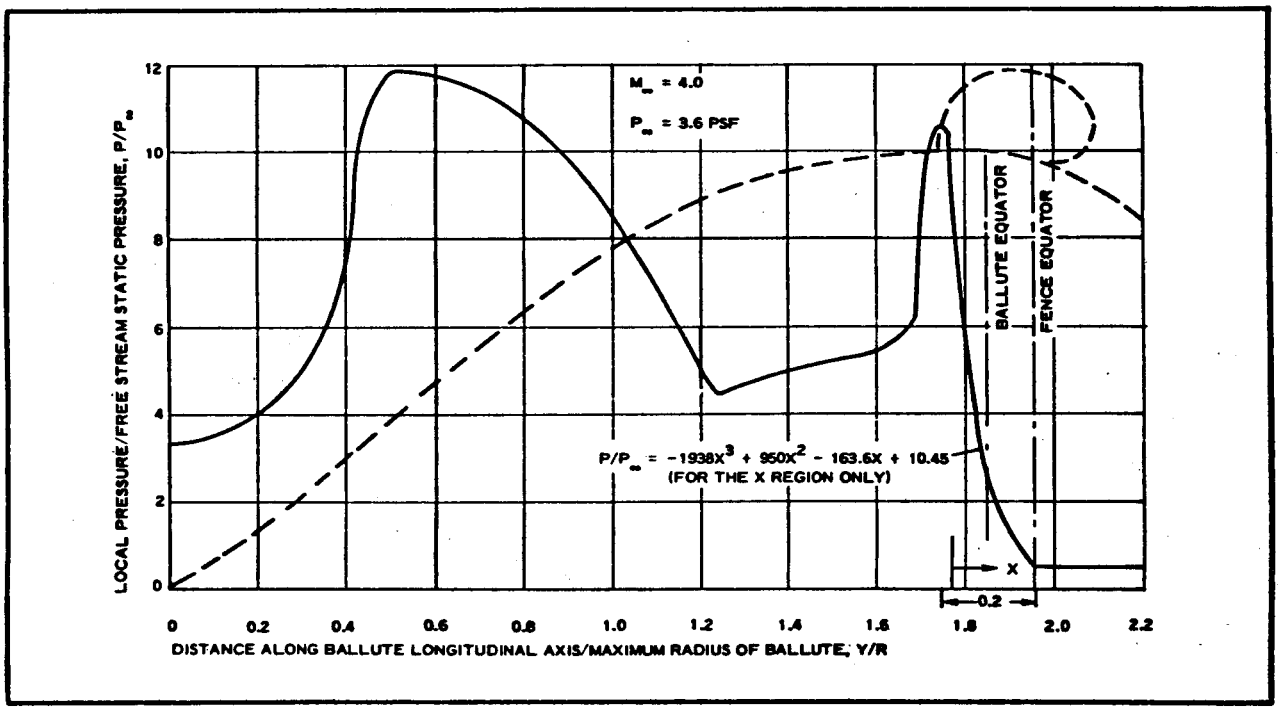

Figure 19 - Equation for BALLUTE Pressure Distribution

The drag from the back half is found by assuming that the pressure over the back of the burble fence and the BALLUTE proper is uniform. To this loading is added the load from the front half of the burble fence.

Front Half - The front half of the cross section of the burble fence is considered to be a circular arc as shown in Figure 20.

The pressure is constant at $p_o/p_\infty = 10.45$ over the portion from 0.02 R to 0.0872 R and then varies as (see Figure 19):

$$p_o/p_\infty = -1938\ X^3 + 950\ X^2 - 163.6\ X + 10.45. \qquad (30)$$

The corresponding drag is given by

$$D_{tb} = (10.45)(0.182)\pi p_\infty\ R^2 + \int_{0.0872R}^{0.2R} 2\pi(R + y)\ p_o\ dy, \qquad (31)$$

where

$$y = \sqrt{0.0076R^2 + 0.36\ R_x - x^2}\ . \qquad (32)$$

This equation is integrated numerically in Table VI.

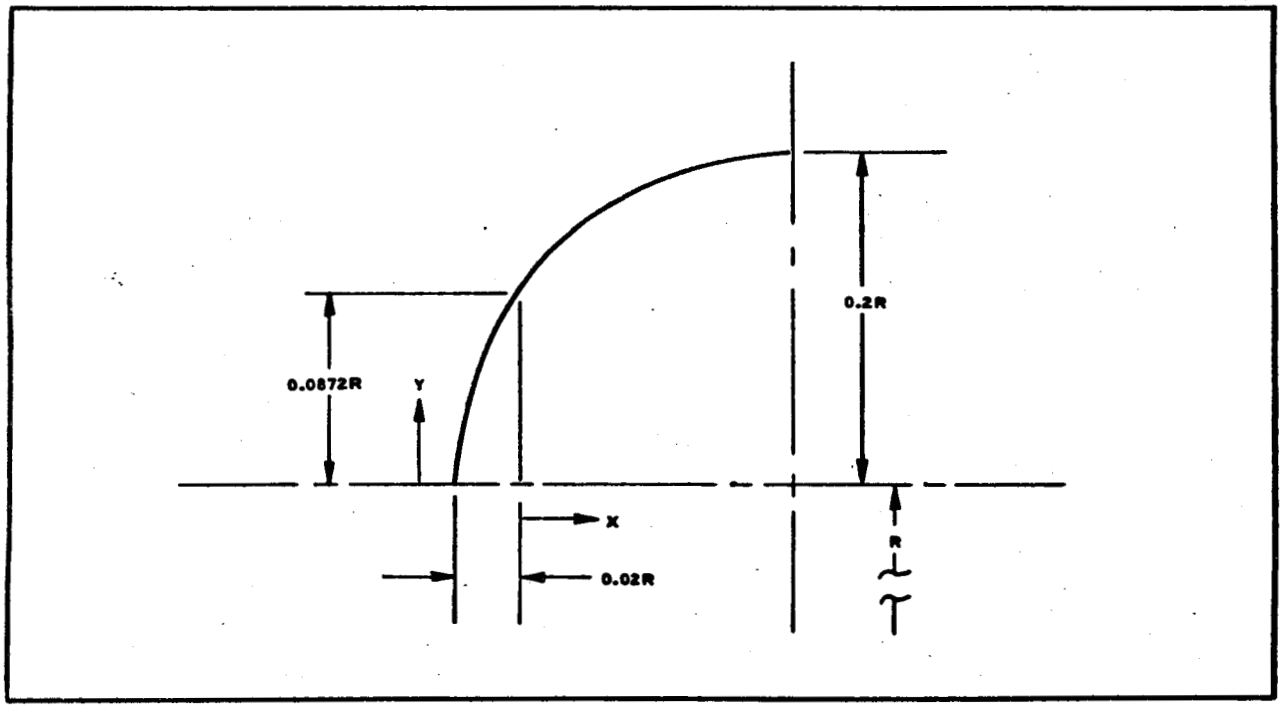

Figure 20 - Cross Section of Front Half of Burble Fence

TABLE VI - EXTERNAL PRESSURE AND DRAG ON FRONT OF FENCE

X/R	p_o/p_∞	1 + Y/R	$(1 + Y/R)^2$	$\Delta A/\pi R^2$	$(p_o/p_\infty)_{Ave}$	$\Delta D_{fb}/p_\infty \pi R^2$
0	10.45	1.0872	1.182	0.182	10.45	1.902
0.01	8.91	1.1052	1.221	0.039	9.68	0.378
0.03	6.35	1.1322	1.282	0.061	7.63	0.465
0.05	4.40	1.152	1.327	0.045	5.375	0.242
0.07	2.99	1.167	1.362	0.035	3.695	0.129
0.09	2.01	1.1785	1.389	0.027	2.5	0.068
0.11	1.37	1.1873	1.410	0.021	1.69	0.035
0 13	0.98	1.1938	1.425	0.015	1.175	0.018
0.15	0.74	1.1977	1.434	0.009	0.86	0.008
0.17	0.57	1.1996	1.439	0.005	0.655	0.003
0.18	0.45	1.2	1.44	0.001	0.51	0.001
						Total = 3.249

Therefore, the total drag from the back half is given by:

$$D_r = D_{tb} + D_{rb} + D_{rB} \tag{33}$$

or, for the PEPP BALLUTE,

$$\frac{D_r}{p_\infty \pi R^2} = 3.249 - 0.45(1 + 0.44)$$

$$= 2.601. \tag{34}$$

Distributing this drag around the equator gives:

$$N_{D_r} = \frac{D_r}{2\pi R} = 1.3\, R p_\infty . \tag{35}$$

Next, consider equilibrium of forces (parallel to the axis of revolution) in the front half of the BALLUTE (see Figure 21).

$$2\pi X N_\phi \sin\phi = 2\pi R N_r - 2\pi \int_o^{R-X} p\,(R - z)\,dz$$

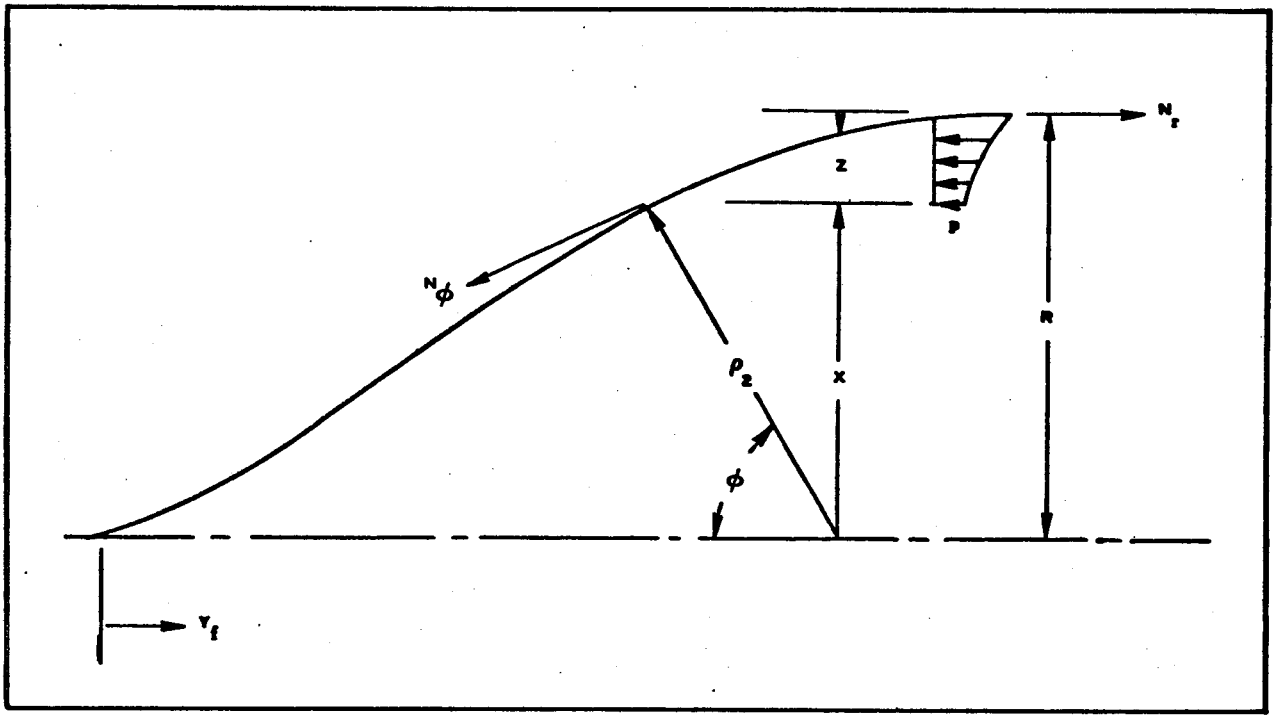

Figure 21 - Equilibrium on Parallel Circle of Radius X
(Front Half of BALLUTE)

$$N_\phi = \frac{RN_r - R\int_o^{R-X} p\left(1 - \frac{z}{R}\right)dz}{x \sin \phi} \tag{36}$$

where

$$N_r = N_{Dr} + \frac{p_i R}{2}$$

$$= \left(1.3 + \frac{33.6}{2}\right) R p_\infty$$

$$= 18.1 R p_\infty \ . \tag{37}$$

and

$$p = p_i - p_o$$

$$= \left(33.6 - \frac{p_o}{p_\infty}\right) p_\infty \tag{38}$$

The integral of Equation 36 is evaluated numerically in Table VII along with the drag on the front of the BALLUTE, D_t.

From Table VII,

$$\frac{D_t}{p_\infty \pi R^2} = 2 \sum_0^1 \frac{p_o}{p_\infty} \frac{\Delta z}{R} \left(1 - \frac{z}{R}\right)$$

$$= 2(4.132)$$

$$= 8.264. \qquad (39)$$

The total drag is given by (see Equations 34 and 39)

$$D = D_t + D_r \qquad (40)$$

or, for the PEPP BALLUTE,

$$\frac{D_t}{p_\infty \pi R^2} = 8.264 + 2.601$$

$$= 10.865 . \qquad (41)$$

In particular, for $p_\infty = 3.6$ psf and $R = 7.5$ ft.,

$$D = (10.865)(3.6)\pi(7.5)^2$$

$$= 6920 \text{ lb.} \qquad (42)$$

The corresponding drag coefficient when:

$$q = 0.7 M_\infty{}^2 p_\infty$$

$$= (0.7)(4)^2(3.6)$$

$$= 40 \text{ psf,} \qquad (43)$$

becomes

$$C_D = \frac{D}{q \pi R^2}$$

$$= \frac{D}{0.7 M_\infty{}^2 p_\infty \pi R^2}$$

TABLE VII - NUMERICAL INTEGRATION OF PRESSURE DISTRIBUTION

$\frac{X}{R}$	$\frac{Y}{R}$	$\frac{p_o}{p_\infty}$	$\frac{p}{p_\infty}$	$\frac{Z}{R}$	$\frac{p_o}{p_\infty}\frac{\Delta Z}{R}$	$\frac{p}{p_\infty}\frac{\Delta Z}{R}$	$\frac{p_o}{p_\infty}\frac{\Delta Z}{R}\left(1-\frac{Z}{R}\right)$	$\frac{p}{p_\infty}\frac{\Delta Z}{R}\left(1-\frac{Z}{R}\right)$	$\sum_0^{1-X/R}\frac{p_o}{p_\infty}\frac{\Delta Z}{R}\left(1-\frac{Z}{R}\right)$	$\sum_0^{1-X/R}\frac{p}{p_\infty}\frac{\Delta Z}{R}\left(1-\frac{Z}{R}\right)$
0.0	0.0	3.3	30.3	1.00	0.082	1.51	0.0	0.0	4.132	12.99743
0.05	0.08207	3.4	30.2	0.95	0.17	1.51	0.0085	0.0755	4.132	12.99743
0.1	0.15640	3.7	29.9	0.9	0.185	1.495	0.0185	0.1495	4.1235	12.92193
0.15	0.22547	4.2	29.4	0.85	0.21	1.47	0.0315	0.2205	4.105	12.77243
0.2	0.29085	4.95	28.65	0.8	0.2475	1.4325	0.0495	0.2865	4.0735	12.55193
0.25	0.35361	6.0	27.6	0.75	0.30	1.38	0.075	0.345	4.024	12.26543
0.3	0.41452	8.4	25.2	0.7	0.42	1.26	0.126	0.378	3.949	11.92043
0.35	0.47424	11.35	22.25	0.65	0.5675	1.1125	0.1986	0.3894	3.823	11.54243
0.4	0.53330	11.8	21.8	0.6	0.59	1.09	0.236	0.436	3.62240	11.15302
0.45	0.59218	11.7	21.9	0.55	0.585	1.095	0.26325	0.49275	3.38840	10.71703
0.5	0.65142	11.5	22.1	0.5	0.575	1.105	0.2875	0.5525	3.12515	10.22428
0.55	0.71172	11.25	22.35	0.45	0.5625	1.1175	0.30938	0.61463	2.83765	9.67178
0.6	0.77387	10.9	22.7	0.4	0.545	1.135	0.327	0.681	2.52827	9.05715
0.65	0.83881	10.35	23.25	0.35	0.5175	1.1625	0.3264	0.75563	2.20127	8.37615
0.7	0.90773	9.65	23.95	0.3	0.4825	1.1975	0.33775	0.83825	1.86487	7.62052
0.75	0.98223	8.7	24.9	0.25	0.435	1.245	0.32625	0.93375	1.52712	6.78227
0.8	1.06481	7.5	26.1	0.2	0.375	1.305	0.3	1.044	1.20087	5.84852
0.85	1.15956	5.85	27.75	0.15	0.2925	1.3875	0.24863	1.179375	0.90087	4.80452
0.9	1.27405	4.5	29.1	0.1	0.225	1.455	0.2025	1.3095	0.65224	3.62514
0.95	1.42841	4.95	28.65	0.05	0.198	1.146	0.1881	1.0387	0.44974	2.31564
0.98	1.15956	5.25	28.35	0.02	0.168	0.9072	0.16464	0.88906	0.26164	1.22694
0.994	1.69000	6.1	27.5	0.006	0.0458	0.2063	0.04553	0.205062	0.097	0.33788
0.995	1.70005	8.5	25.1	0.005	0.0255	0.0753	0.025373	0.07492	0.05147	0.13282
1.0	1.75000	10.45	23.15	0.0	0.026	0.0579	0.0261	0.0579	0.0261	0.0579

$$= \frac{10.865}{(0.7)(16)}$$

$$= 0.97 \qquad (44)$$

The meridian force, N_ϕ, of Equation 36 may be determined by using the values of Table VII along with values of $X\sin\phi$ from Table V and N_r as given by Equation 37. The circumferential force, N_θ, is given by the well-known membrane equation:

$$\frac{N_\phi}{\rho_1} + \frac{N_\theta}{\rho_2} = p$$

or

$$N_\theta = \rho_2\left(p - \frac{N_\phi}{\rho_1}\right). \qquad (45)$$

Assuming that the bias fabric combines with the meridians to behave as a three-thread-set fabric, it is easily shown that,

$$N_\theta = f, \qquad (46)$$

$$N_\phi = f + \frac{nT_m}{2\pi X}, \qquad (47)$$

or,

$$T_m = \frac{2\pi X}{n}(N_\phi - f). \qquad (48)$$

The shear stress between the fabric and the meridian is given by

$$f_s = \frac{\Delta T_m}{\Delta_s}, \qquad (49)$$

where Δ_s is given in Table V. The above expressions are evaluated in Table VIII.

Using the maximum values from Table VIII along with the design values for N, R, and p_∞ gives:

$$f = 14.85\, p_\infty R$$

$$= (14.85)(3.6)(7.5)(1/12)$$

$$= 33.4 \text{ lb/in.}$$

$$f_s = 210 \frac{p_\infty R}{n}$$

$$= \frac{210}{14.85} \frac{33.4}{48}$$

$$= 9.85 \text{ lb/in.}$$

$$T_m = 78.5 \frac{p_\infty R^2}{n}$$

$$= 78.5 \frac{3.6}{48} (7.5)^2$$

$$= 332 \text{ lb.}$$

The above fabric stress acts across the meridional and cross-gore seams, which are the weakest elements of the BALLUTE. These French fell seams are stitched with one row, 4 to 6 stitches per inch and two rows, 6 to 8 stitches per inch using Nomex thread (see Reference Drawing 620A000-002). The minimum strength in any test was found to be F_{tu} = 80 lb/in. Again, using a factor of safety of 1.5 along with the dynamic factor of 1.5, i.e. $N = (1.5)^2 = 2.25$, gives the following minimum margin of safety:

$$M.S. = \frac{F_{tu}}{Nf} - 1$$

$$= \frac{80}{(2.25)(33.4)} - 1$$

$$= +0.06.$$

The fabric is sewn to the meridian straps in a manner similar to the splices in the fabric (see Reference Drawing 620A000-002). The shear strength between the fabric and meridian strap is estimated to be the same as for the fabric seam, i.e., F_{tu} = 80 lb/in. Therefore,

$$M.S. = \frac{80}{(2.25)(9.85)} - 1$$

$$= +2.6.$$

The meridians are Nomex webs. There are no splices in these webs of the BALLUTE proper and the plying efficiency for the two webs is close to 100 percent.

The minimum strength of the tests was found to be, T_u = 750 lb. Therefore, the margin of safety is

$$M.S. = \frac{T_u}{NT_m} - 1$$

$$= \frac{750}{(2.25)(332)} - 1$$

$$= +0.000$$

Burble Fence - Since the burble fence is scaled from that used on the TB-1 BALLUTE, the cross section of the burble fence does not necessarily yield the constant one-to-one stress condition for the loadings of this application. This condition, however, is relatively unimportant since the stress level is much less than that of the basic BALLUTE, where, as has already been seen, minimum gage considerations govern the fabric selection. The conditions of primary interest are the maximum fabric stresses and loads on the connections of the fence to the BALLUTE. Also, to have the desired minimum drag area, the outer circumference of the fence must remain at least equal to that of the design 10-percent fence.

The solid curve of Figure 22 is the tailored cross section of the fence (also, see Figure 18) and the dashed curve represents the deformed stable shape under internal pressure only. The deformed shape under the drag load is expected to lie between these two curves and will be estimated.

First, consider the pressure-stable shape, which may be determined from geometry by neglecting circumferential stiffness, i.e., the fence behaves as a cylinder. The validity of this approximation will be shown later. Also, if the warp and fill directions of the fabric were oriented in the meridional and circumferential directions, the increase in circumference indicated

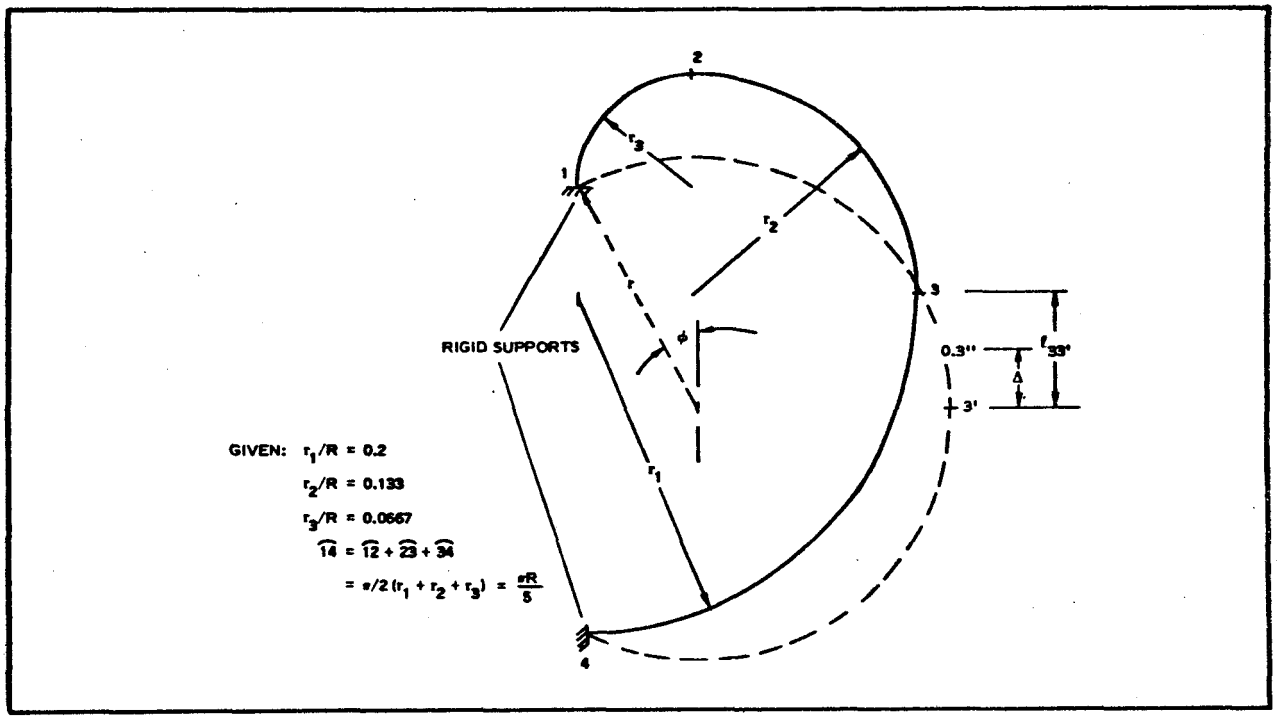

Figure 22 - Tailored and Pressure-Stable Cross Section of Burble Fence

by the movement of point 3 to point 3' could not occur and wrinkling in the vicinity of point 4 would be expected. However, bias orientation of the fabric more easily allows such deformation and a minimum amount or no wrinkling is expected.

The equilibrium shape is shown by the dashed curve and the radius and central angle are determined below:

$$2r\left(\phi + \frac{\pi}{2}\right) = \frac{\pi R}{5} , \tag{50}$$

$$2r \cos \phi = r_1 + r_2 - r_3$$

$$= 0.2667R, \text{ and} \tag{51}$$

$$\cos \phi = \sin \left(\phi = \frac{\pi}{2}\right); \tag{52}$$

therefore,

$$\frac{\sin\left(\phi + \frac{\pi}{2}\right)}{\phi + \frac{\pi}{2}} = \frac{0.2667}{\frac{\pi}{5}}$$

$$= \frac{1.3333}{\pi}$$

$$= \frac{4}{3\pi}$$

$$= 0.42441 \quad (53)$$

Solving Equation 53 gives,

$$\phi + \frac{\pi}{2} = 118.5 \text{ deg or } \phi = 28.5 \text{ deg}, \quad (54)$$

$$r/R = \frac{\pi}{10\left(\phi + \frac{\pi}{2}\right)}$$

$$= \frac{180}{(10)(118.5)}$$

$$= 0.152, \quad (55)$$

$$(r/R)\sin\phi = (0.152)(0.4772)$$

$$= 0.0726, \text{ and}$$

$$(r/R)(1 + \sin\phi) = 0.2246 \text{ versus } (1/R)(r_2 + r_3) = 0.2 \quad (56)$$

The membrane forces are the same as for a cylinder:

$$N_\phi = pr$$

$$= (0.833)(0.152)(90)$$

$$= 11.4 \text{ lb/in., and} \quad (57)$$

$$N_\theta = \frac{pr}{2}$$

$$= 5.7 \text{ lb/in.} \quad (58)$$

To show that the two-dimensional approximation is valid, the N_ϕ force of Equation 57 is compared with the maximum and minimum meridional stresses in a pressurized torus.

From the shell theory, [8]

$$N_\phi = \frac{pr_o}{2}\left(1 + \frac{R_t}{r}\right), \tag{59}$$

where

$$r_o = r$$

$$= 0.152\ R, \text{ and} \tag{60}$$

$$R_t = R + r \sin\phi$$

$$= \left[1 + (0.152)(0.4772)\right]R$$

$$= 1.0726\ R; \tag{61}$$

then for $N_{\phi\ min'}$ $r = R_t + r_o = (1.0726 + 0.152)\ R = 1.2246\ R.$ (62)

Therefore,

$$N_{\phi\ min'} = \frac{pr}{2}\left(1 + \frac{1.0726}{1.2246}\right)$$

$$= 0.939\ pr \text{ versus } pr. \tag{63}$$

For $N_{\phi\ max'}$ $r = R_t - r_o \sin\phi = (1.0726 - 0.0726)R = R.$ (64)

Therefore,

$$N_{\phi\ max} = \frac{pr}{2}(1 + 1.0726)$$

$$= 1.0363\ pr \text{ versus } pr. \tag{65}$$

Thus, the variation on the assumed N_ϕ force is only + 3.63 to - 6.1 percent.

Estimated Deformed Shape - Consider points 3 and 3' and between them the distance $\ell_{33'}$ (see Figure 22) given from geometry and the preceding equations:

$$\ell_{33'} = r\cos\phi - r_2 + r_3$$

$$= \frac{1}{2}(r_1 + r_2 - r_3) - r_2 + r_3$$

$$= \frac{1}{2}(0.2667\ R) - 0.1333\ R + 0.0667\ R$$

$$= 0.0667\ R. \tag{66}$$

Consider the movement of point 3' due to the applied drag, which is assumed to be given by the first two terms of Equation 23, i.e.,

$$D_b = D_{tb} + D_{rb}$$

$$= (3.249 - 0.45)\, p_\infty \pi R^2$$

$$= 2.8 p_\infty \pi R^2$$

$$= (2.8)(3.6)\pi (7.5)^2$$

$$= 1785 \text{ lb.} \qquad (67)$$

Point 3' moves to the left and upward to the position 3" (see Figure 22). The corresponding deflection, Δ, may be conservatively estimated by considering the drag as a concentrated line load applied to point 3' and using the analysis of Appendix C.

The applied load, P, of Appendix C thus is equal to:

$$P = \frac{D_b}{2\pi(R + r + r \sin \phi)}$$

$$= \frac{2.8\, p_\infty \pi R^2}{2\pi R\left[1 + 0.152\ (1 + 0.4772)\right]}$$

$$= 1.142\, p_\infty R$$

$$= (1.142)(3.6)\frac{7.5}{12}$$

$$= 2.57 \text{ lb/in.} \qquad (68)$$

The internal pressure, undeformed radius, and central angle are, respectively,

$$p = C_{pi}\, q$$

$$= (3)\left(\frac{40}{144}\right)$$

$$= 0.834 \text{ psi,} \qquad (69)$$

$$R_o = 0.152\ R$$

$$= (0.152)(7.5)(12)$$

$$= 13.68 \text{ in., and} \tag{70}$$

$$\alpha_o = 90 - \phi$$

$$= 90 - 28.5$$

$$= 61.5 \text{ deg;}$$

$$2 \sin \alpha_o = 1.75754. \tag{71}$$

Then, by substituting into Equations C-17 and C-18,

$$\alpha_1 = 180 - 118.5\ X, \text{ and}$$

$$\alpha_2 = 180 - 118.5\ Y.$$

A trial and error solution of Equations C-19 and C-20 yields X = 0.945 and Y = 1.05; therefore, X/Y = 0.9.

Then α_1 = 68 deg 10.5 min, $\sin \alpha_1 = 0.92832$, $\cos \alpha_1 = 0.37177$,

α_2 = 55 deg 34.5 min, $\sin \alpha_2 = 0.82487$, $\cos \alpha_2 = 0.56523$,

ω_1 = 1 deg 12 min, $\sin \omega_1 = 0.020942$, $\cos \omega_1 = 0.999781$,

ω_2 = 1 deg 20 min, $\sin \omega_2 = 0.023269$, and $\cos \omega_2 = 0.999729$.

Substitution of these values into Equations C-1 through C-9 of Appendix C yields the remaining unknowns and provides a check of the solution:

$$r_1 = \frac{\pi - \alpha_o}{\pi - \alpha_1}\ r_o$$

$$= \frac{180 - 61.5}{180 - 68.175}\ (13.68)$$

$$= 14.5 \text{ in.,} \tag{72}$$

$$r_2 = \frac{\pi - \alpha_o}{\pi - \alpha_2}\ r_o$$

$$= \frac{118.5}{180 - 55.575}\ (13.68) = 13 \text{ in.} \tag{73}$$

$$F_1 = pr_1$$
$$= (0.834)(14.5)$$
$$= 12.1 \text{ lb/in.}, \quad (74)$$
$$F_2 = pr_2$$
$$= (0.834)(13)$$
$$= 10.85 \text{ lb/in.} \quad (75)$$

Therefore, the solution checks as follows: $F_1 \sin \omega_1 = F_2 \sin \omega_2$, or

$$(12.1)(0.02094) = (10.85)(0.023296)$$
$$0.2534 = 0.2525.$$

Finally, the deflection is given by:

$$\Delta = r_1 \left[\sin (\alpha_1 - \omega_1) - \sin \omega_1\right] - r_o \sin \alpha_o$$
$$= 14.5 \text{ (sin 66 deg 58.5 min - 0.020942) - (13.68)(0.877882)}$$
$$= (14.5)(0.920334 - 0.020942) - 12.022$$
$$= 13.041 - 12.022 = 1.019 \text{ in.},$$

or

$$\Delta = r_o \sin \alpha_o - r_2 \left[\sin (\alpha_2 + \omega_2) + \sin \omega_2\right]$$
$$= 12.022 - 13 \left[\sin 56 \text{ deg } 54.5 \text{ min} + 0.02369\right]$$
$$= 12.022 - (13)(0.837799 + 0.023269)$$
$$= 12.022 - 11.194$$
$$= 0.828 \text{ in.}$$

Since this work is only an estimate of the deflection, no further trials are warranted and the above discrepancy in Δ will be accepted with an average value of $\Delta = 0.92$ in. Then,

$$\frac{\Delta}{R} = \frac{0.92}{(7.5)(12)} = 0.0102 \quad (76)$$

Comparing Equation 76 with the distance ℓ_{33}, as given by Equation 66 indicates that the deflected burble fence will lie closer to the pressure stable shape than it will to the tailored shape.

(d) Fabric Stresses

Margin of Safety - As mentioned previously, a 2-to-1 stress ratio exists in the burble fence for all practical purposes. The bias fabric of the burble fence then will tend to rack or pantograph since it is stable for a 1-to-1

stress ratio. If a restraint to this racking such as that provided by the elastomer is neglected, the fabric deforms to a new bias angle that is the hose angle, 54 deg 44 min. This is seen easily from the statics of a two-thread-set system subjected to the 2-to-1 stress ratio as shown in Figure 23. In Figure 23,

$$\frac{\sigma_Y}{\sigma_X} = 2 \; . \tag{77}$$

By statics, in the X direction:

$$2\sigma_B \sin^2 \phi = \sigma_Y, \tag{78}$$

and in the Y direction:

$$2\sigma_B \cos^2 \phi = \sigma_X. \tag{79}$$

Dividing Equation 78 by Equation 79 and equating to Equation 77 gives,

$$\tan^2 \phi = 2;$$

therefore,

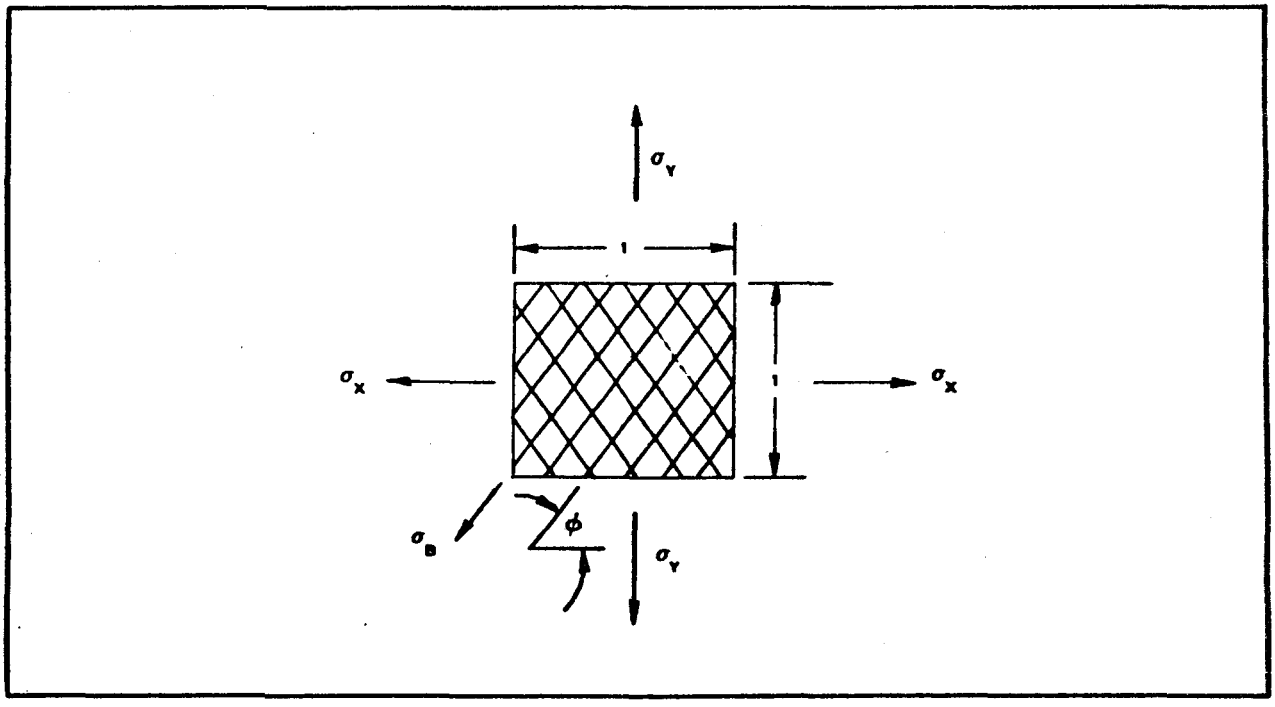

Figure 23 - Statics of Two-Thread Sets Under a 2-to-1 Stress Ratio on the Bias

$$\phi = \tan^{-1}\sqrt{2}$$

$$= 54 \text{ deg } 44 \text{ min.} \quad (80)$$

Then,

$$\sigma_B = \frac{\sigma_Y}{2\sin^2\phi} = \frac{\sigma_X}{2\cos^2\phi} = \frac{\sigma_Y}{2(0.8165)^2} = \frac{\sigma_X}{2(0.5774)^2}$$

$$= \frac{\sigma_Y}{1.236} = \frac{X}{0.668} \quad (81)$$

Now, σ_Y corresponds to the meridian stress in the burble fence, N_ϕ. The three maximum values of the stress that may be considered are:

1. On the tailored shape,

$$N_\phi = pr_1 = (0.833)(0.2)(90) = 15 \text{ lb/in.},$$

2. On the pressure stable shape (Equation 57),

$$N_\phi = 11.4 \text{ lb/in., and}$$

3. On the estimated deformed shape (Equation 74),

$$N_\phi = 12.1 \text{ lb/in.}$$

Taking the largest of these values and substituting into Equation 81 gives a fabric stress of

$$\sigma_B = \frac{N_\phi}{1.236} = \frac{15}{1.236} = 12.15 \text{ lb/in.}$$

The fabric of the burble fence is the same as that of the BALLUTE. The margin of safety then is:

$$\text{M.S.} = \frac{F_u}{N\sigma_B} - 1 = \frac{80}{(2.25)(12.15)} - 1 = +1.92.$$

BALLUTE and Fence Seams - Both the BALLUTE and fence seams are conservatively considered by applying the maximum meridional burble fence stress as a severe peel loading on the seam as shown in Figure 24.

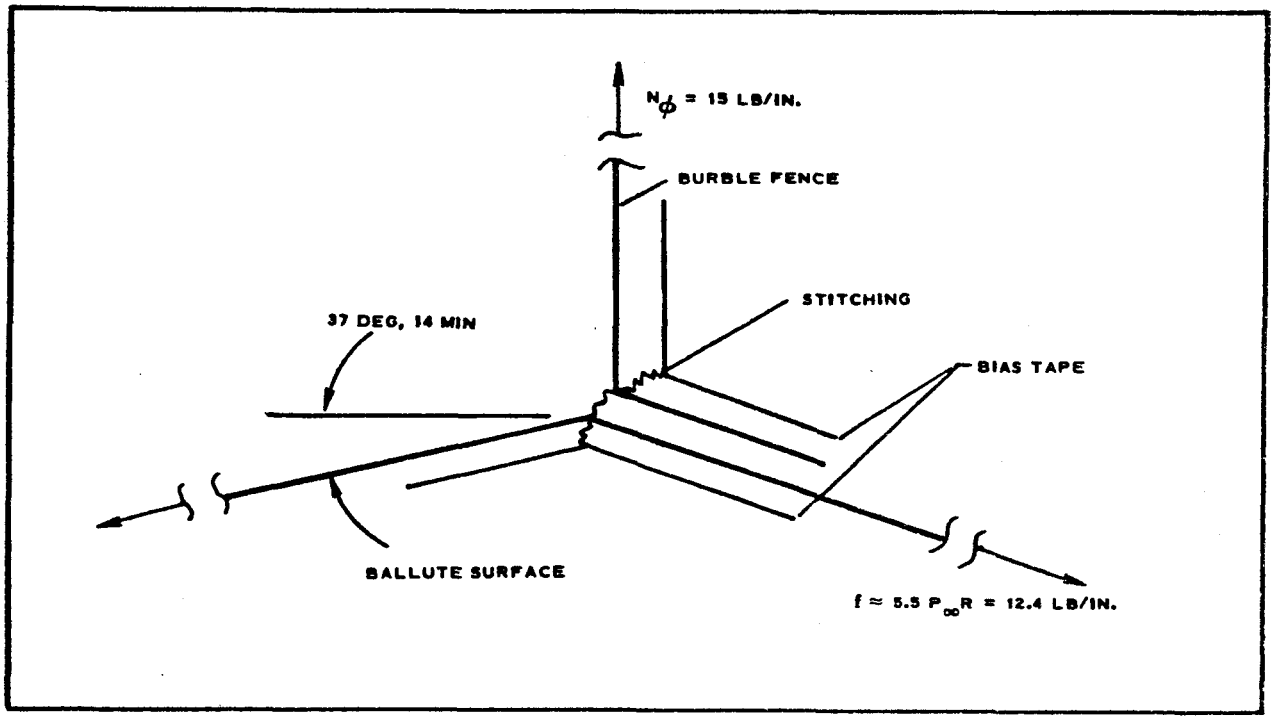

Figure 24 - BALLUTE Burble Fence Seam

In Figure 24, the fabric stress at the equator in the BALLUTE is used to determine the angle of 37 deg 14 min from statics of the uniaxial loading (see Table VIII). Because this stress level is somewhat low and a biaxial stress condition actually exists, the local deformation of the BALLUTE under these seams will not be as great as indicated in Figure 24.

BALLUTE Inlets - Each inlet is approximated by a segment of a circular torus as shown in Figure 25. The pressure in the inlet is equal to the internal pressure in the BALLUTE; the pressure around the outside of the inlet is conservatively assumed to be zero (gage). The principal stresses then are given from the shell theory:[8]

$$N_\phi = \frac{pr_c}{2} , \tag{82}$$

$$N_\phi = \frac{pr_c}{2}\left(1 + \frac{R}{r}\right) . \tag{83}$$

TABLE VIII - FABRIC STRESSES, SHEAR STRESSES, AND MERIDIAN TENSIONS

$\frac{X}{R}$	$\frac{N_\phi}{p_\infty R}$	$\left(\frac{N_\phi}{p_\infty R}\right)\left(\frac{R}{\rho_1}\right)$	$\frac{p}{p_\infty} - \left(\frac{N_\phi}{p_\infty R}\right)\left(\frac{R}{\rho_1}\right)$	$\frac{f}{p_\infty R}$	$\frac{N_\phi - f}{p_\infty R}$	$\frac{nT_m}{p_\infty R^2}$	$\Delta\frac{nT_m}{p_\infty R^2}$	$\frac{nf_s}{p_\infty R}$
0.0	. . .	. . .	. . .	0.0	. . .	40.0	. . .	. . .
0.05	121.0	-54.5	84.7	5.03	116.0	36.5	4.6	24.8
0.1	63.1	-26.0	55.9	6.81	56.3	35.4	2.4	13.7
0.15	44.3	-14.4	43.8	8.2	36.1	34.1	3.2	19.1
0.2	35.1	-8.82	37.47	9.5	25.6	32.2	3.8	23.4
0.25	30.0	-5.61	33.21	10.7	19.3	30.3	2.8	17.6
0.3	26.8	-3.4	28.6	11.15	15.6	29.4	0.6	3.8
0.35	24.5	-1.76	24.01	11.0	13.5	29.7	1.2	7.7
0.4	22.8	-0.381	22.18	11.6	11.2	28.2	4.0	25.9
0.45	21.5	0.93	20.97	12.38	9.1	25.7	4.3	27.8
0.5	20.5	2.35	19.75	12.9	7.6	23.9	2.9	18.6
0.55	19.8	3.77	18.58	13.2	6.6	22.8	2.0	12.7
0.6	19.2	5.18	17.52	13.38	5.8	21.9	1.6	9.9
0.65	18.7	6.57	16.68	13.53	5.2	21.2	1.7	10.2
0.7	18.3	7.96	15.99	13.65	4.6	20.2	1.9	10.9
0.75	17.9	9.4	15.5	13.79	4.1	19.3	2.1	11.3
0.8	17.6	10.85	15.25	14.0	3.6	18.1	2.7	13.3
0.85	17.3	12.7	15.05	14.18	3.1	16.6	5.1	22.0
0.9	17.2	13.65	15.45	14.85	2.3	13.0	-6.1	-21.3
0.95	17.1	15.1	13.55	13.3	3.8	22.7	-23.4	-71.5
0.98	17.5	16.7	11.65	11.58	5.9	36.4	-43.6	-161.0
0.995	17.9	17.8	7.3	7.29	10.6	66.3	-42.1	-210.0
1.0	18.0	18.0	5.15	5.5	12.5	78.5	. . .	. . .

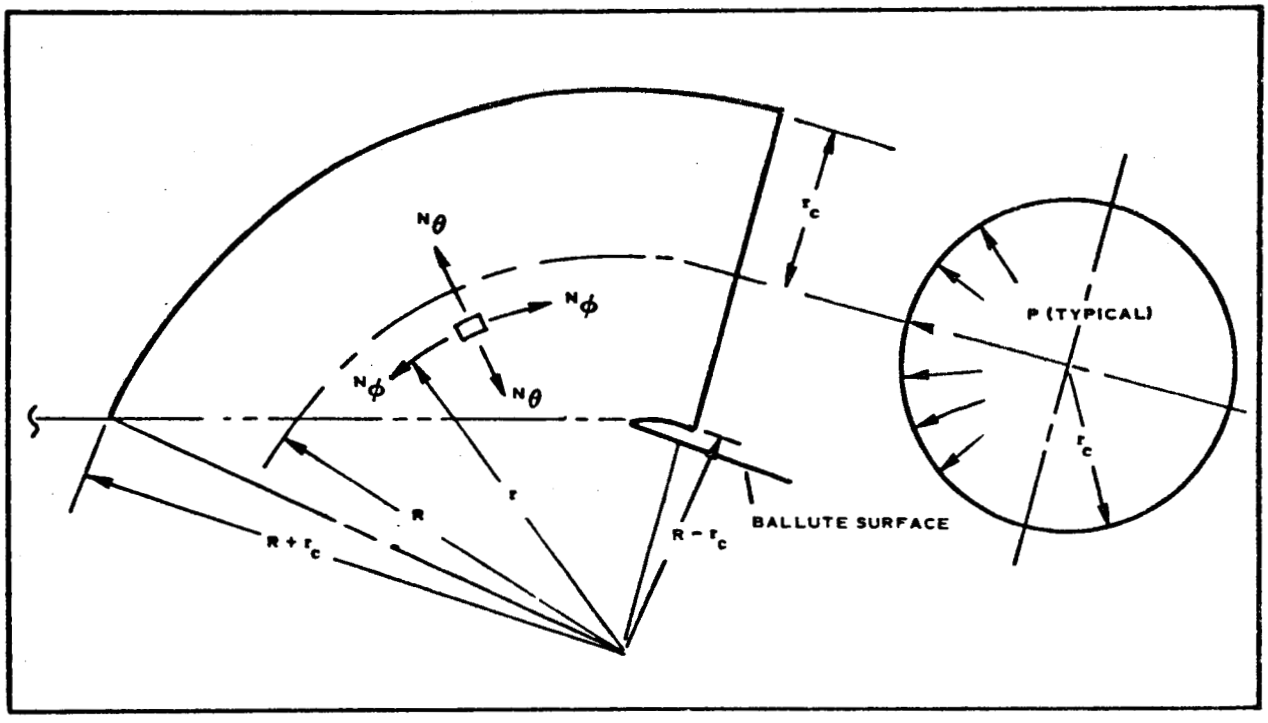

Figure 25 - BALLUTE Inlet

In Equations 82 and 83, the nomenclature of Figure 25 is used. The principal stresses are obtained by substituting the following values;

$$p = C_{pi}q = (3)(40) = 120 \text{ psf} = 0.833 \text{ psi}$$

$$r_c = 5 \text{ in.}$$

$$R = 13.75 \text{ in. (scaled).}$$

The values for r_c and R were taken from Drawing 620A000-002. The maximum fabric stress is given by Equation 83 as

$$N_{\theta \max} = \frac{pr_c}{2}\left(1 + \frac{R}{R - r_c}\right)$$

$$= \frac{(0.833)(5)}{2}\left(1 + \frac{13.75}{8.75}\right)$$

$$= 5.35 \text{ lb/in.}$$

and the margin of safety is:

$$M.S. = \frac{F_u}{NN_{\theta\ max}} - 1$$

$$= \frac{80}{(2.25)(5.35)} - 1$$

$$= +5.65$$

b. Riser and Bridle Assembly

(1) Description

A sketch of the riser and bridle assembly at maximum line stretch and with the deployment bag closed is shown in Figure 26. Sketches of the components are shown in Figures 27 through 31. The webbing of the assembly is composed of three materials: the 750-lb Nomex, 5,500-lb dacron, and 10,000-lb nylon. Load-elongation curves for the latter two materials are shown in Figures 32 and 33. Figure 34 shows the load-elongation curves for 500-lb Nomex that was used as a basis for estimating the properties of 750-lb Nomex, which was not available for testing at this writing.

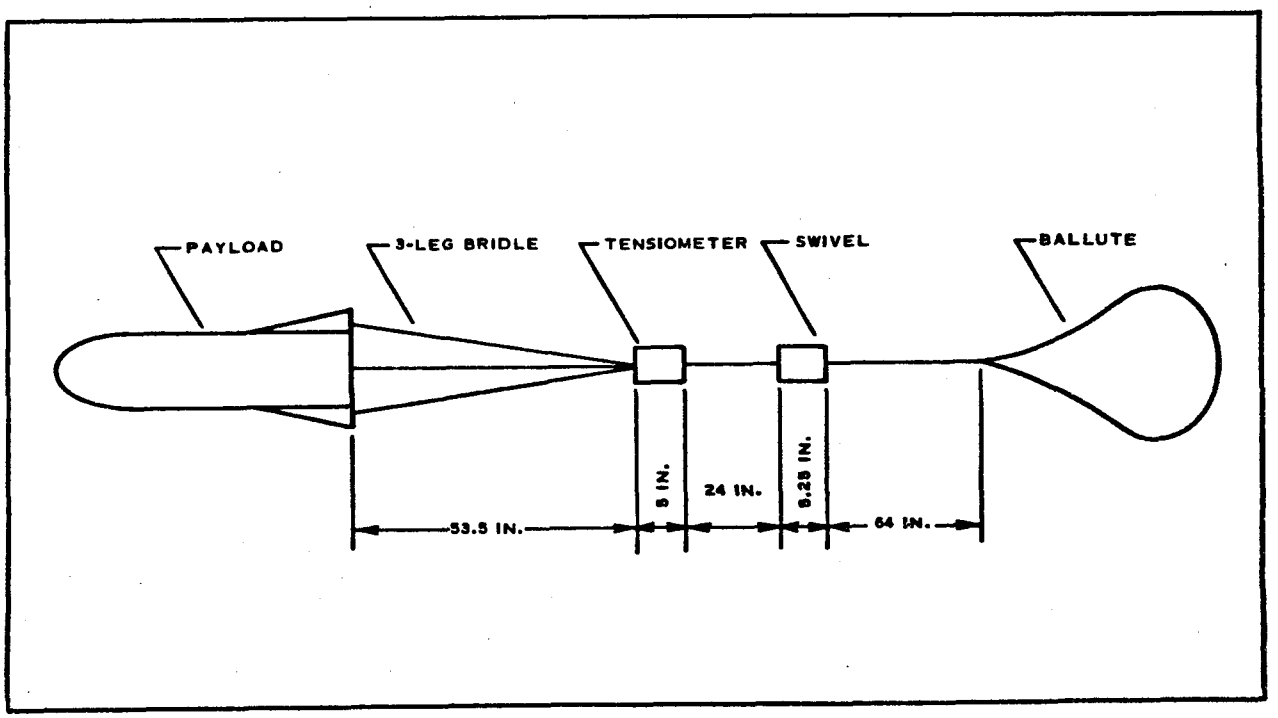

Figure 26 - Riser and Bridle Assembly (Stretched)

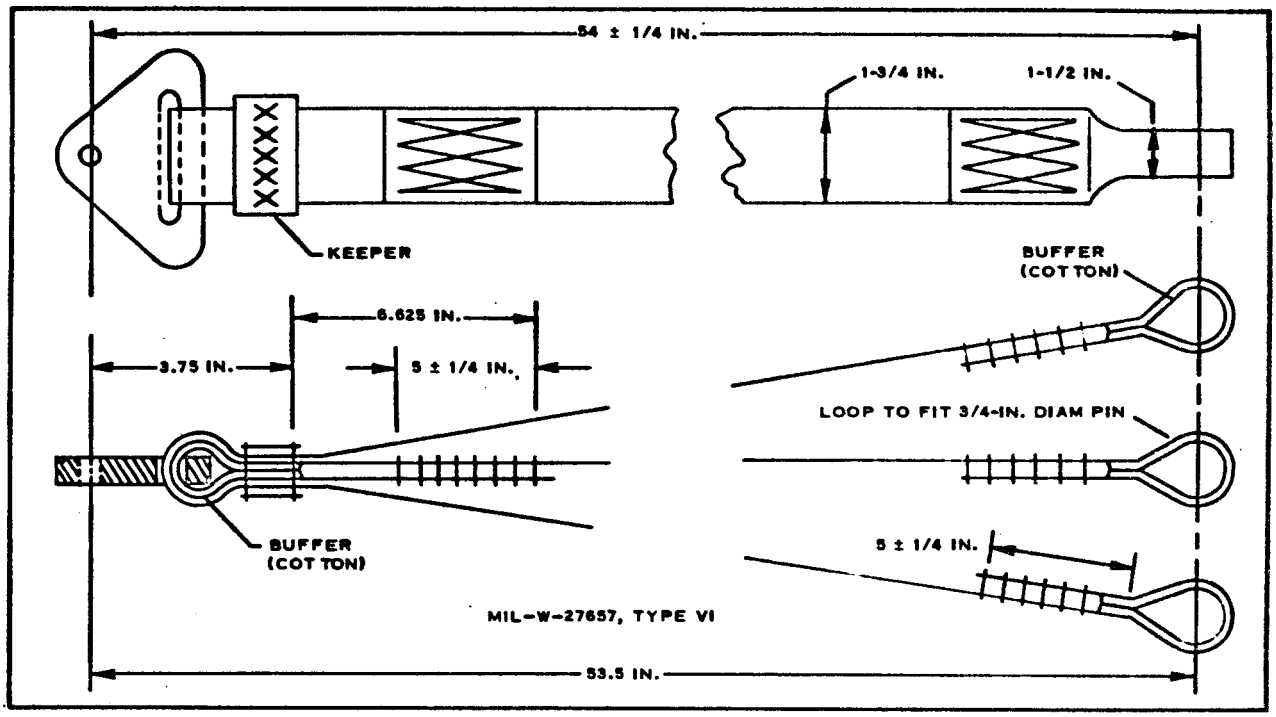

Figure 27 - Three-Leg Bridle

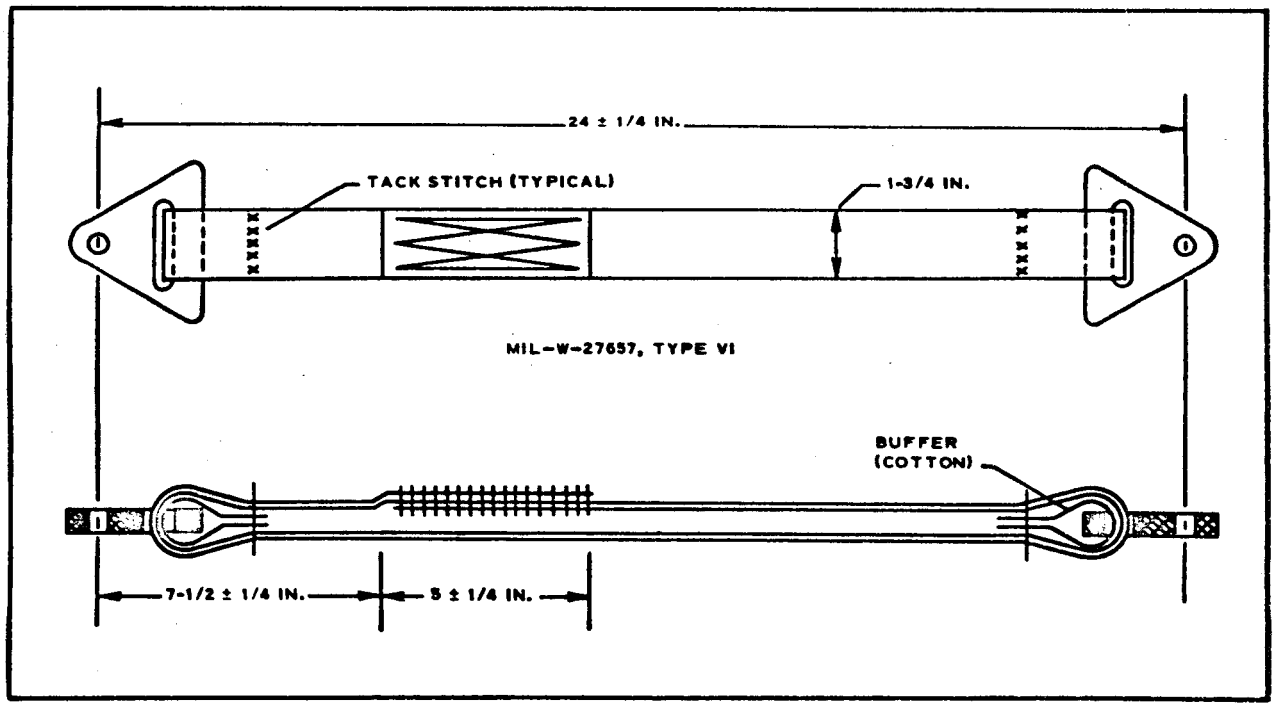

Figure 28 - Intermediate Riser

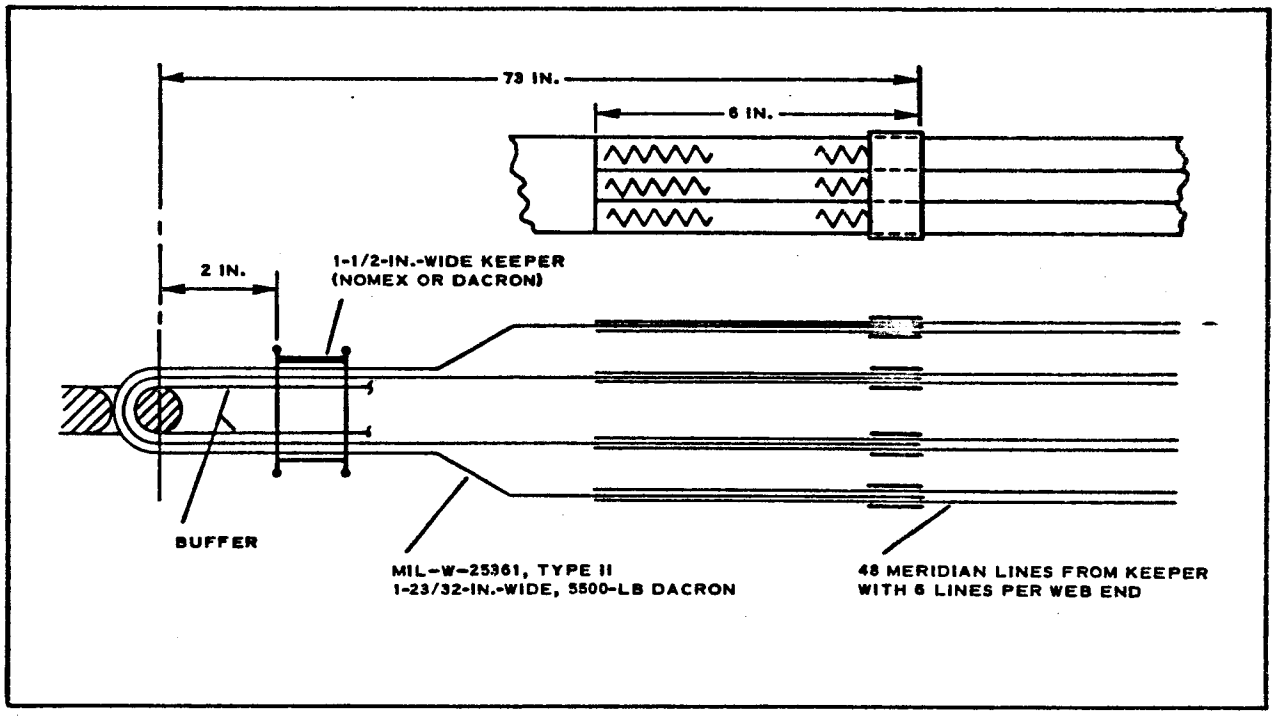

Figure 29 - Cross Section of Riser from BALLUTE to Swivel

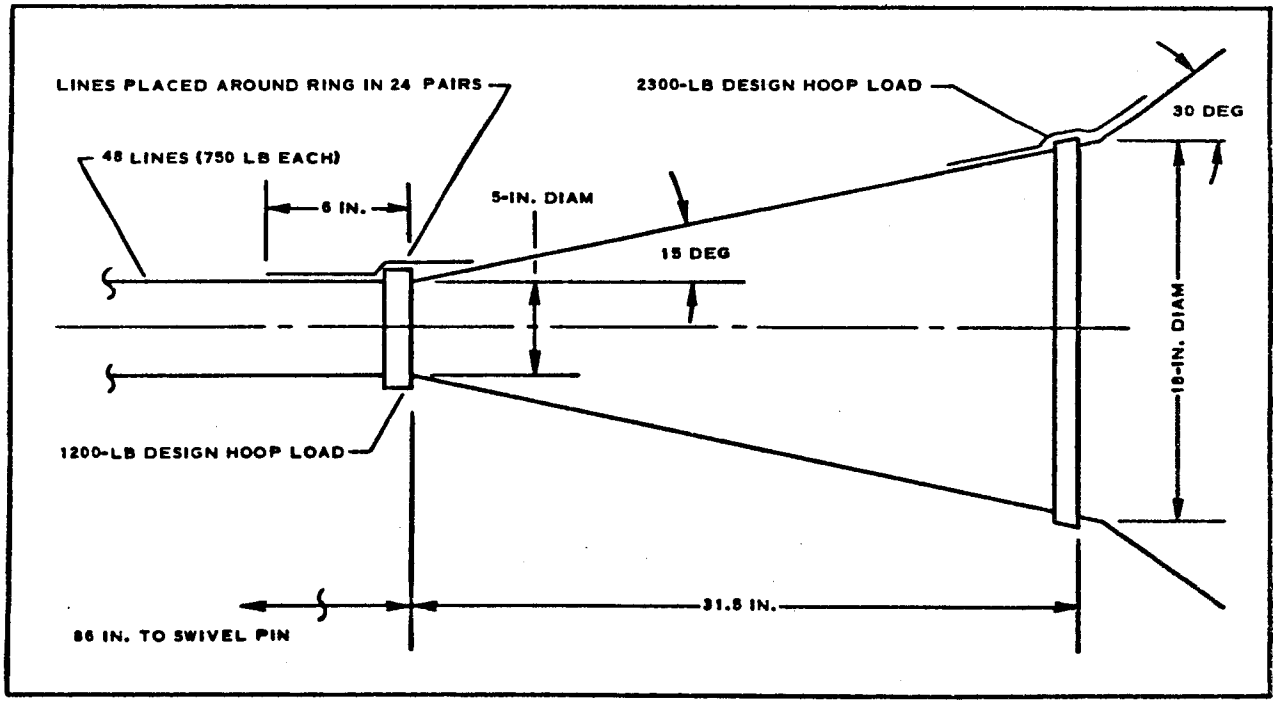

Figure 30 - Keeper Rings at BALLUTE Front

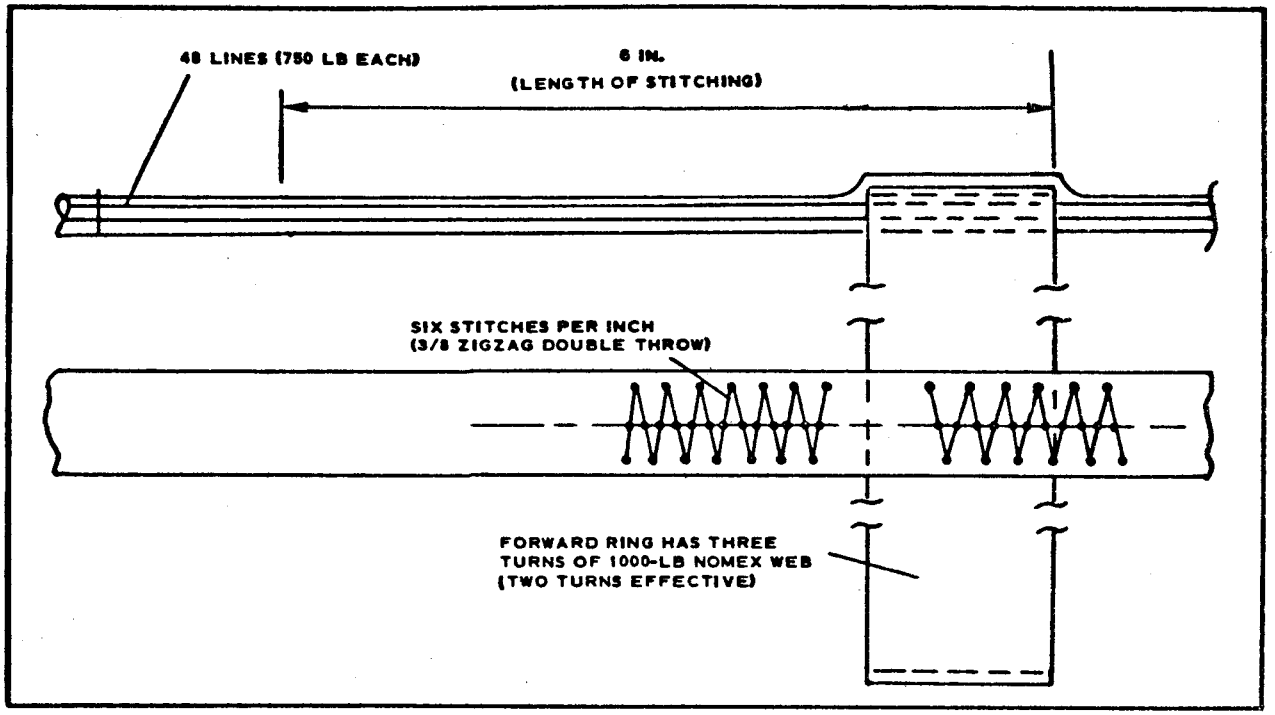

Figure 31 - Forward Keeper Ring

The design conditions, which must be checked, are snatch loads and steady-state drag. The snatch loads occur after the packaged BALLUTE has separated a distance from the payload equal to the length of the riser and bridle lines. The BALLUTE is accelerated to the payload's velocity by the force applied through these lines. The drag is assumed to be constant over the length of the lines and the snatch forces are based on the energy solution given in Reference 2. Since the referenced analysis is for a two-mass system, it may be directly applied by conservatively considering that the mass of the tensiometer is also at the swivel location so that (see Figure 35):

$$m_2 = \frac{W_S + W_T}{g}$$

$$= \frac{1.69 + 1.75}{32.2}$$

$$= 0.107 \text{ slugs.} \qquad (84)$$

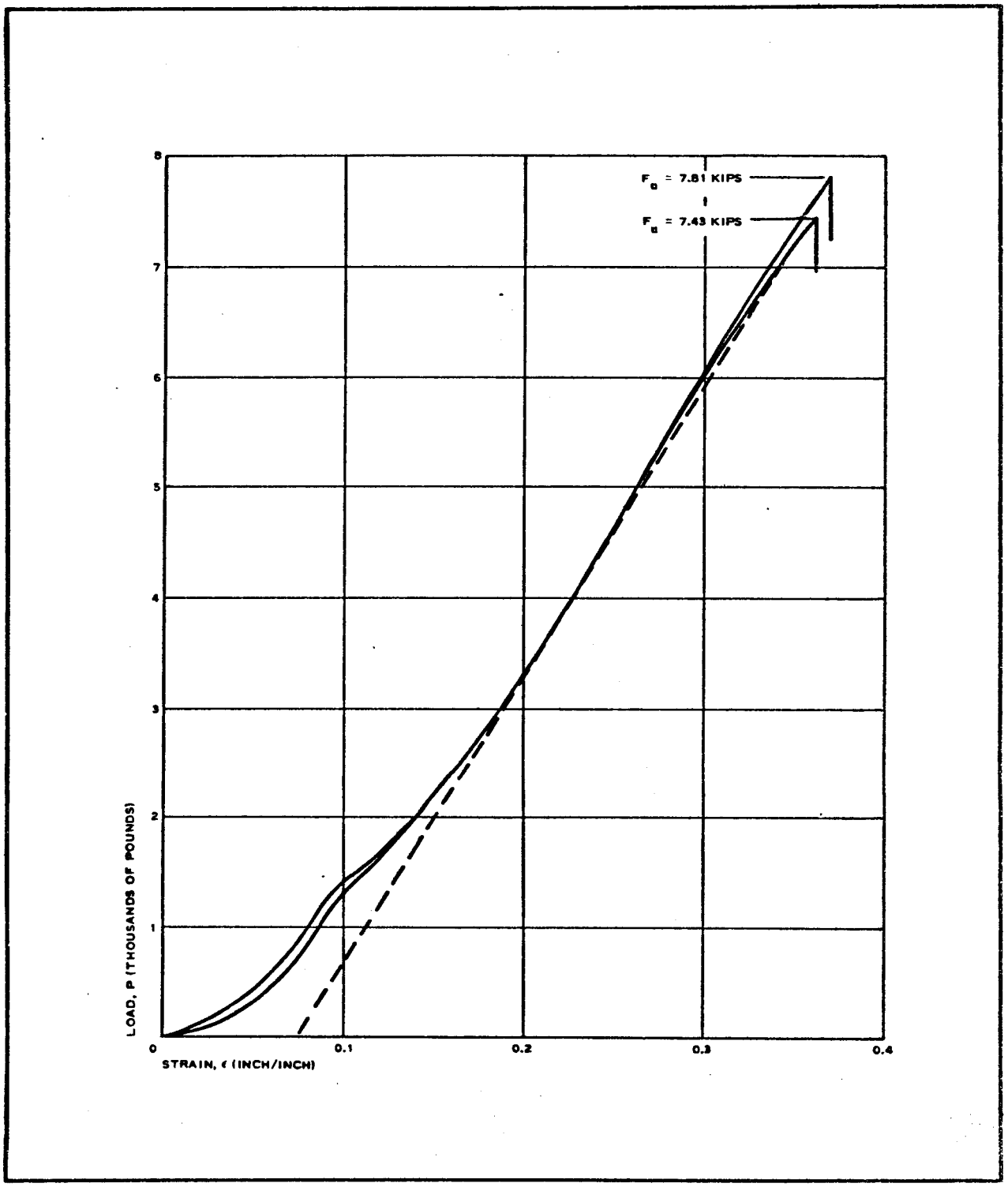

Figure 32 - Load-Strain Relationship of 5500-Lb Dacron Webbing (Two Tests)

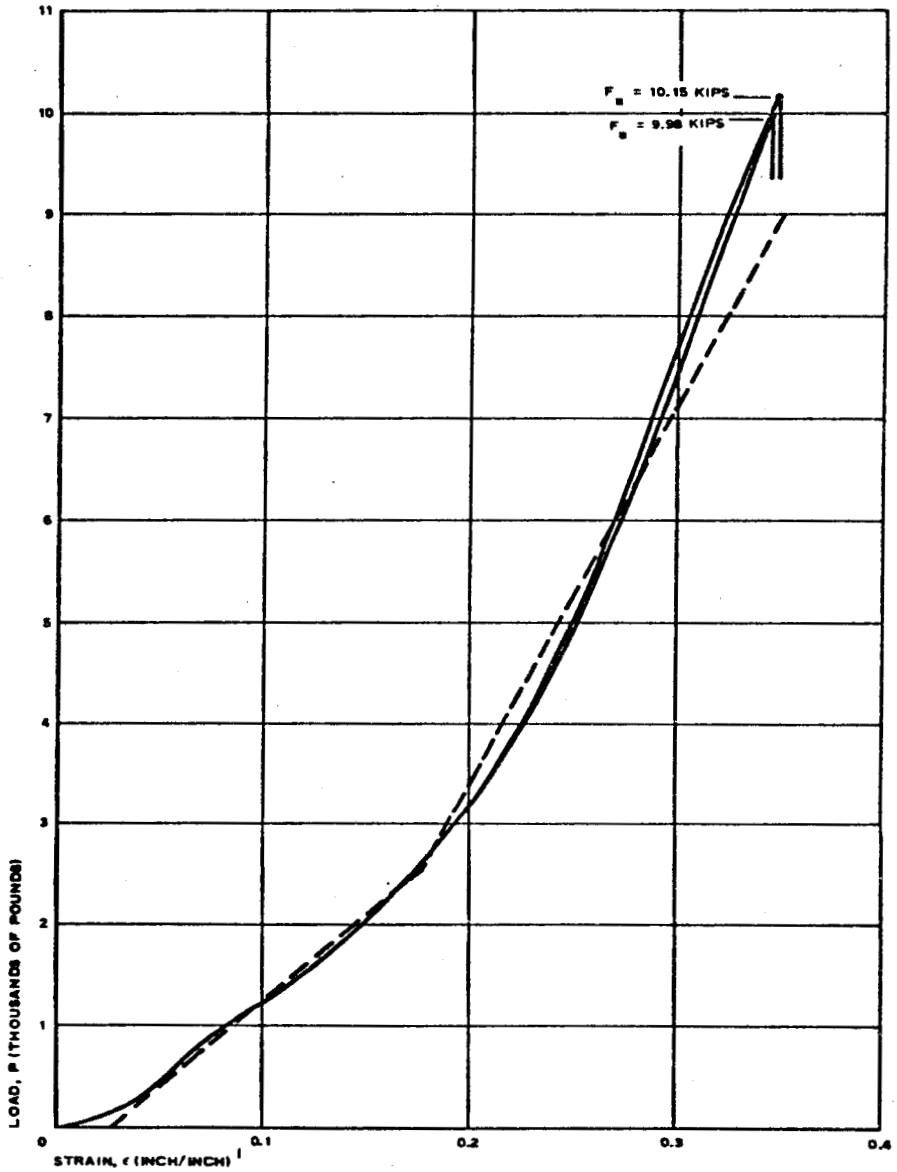

Figure 33 - Load-Strain Relationship of 10,000-Lb Nylon Webbing (Two Tests)

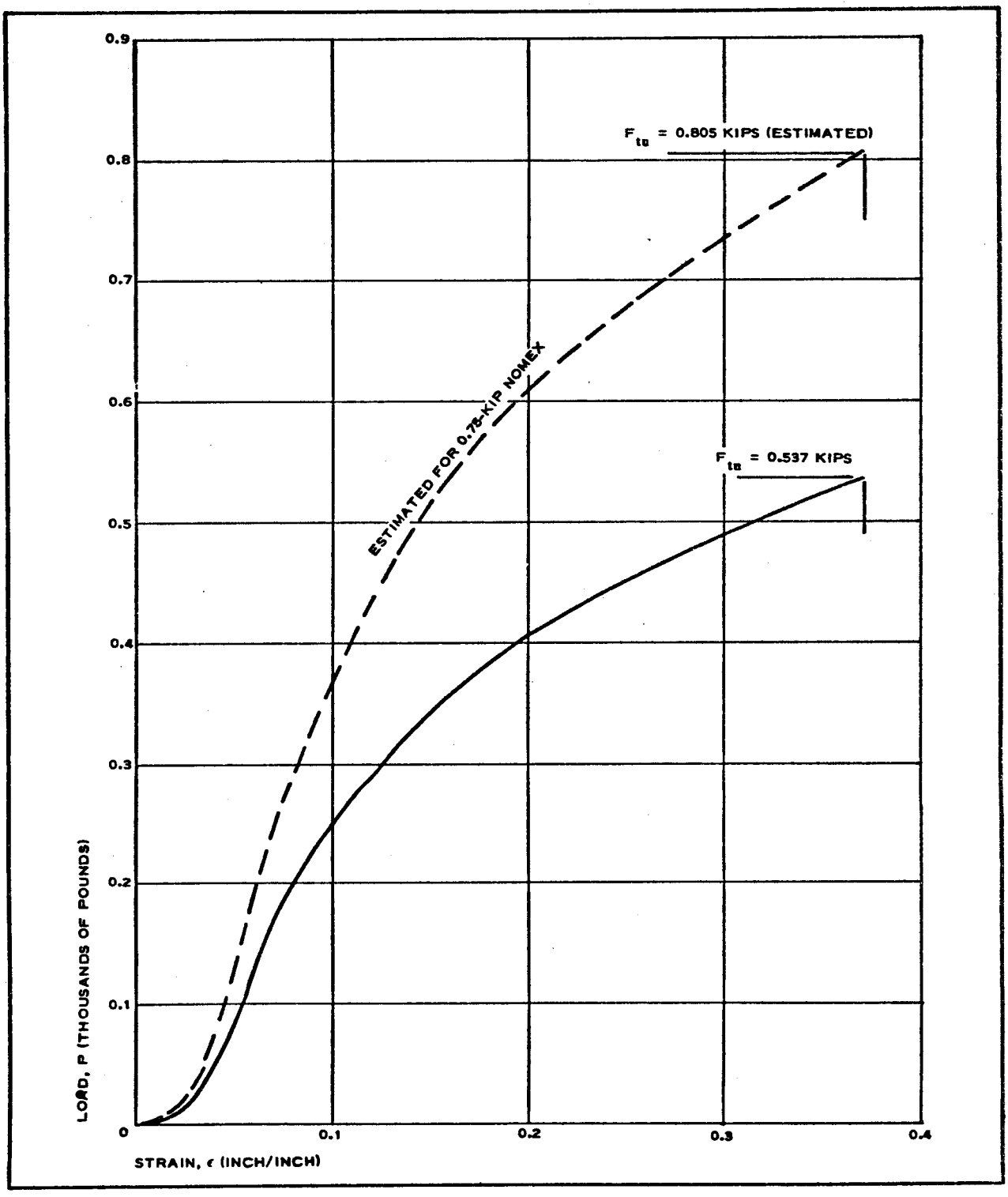

Figure 34 - Load-Strain Relationship of 500-Lb Nomex Webbing (Two Tests)

The mass, m_1, corresponds to the packaged BALLUTE weight that is taken from Appendix B as $W_1 = 43.82$ lb; then,

$$m_1 = \frac{W_1}{g} = \frac{43.82}{32.2} = 1.36 \text{ slugs.} \tag{85}$$

The approach to this analysis is based on the two-mass system of Figure 35. The motion is simple harmonic motion for which the maximum load in the connecting spring is given by Equation IV-16 of Reference 2 as:

$$P_{max} = \frac{E v_o}{\ell \sqrt{\frac{E}{\ell}\left(\frac{1}{m_1} + \frac{1}{m_2}\right)}}. \tag{86}$$

In the problem at hand, the initial velocity is given as $v_o = 120$ fps. The length over which the kinetic energy is absorbed is conservatively taken from Figure 26 as $\ell = 28$ in. Similarly, a conservatively high value for the modulus is used. This is determined by considering Figures 29 and 32. Since the curves of Figure 32 are nonlinear, a linear approximation must be made to use Equation 86. A secant modulus, E, is determined by trial

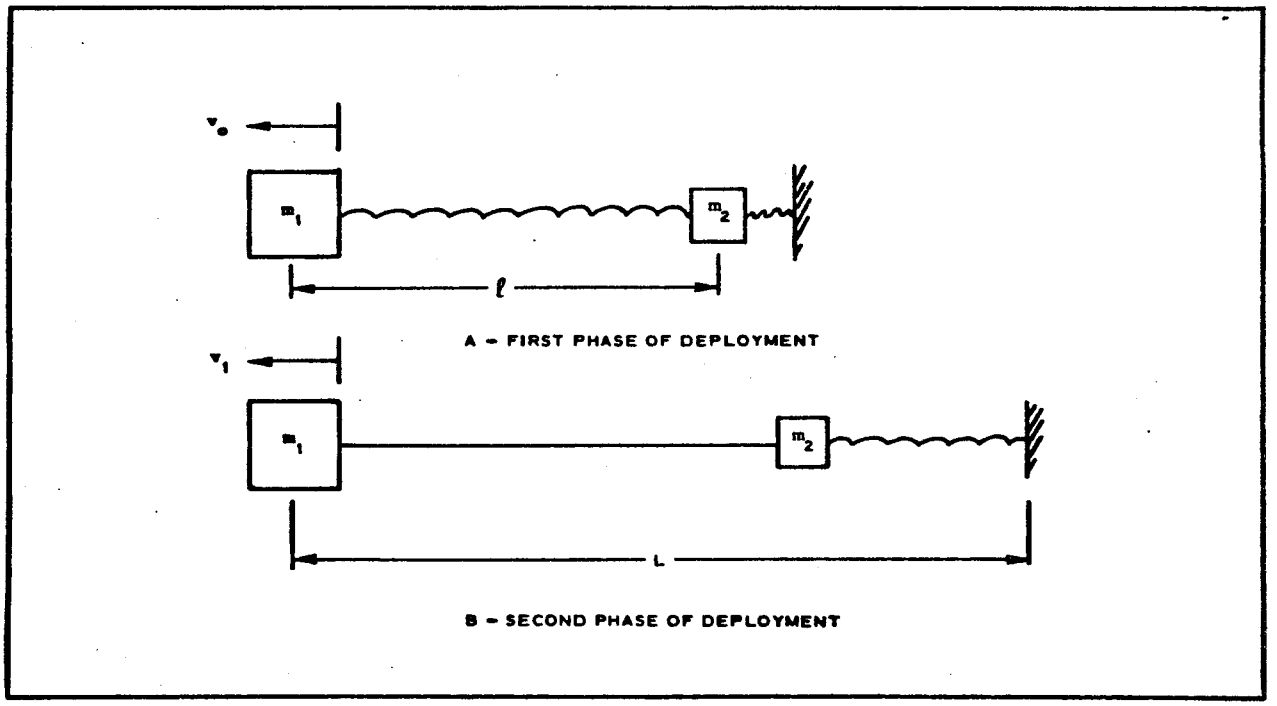

Figure 35 - Schematic of Deployment Previous to Snatch

and error so that the load as given by this modulus (from the curves) agrees with that calculated from Equation 86. The determined value is: E = 4(14.75) = 59 kips. Then, by Equation 86,

$$P_{max} = \frac{120\,E}{\frac{28}{12}\sqrt{\frac{12E}{28}\left(\frac{1}{1.36}+\frac{1}{0.107}\right)}}$$

$$= 24.7\sqrt{E}$$

$$= 24.7\sqrt{59,000}$$

$$= 6 \text{ kips.} \qquad (87)$$

The corresponding strain is:

$$\epsilon = \frac{P_{max}}{E} = \frac{6}{59} = 0.1018 \text{ in./in.} \qquad (88)$$

Since the point determined by $P_{max} = 6/4 = 1.5$ kips and $\epsilon = 0.108$ in./in. lies approximately on the curves of Figure 32, the value of E is considered adequate.

At the instant that the two masses begin to accelerate rearward, they have a common velocity, V_1, which is given by conservation of momentum as:

$$v_1(m_1 + m_2) = v_o m_1; \qquad (89)$$

therefore,

$$v_1 = \frac{m_1 v_o}{m_1 + m_2}$$

$$= \frac{(1.36)(120)}{1.467}$$

$$= 111.1 \text{ fps.}$$

Assuming that the aerodynamic drag acting on the packaged BALLUTE is constant over the length of the riser and bridle line assembly, the kinetic energy at the instant of line stretch is given by:

$$\text{K.E.} = \left(\frac{m_1 + m_2}{2}\right) v_1^2 + DL, \qquad (90)$$

where

$$D = q\,C_D A = (40)(1.5)\frac{\pi}{4}\left(\frac{11}{12}\right)^2 = 39.6 \text{ lb},$$

and, from Figure 26, $L = 53.5 + 5 + 24 + 5.25 + 28 = 115.75$ in. or 6.65 ft; then,

$$\text{K. E.} = \frac{1.467}{2}(111.1)^2 + (39.6)(6.65)$$

$$= 9060 + 264$$

$$= 9324 \text{ ft-lb.}$$

The strain-energy capacity of the riser and bridle line assembly is conservatively estimated on the basis of the straight-line approximations shown in Figure 32 and 33 so that the areas under the straight lines are less than the actual areas under the curves.

(2) Stresses

For the dacron webbing (see Figure 32), the modulus is:

$$E = \frac{7200}{0.35 - 0.075}$$

$$= 26,200 \text{ lb.} \qquad (91)$$

The effective length is taken from Figure 29 as:

$$\ell_e \approx (4)(27) = 108 \text{ in. or } 9 \text{ ft.} \qquad (92)$$

The strain energy for the dacron then is given by

$$(\text{P. E.})_D = \frac{P^2 \ell}{2E} = \frac{9P^2}{2(26200)} = 1.72 \times 10^{-4} P^2. \qquad (93)$$

The two straight lines shown in Figure 33 are used to approximate the curves for the nylon webbing. By letting the subscripts 1 and 2 denote each of these two lines, the moduli are:

$$E_1 = \frac{2500}{0.175 - 0.025} = 16,600 \text{ lb} \qquad (94)$$

and

$$E_2 = \frac{9000 - 2500}{0.35 - 0.175} = 37,100 \text{ lb.} \quad (95)$$

The effective lengths of the bridle and intermediate riser are taken from Figures 27 and 28, respectively, as:

$$\ell_B \approx 3(54 - 3.5) = 151.5 \text{ in. or } 12.6 \text{ ft} \quad (96)$$

and

$$\ell_{IR} \approx 4\left[24 - 2(3.5)\right] = 68 \text{ in. or } 5.6 \text{ ft.} \quad (97)$$

The total effective length, ℓ_e, then is 18.2 ft (12.6 + 5.6 ft). Assuming that the snatch load will be greater than 2500 lb (mortar ejection load is 1450 lb), the strain energy for the nylon is given by:

$$(P.E.)_n = \frac{(2500)^2(18.2)}{2(16600)} + \frac{(2500)(18.2)P}{37100} + \frac{(P - 2500)^2(18.2)}{2(37100)}$$

$$= 2.45 \times 10^{-4} P^2 + \frac{(2500)^2(18.2)}{2}\left(\frac{1}{16600} + \frac{1}{37100}\right)$$

$$= 2.45 \times 10^{-4} P^2 + (625)(9.1)(0.6 + 0.27)$$

$$= 2.45 \times 10^{-4} P^2 + 4590. \quad (98)$$

Adding the strain energy of the dacron and nylon, equating the kinetic energy, and solving for the snatch load, P, gives:

$$(1.72 + 2.45) \times 10^{-4} P^2 + 4950 = 9324, \quad (99)$$

or

$$P^2 = \frac{4374}{4.17} \times 10^4 = 10.5 \times 10^6;$$

then,

$$P = 3.24 \text{ kips.}$$

However, the maximum steady-state drag load from the deployed BALLUTE is larger than either the above snatch load or the load due to deployment of the swivel and tensiometer masses, or:

$$D_{max} = C_d \, q \, A \approx (1)(40)\frac{\pi}{4}(15)^2 = 7,080 \text{ lb.} \quad (100)$$

The ultimate strengths of the components are calculated below using the ultimate strengths from Figures 32, 33, and 34 as multiplied times the corresponding number of webs in each component. A factor of safety, F.S., of 2 is applied along with a fitting factor, F.F., of 1.2 to account for loop strength and plying/splicing efficiency.

The corresponding margins of safety as based on the steady-state maximum drag load given by Equation 100 also were determined for the following items:

1. Bridle (see Figures 27 and 28)

a. $$T_u = \frac{3F_u}{F.F.} = \frac{3(9.98)}{1.2} = 24.9 \text{ kips} \quad (101)$$

b. $$M.S = \frac{T_u}{(F.S.)(D_{max})}\left(\frac{53.5}{54}\right) - 1$$

$$= \frac{24.9}{2(7.08)}(0.99) - 1 = +0.74 \quad (102)$$

2. Intermediate riser (see Figures 28 and 33)

a. $$T_u = \frac{4F_u}{F.F.} = \left(\frac{4}{3}\right)(24.9) = 33.2 \text{ kips} \quad (103)$$

b. $$M.S. = \frac{33.2}{(2)(7.08)} - 1 = 1.33 \quad (104)$$

3. Dacron webs from swivel to meridians (see Figures 29 and 32)

a. $$T_u = \frac{4F_u}{F.F.} = \frac{(4)(7.43)}{1.2} = 24.7 \text{ kips} \quad (105)$$

b. $$M.S. = \frac{24.7}{14.16} - 1 = +0.74 \quad (106)$$

4. Nomex meridians (see Figures 30 and 34), using F_u = 750 lb as guaranteed minimum

a. $$T_u = \frac{48F_u}{F.F.} = \frac{(48)(750)}{1.2} = 30 \text{ kips} \quad (107)$$

b. $$M.S. = \frac{T_u \cos 30 \text{ deg}}{(F.S.)(D_{max})} - 1 = \frac{30}{14.16}(0.866) - 1$$

$$= +0.83 \qquad (108)$$

Increasing the length of the BALLUTE main riser to 73 in. by the specification change will result in greater energy absorption and consequently does not warrant recalculation of the bridle and riser safety margins.

c. List of Structural Symbols

A = area, sq ft

B = one-half the gore width, ft

C = length along the center of a gore, ft

C_D = drag coefficient

C_{pi} = internal pressure coefficient

D = drag, lb

E = secant modulus of elasticity, lb

$F.F.$ = fitting factor

$F.S.$ = factor of safety

F_u = ultimate steady-state fabric stress, lb/ft

F'_u = ultimate flag-snapping fabric stress, lb/ft

f = fabric stress, lb/in.

f_s = fabric to meridian shear stress, lb/in.

g = number of deployment g's

j = denotes particular cross seam for reference

K = meridian load factor

K_f = fabric strength-weight ratio, ft

K.E. = kinetic energy, ft-lb

k_m = meridian strength-weight ratio, ft

ℓ = length, ft

M.S. = margin of safety

M_∞ = mach number

m = number of laps in a meridian seam

m_c = number of laps in a circumferential seam

N = design factor

N_ϕ, N_r = meridian membrane forces, lb/in.

N_θ = circumferential membrane force, lb/in.

n = number of meridians

n_{bm} = number of meridian seams of the burble fence

n_g = number of gores

P = load, lb

p = differential pressure, psf

P.E. = strain energy, ft-lb

p_i = internal pressure (gage), psf

p_o = external pressure, psf

p_∞ = ambient pressure, psf

q = dynamic pressure, psf

R = equatorial BALLUTE radius, ft

R.T. = room temperature, F

r, r_1, r_2, r_3 = radii of the burble fence cross section, in.

T = temperature, F

T_m = meridian tension, lb

T_u = ultimate steady-state meridian load, lb

T'_u = ultimate deployment shock meridian load, lb

V = volume, cu ft

v_l = velocity, fps

W_p = payload weight, lb

W_s = weight of swivel, lb

W_T = weight of tensiometer, lb

w = width of seam, ft

X = radius to any point on the BALLUTE meridian, ft

x = cartesian coordinate in X direction

Y = coordinate taken parallel to the axis of revolution, ft

y = cartesian coordinate in Y direction

Z = equatorial radius, R, minus the radius to any point on the BALLUTE meridian, X

α = central angles of deformed burble fence, deg

γ = density, oz/sq yd

Δ = deflection of the burble fence, in.

Δ_s = elemental arc length, ft

θ_b = angle that defines burble fence location, deg

ρ_1, ρ_2 = meridional and circumferential principal radii of curvature, respectively, ft

σ_B, σ_X, σ_Y = stresses in the bias fabric, lb/in.

ϕ = angle defining the slope of the meridian profile, deg

ω = angle defining burble fence deflection, deg

Subscripts

B = BALLUTE

b = burble fence

c = circumferential

e = effective

f = fabric

m = meridian

o = initial

p = payload

r = rear

s = bias splices

t = front

θ = circumferential direction

ϕ = meridional direction

∞ = free stream

SECTION VI - THERMAL ANALYSIS

1. SUMMARY

A thermal analysis of the BALLUTE was conducted to determine the maximum temperature that the fabric may sustain from aerodynamic heating. The design conditions for the BALLUTE flight test were outlined in Section II. Trajectory calculations based upon these conditions indicated that after deployment, the combined payload/BALLUTE system decelerates rapidly from an initial Mach number of four during transit in the upward phase of the trajectory. The maximum temperature of the fabric was predicted to be about 400 F during ascent. Aerodynamic heating during descent was considered to be negligible, since the flight Mach number during descent barely exceeds one. The trajectory calculations also indicated that aerodynamic heating during re-entry apparently would be negligible compared to the heating expected subsequent to deployment.

2. FLOW FIELD

A schematic of the payload/decelerator configuration is shown in Figure 36. To calculate the convective heat transfer coefficient and the heat flux rates at the decelerator surface, the flow field at this surface must be defined. The following type of flow field model was assumed to represent the flow over the decelerator surface.

Upon decelerator deployment and inflation, the airflow ahead of the payload passes through the bow shock which stands off at the nose of the payload, expands over the payload, enters the wake ahead of the decelerator, and then flows over the decelerator. A cylindrical type of viscous wake is assumed to form between the payload and the decelerator as a result of flow interaction between these two vehicles. The viscous wake is assumed to have a diameter equal to the diameter of the payload. The Mach number at the edge of the viscous wake is assumed to be produced by air ahead of the payload being compressed during passage through the bow shock and then expanded to the

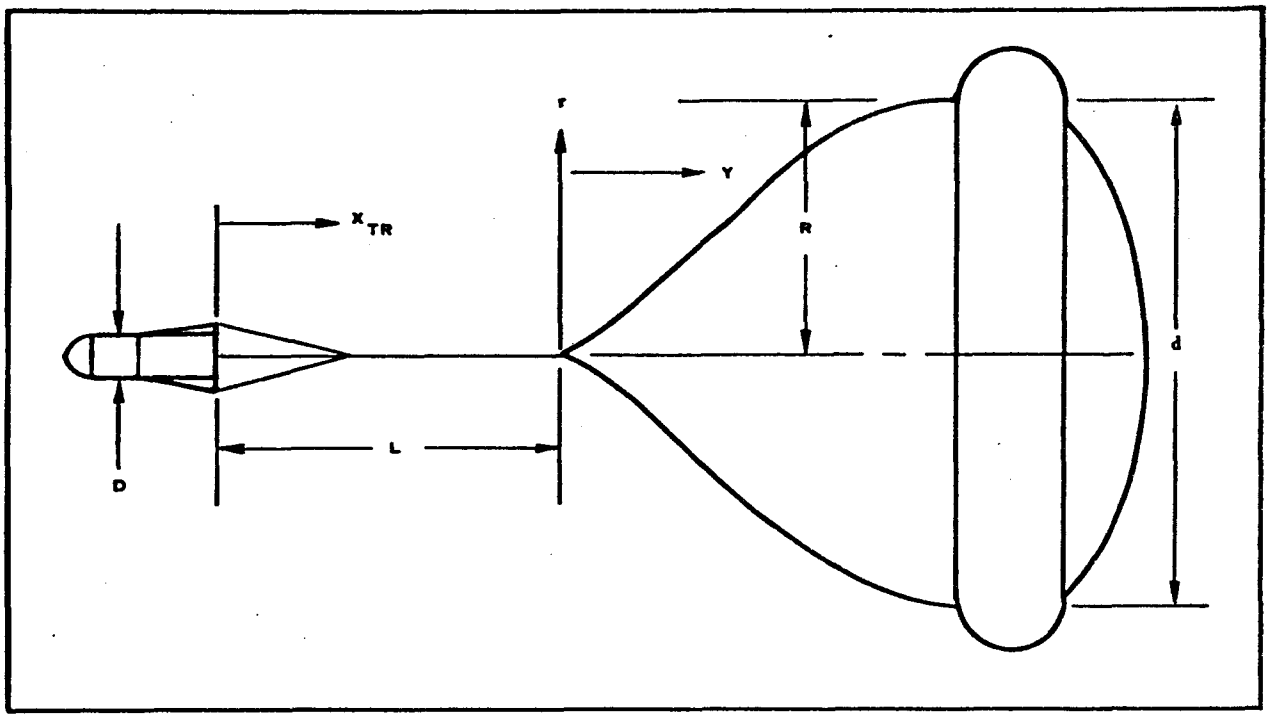

Figure 36 - Parameters of Payload/BALLUTE Configuration

free stream pressure downstream at the edge of the viscous wake. Although normally a velocity gradient exists in this inviscid portion of the wake away from the viscous wake, a constant velocity gradient was assumed to exist whose Mach number was fixed by expanding the compressed air behind the bow shock to a free stream pressure. The pressure at the BALLUTE surface then was calculated on the basis of the tangent cone theory for a cone apex semiangle of 40 deg at the Mach number of the inviscid wake.

Once the flow field at the decelerator surface is defined, the heat transfer coefficient and then the heat flux rates to the surface can be calculated. Since the maximum temperature rise of the decelerator material was of importance in this design study, the analysis was limited to the position on the surface where the maximum heat flux rate occurs. Experimental wind tunnel studies of trailing BALLUTE decelerators, with a d/D ratio much smaller than the design under consideration, indicated that maximum heating should occur at a decelerator location of Y/R = 0.7. Therefore, this station was selected for analysis pending a more exacting definition of the flow field about this large diameter decelerator.

3. ANALYSIS

The calculated cold wall heat flux rates to the surface at Station 0.7 are shown in Figure 37 as a function of time. The re-entry heat flux rates are not shown because of the very low magnitude of the heat flux rates during re-entry. The laminar heat flux rates were calculated using the following relationship:

$$(\dot{q}_{cw}) = 0.332(Re^*)^{-0.5} \rho^* u'(H_1 - h_{cw}) . \quad (109)$$

The turbulent heat flux rates were calculated using the following equation:

$$(\dot{q}_{cw})_t = 0.0296(Re^*)^{-0.2} (Pr)^{-2/3} \rho' u'(H_1 - h_{cw}) . \quad (110)$$

The maximum heat flux rates occur at deployment. While this initial heat flux rate shown in Figure 37 begins with the actual initiation of deployment, the heating rates shown for the incremental time period of deployment are not representative because of the finite time required for the decelerator to inflate.

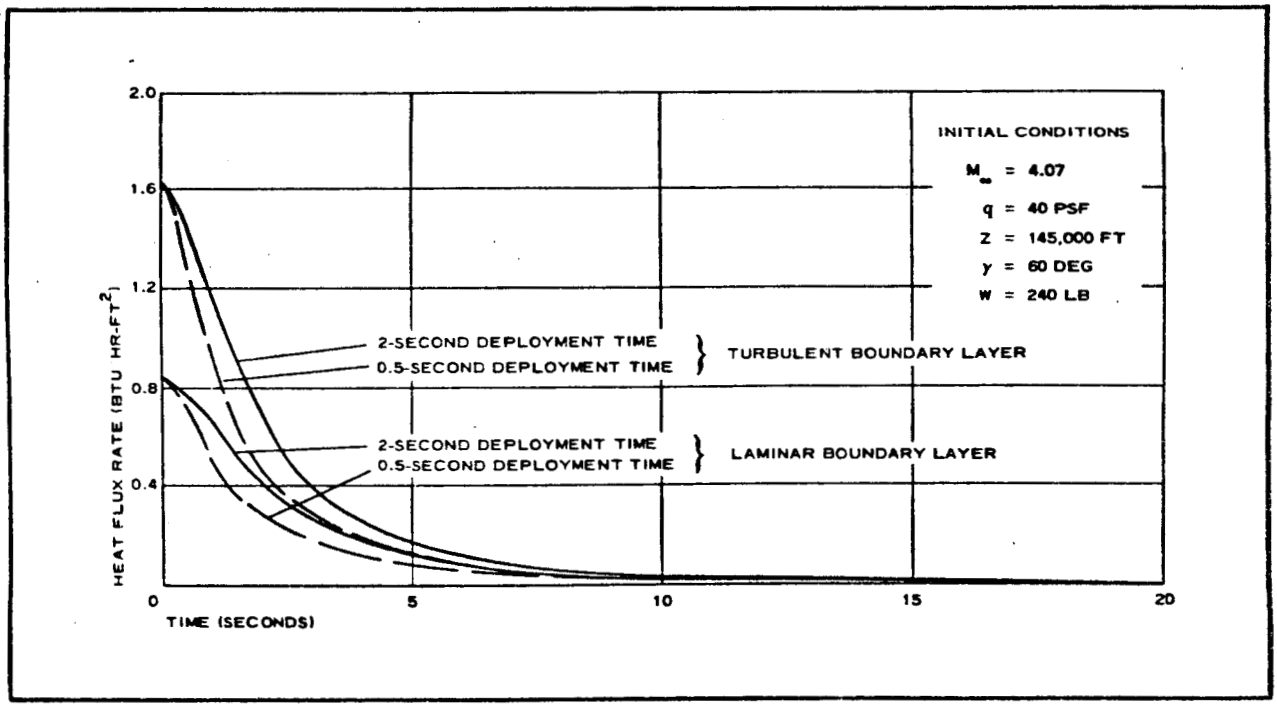

Figure 37 - Cold Wall Heat Flux Rates

In conjunction with the heat flux rate calculations, an attempt was made to estimate the state of wake based upon the unified wake transition criteria.[9] The results of this analysis are shown in Figure 38. Two locations are shown as functions of the upstream Mach number variation. The lower location is for a position one foot aft of the base of the payload, which shows that a free wake should remain laminar at this location. The upper trace is for a location 10 ft aft of the base of the payload, which shows that a free wake may be turbulent near the approximate location of the decelerator. A Reynolds number based on length on the payload indicated that the boundary layer over the payload would be laminar at the time of deployment. The conclusion from the results of this estimate is that the flow over the decelerator may be turbulent and that the turbulent heat flux rates shown in Figure 37 should be used to evaluate the temperature rise in the decelerator fabric.

The fabric temperature as a function of the time from deployment and the turbulent heat flux rate for a two-second deployment time is presented in Figure 39. The adiabatic wall temperature variation is also presented for both estimated deployment times showing the relative magnitude of this driving temperature. The temperature response of the fabric material decelerator was calculated on the basis of transient one-dimensional heat conduction in a slab using the following heat conduction relationships:

1. In a slab

$$\frac{\partial T}{\partial t} = \alpha \frac{\partial^2 T}{\partial y^2} \tag{111}$$

2. At the outer surface

$$h_c(T_{aw} - T_w) - \epsilon \sigma T_w^4 = -k\left\{\frac{\partial}{\partial y}\left[T(0,\ t)\right]\right\} \tag{112}$$

3. At the inner wall

$$\left.\frac{\partial T}{\partial y}\right|_{y = \delta} = 0 \tag{113}$$

The decelerator material was assumed to be Nomex, possessing the following properties:

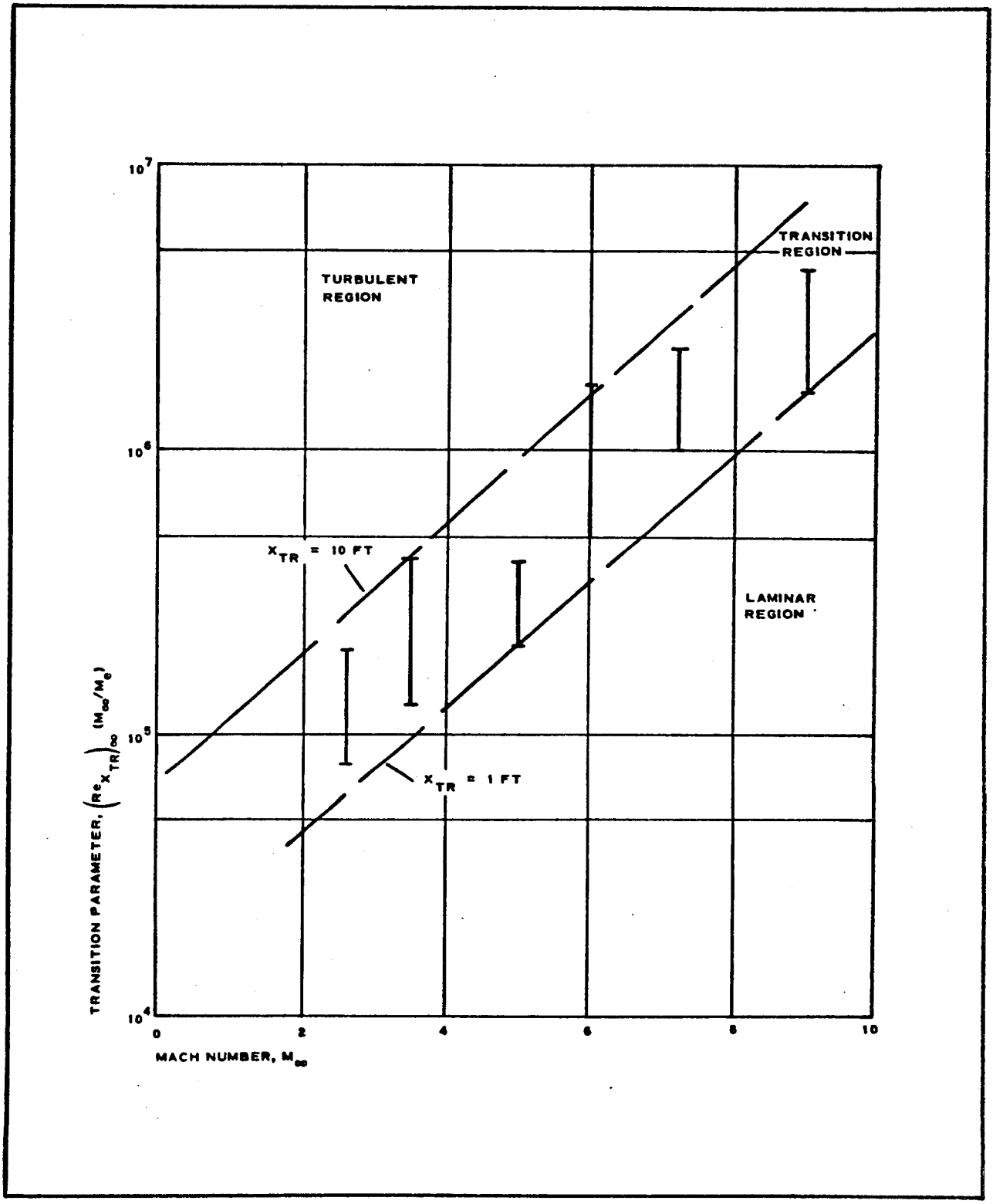

Figure 38 - Unified Wake Transition Correlation

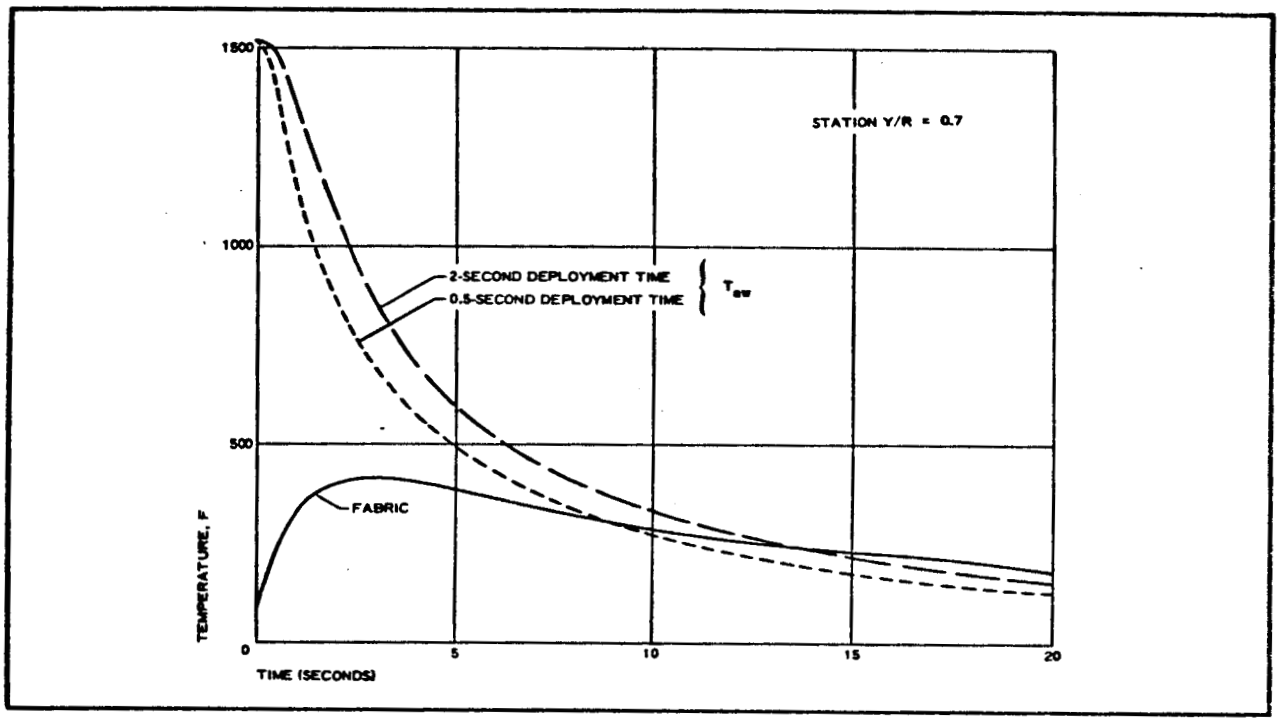

Figure 39 - Temperature History of Fabric

$W/A = 0.01544$ psf or 2.2 oz/sq yd

$\delta = 0.0048$ in.

$k = 0.01$ Btu/hr-ft/F

$c = 0.35$ Btu/lb/F

$\epsilon = 0.8$

4. CONCLUSIONS

The results of the temperature response calculation show a quick rise to about 400 F during the first four seconds of exposure followed by a gradual cooling period as the payload/BALLUTE system continues upward. Since there is a negligible amount of heating during re-entry, no temperature rise in the fabric is expected. The maximum temperature for design purposes may be assumed to be 400 F.

5. LIST OF THERMAL SYMBOLS

A = surface area, sq ft

c = specific heat, Btu/lb/F

d = BALLUTE diameter, ft

D = payload diameter, ft

h_c = convective heat transfer coefficient, Btu/hr/sq ft/F

h_{cw} = cold wall enthalpy, Btu/lb

H_l = total enthalpy, Btu/lb

k = thermal conductivity, Btu/hr/ft/F

L = length, ft

M_∞ = free stream Mach number

Pr = Prandtl number

q = dynamic pressure, psf

$(\dot{q}_{cw})_l$ = laminar cold wall heat flux rate, Btu/sq ft/sec

$(\dot{q}_{cw})_t$ = turbulent cold wall heat flux rate, Btu/sq ft/sec

Re^* = Reynolds number evaluated by using reference enthalpy method

R = radius of BALLUTE, ft

r = local BALLUTE radius, ft

T = temperature, F

T_w = surface temperature, F

T_{aw} = adiabatic wall temperature, F

u' = velocity at BALLUTE surface, fps

W = weight, lb

X_{TR} = length from payload base, ft

y = local material depth, ft

Z = altitude, ft

α = thermal diffusivity, sq ft/hr

γ = flight angle with respect to horizontal, deg

δ = total material thickness

ϵ = surface emissivity

ρ' = density at BALLUTE surface, pcf

ρ^* = density of air evaluated using reference enthalpy method, pcf

σ = Stefan-Boltzmann constant, 0.173×10^{-8} Btu/hr/sq ft/R^4

τ = time, sec

SECTION VII - DESIGN VALIDATION AND MATERIAL PROPERTIES

1. SELECTION OF MATERIALS

A lightweight high-strength BALLUTE fabric was selected because an 18-ft-diameter BALLUTE had to be packed into approximately one cubic foot. The sterilization requirement plus the temperature range of the BALLUTE narrowed the basic material selection. Dacron and/or Nomex using silicone, Viton, polyurethane, or Dyna-Therm as the elastomeric coating were considered. The choice of Nomex cloth over dacron was made because the strength-to-weight ratio at the operating temperature was more favorable. Nomex cloth (2.15 oz/sq yd) with a tensile strength of 103.0 lb/in. (warp) and 102 lb/in. (fill) allowed the cloth to be calendered and still meet the strength requirements set by the stress analysis. Calendering reduced the cloth porosity from 19 cfm to less than 2 cfm, also, reducing the coating weight required to reach the desired permeability of 0.02 cu ft/sq ft/min at 0.5 in. of water (using air).

In the selection of an elastomer, polyurethane was eliminated because blocking occurred during the sterilization test cycle when it was packaged above 30 pcf. Dyna-Therm was not as flexible as the other elastomers and cracks occurred when it was rotoflexed for 1000 cycles. Silicones, which were very flexible, did not bond well to the calendered Nomex cloth and were difficult to apply at a weight of less than 1.0 oz/sq yd. Viton appeared to be best suited for this application. After etching the Nomex with a cyanic dip and then machine coating Viton (15 percent solids), the fabric density was 2.6 oz/sq yd. The porosity was less than 0.02 cu ft/sq ft/min at 0.5 in. of water (using air) and more than met the requirements. This low porosity was accomplished with a coating that was less than one mil thick. The meridian tapes also were Nomex. Because of the small selection of Nomex webbings and tapes that were available, special tapes had to be woven to meet the requirements of Goodyear Aerospace. After contacting several mills, one agreed to weave a pattern that would be 9/16-in. wide and have a breaking strength of 750 lb. The inlet cords were another problem. To meet delivery schedules, Goodyear Aerospace developed and braided the

Nomex inlet cord. All other webbing and tape were available from vendors as stock items.

The deployment bag material was dacron and all the reinforcement and webbing was dacron. With a good selection of dacron in the 200- to 300-lb/in. range, a cloth capable of restraining the BALLUTE when packaged for deployment was chosen.

2. SEAMING METHODS

The panel, gore, and inlet seams are identical felled seams (0.56-in. wide), using two rows of Nomex size E thread with 5 to 7 stitches per inch (spi), and one row of E thread with 4 to 6 spi as shown in Figure 40.

The burble fence attachment seams were sewn with a Type 304 zigzag stitch. This stitch was used to allow the bias gore to lobe and still not cause the sewing to fail. Figure 41 shows the burble fence forward attachment seam and Figure 42 shows the burble fence aft attachment seam.

The attachment of the meridian to the riser was accomplished by sewing 12 meridians to each leg of the riser as shown in Figure 43.

3. TEST VALUES FOR MATERIALS

Tables IX through XIX list the physical characteristics of materials used in PEPP. All of the cloth tensile tests were conducted by the raveled strip method. All testing was done at a load rate of 12 ipm, 6-in. gauge length, 5-ipm chart speed, 75 F, and RH = 45 percent, except for the test described in Table XIX where a 1-ipm load rate was used.

The joint between the main riser line and the meridians was tested for 120 hr at 257 F (see Figure 43). After Test 1, the tensile strength of the joint was 5710 lb; after Test 2, 5610 lb.

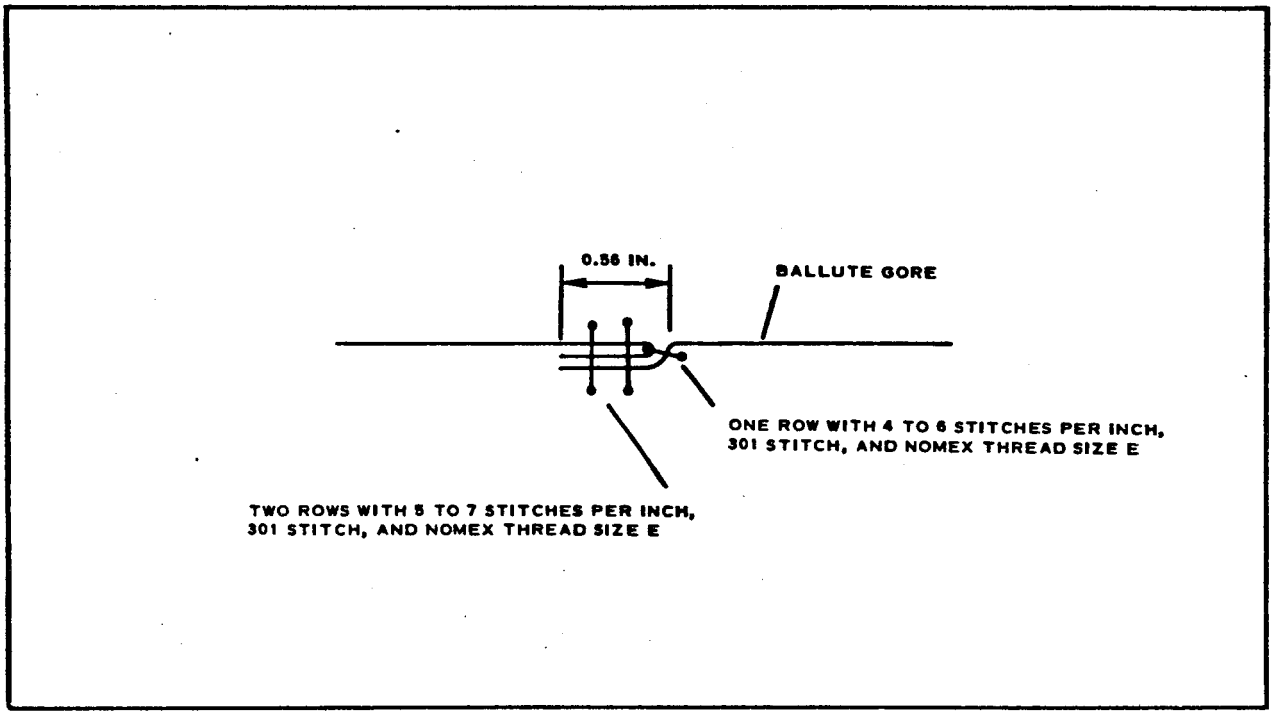

Figure 40 - Panel, Gore, and Inlet Seam

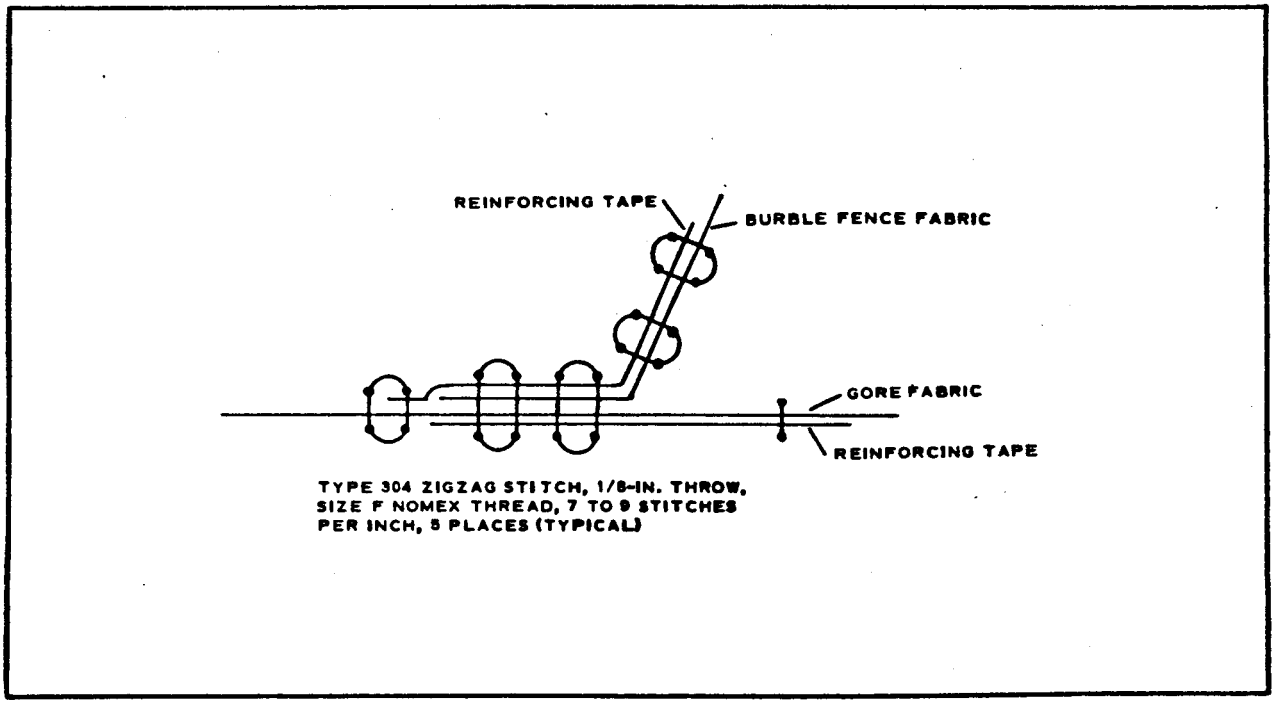

Figure 41 - Forward Burble Fence Seam

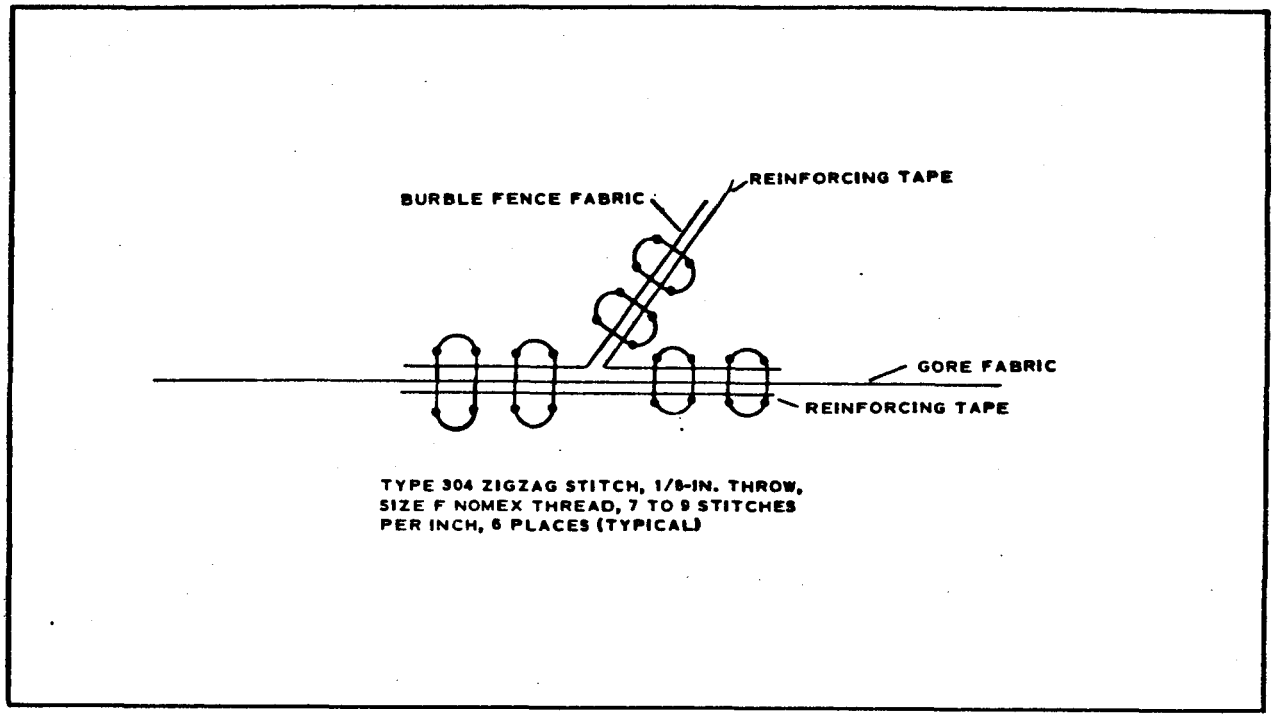

Figure 42 - Aft Burble Fence Seam

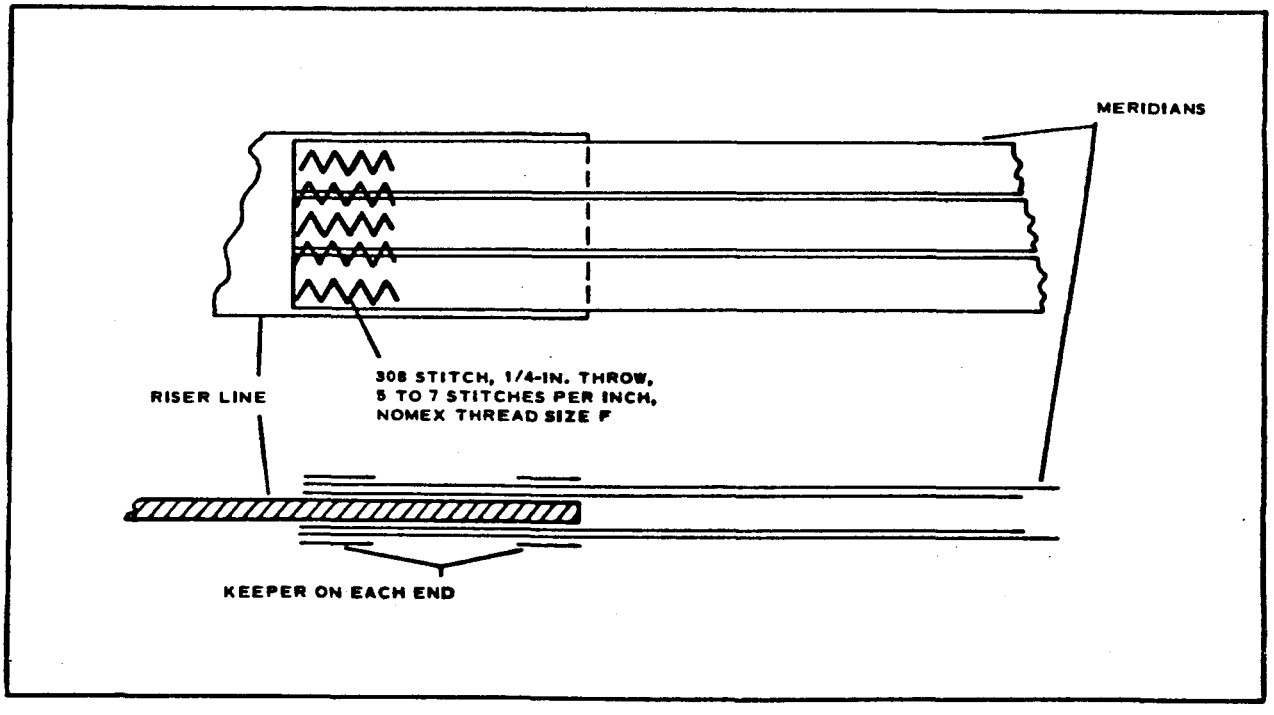

Figure 43 - Attachment of Meridian to Riser

TABLE IX - PHYSICAL CHARACTERISTICS OF HT-101 NOMEX BEFORE COATING

Characteristic	Value
Tensile strength of warp/fill directions (raveled strip method)	97.5*/88.1+ lb/in.
Tear strength	10.4*/8.4 lb+
Elongation	23.8*/23.0+ percent
Porosity	1.83 cfm
Thickness	0.003 mil
Weight	2.15 oz/sq yd
Thread count	80/77

*Warp direction.

+Fill direction.

TABLE X - PHYSICAL CHARACTERISTICS OF HT-101 AFTER COATING WITH VITON CODE NO. GX601V0300

Characteristic	Value
Tensile strength of W/F	99.1/98.9 lb
Tear strength	9.0/7.5 lb
Elongation	27.9/28.0 percent
Porosity	Less than 0.02 cu ft/-sq ft/min at 0.5 H_2O (using air)
Thickness	0.0038 mil
Weight	2.52 oz/sq yd
Thread count	80/80

TABLE XI - PHYSICAL CHARACTERISTICS OF FABRIC AFTER 120 HR AT 257 F

Characteristic	Value
Tensile strength of W/F	102.8/94.0 lb
Tear strength	9.1/7.9 lb
Elongation	28.0/26.0 percent
Porosity	Less than 0.02 cu ft/sq ft/-min at 0.5 H_2O (using air)
Thickness	0.0038 mil
Weight	2.52 oz/sq yd
Thread count	80/80

TABLE XII - TENSILE STRENGTH OF MAIN GORE

Range of values	Strength (lb/in.)
Before sterilization	
High	82.5
Low	79.4
Average	81.4
After 120 hr at 257 F	
High	80.5
Low	73.2
Average	77.7

TABLE XIII - TENSILE STRENGTH OF FORWARD SEAM OF BURBLE FENCE

Range of values	Strength (lb/in.)
Before sterilization	
High	86.7
Low	84.2
Average	85.0
After 120 hr at 257 F	
High	87.7
Low	84.3
Average	85.7

TABLE XIV - TENSILE STRENGTH OF AFT SEAM OF BURBLE FENCE

Range of values	Strength (lb/in.)
Before sterilization	
High	82.0
Low	80.2
Average	81.0
After 120 hr at 257 F	
High	82.1
Low	79.2
Average	80.9

TABLE XV - TENSILE STRENGTH OF MERIDIAN TAPE (PATTERN 1135, 9/16-IN. WIDE)

Range of values	Strength (lb)
Before sterilization	
High	774.0
Low	766.0
Average	770.0
After 120 hr at 257 F	
High	780.0
Low	760.0
Average	776.0

TABLE XVI - TENSILE STRENGTH OF NOMEX BRAIDED CORD

Range of values	Strength (lb)
Before sterilization	
High	369.0
Low	366.0
Average	367.0
After 120 hr at 257 F	
High	370.0
Low	358.0
Average	366.0

TABLE XVII - TENSILE STRENGTH OF DACRON DEPLOYMENT BAG MATERIALS (PATTERN 15292)

Range of values	Strength of W/F (lb/in.)
Before sterilization	
High	395.0/312.0
Low	383.0/302.0
Average	385.8/308.4
After 120 hr at 257 F	
High	398.0/316.0
Low	381.0/297.0
Average	387.6/308.2

TABLE XVIII - TENSILE STRENGTH OF DACRON TAPE (PATTERN 1127, 3/4-IN. WIDE)

Range of values	Strength (lb)
Before sterilization	
High	742.0
Low	731.0
Average	736.5
After 120 hr at 257 F	
High	738.0
Low	722.0
Average	730.6

TABLE XIX - TENSILE STRENGTH OF MAIN RISER LINE DACRON WEBBING (MIL-W-25361, TYPE II)

Range of values	Strength (lb)
Before sterilization	
High	7200
Low	6700
Average	6950
After 120 hr at 257 F	
High	7700
Low	6200
Average	6723

SECTION VIII - DEVELOPMENTAL TESTING

1. INTRODUCTION

Two types of developmental testing were specified in Contract MC 7-709030: helicopter drop testing and vacuum chamber mortar deployment.

2. DROP TESTS

a. Objectives

The objectives of the BALLUTE drop test program were to demonstrate:

1. Separation of the BALLUTE pack and payload
2. Unfolding of the BALLUTE from its deployment bag
3. Self inflation of the BALLUTE by ram-air induction through the eight erectable fabric inlets
4. Terminal velocity characteristics (envelope shape, stability, and apparent drag coefficient)

Two drop tests of the packaged BALLUTE and 206-lb payload were conducted at the NASA Wallops Station on July 26 and 27 of 1967.

b. Description of Test System Components

The drop system (see Figure 44) is comprised of the payload, 4-ft pickup line, 3-leg bridle (54 in. long), 25-ft intermediate riser for the first drop on 26 July 1967, 55-in. riser that is permanently attached to the 18-ft-diam BALLUTE, deployment bag, and 16-ft static line. For the second drop on 27 July 1967, a 12.5-ft intermediate riser was used. Table XX itemizes these components. The BALLUTE was packed in accordance with procedures outlined in a Goodyear Aerospace report.[10]

Shown in Figure 45 is a schematic of the simulated payload, which has an 11.5-in. ID cylinder, 36 in. long. The forward 18 in. of this vehicle is filled with a concrete aggregate to bring the total vehicle weight to 206 lb. The lug at the aft end is provided as a helicopter pickup point. The forward lug is located at the center of gravity and is provided for ground handling. The bridle attachment points are located inside and at the forward end of the

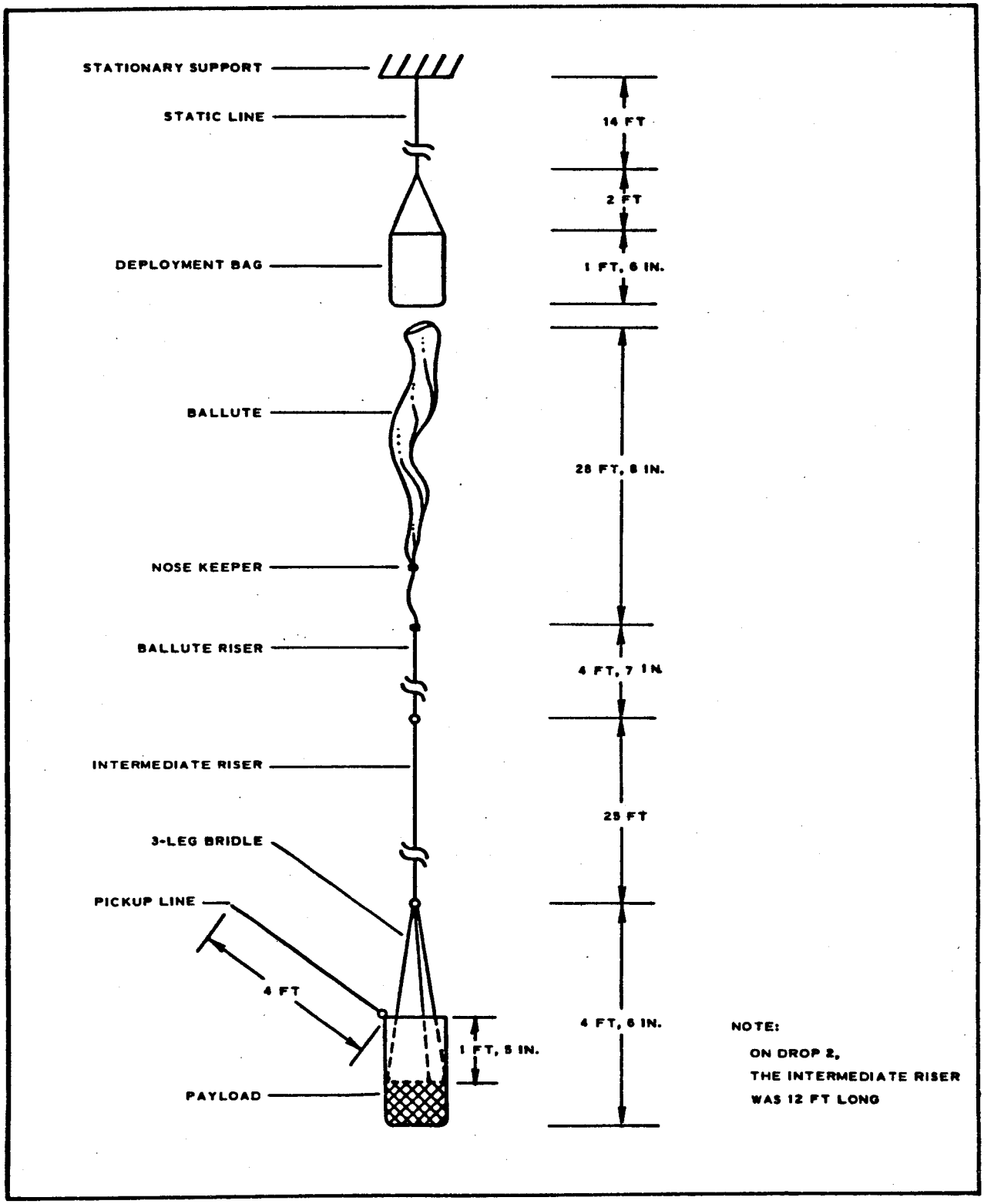

Figure 44 - Configuration of Drop System

TABLE XX - BALLUTE COMPONENTS

Item	Part No.	Quantity
206-lb payload	11.5-in. ID X 36 in.	1
BALLUTE	602A000-002-101	1
Bridle	602A000-004-103	1
Deployment bag	602A000-003-101	1
Intermediate riser	25 ft long	1
Static line	16 ft long	1
Pickup line	4 ft long	1
Connector link	MS22002-4	2

aft 18-in. segment. The packaged BALLUTE and riser were contained in this volume during ascent.

The BALLUTE has a basic body diameter of 15 ft, but the burble fence increases the total diameter to 18 ft (see Figure 46).

c. Pretest Preparation

The three-leg bridle was attached to the three brackets located inside the payload as shown in Figure 47. These brackets then were taped to prevent the nylon webbing from snagging during deployment. In addition, to prevent chafing of the bridle legs during descent, the bridle legs were individually taped in the area adjacent to the aft end of the payload. The intermediate riser was systematically folded and locked as shown in Figure 48. This riser was attached to the three-leg bridle with a connector link (MS 22002-4) and both parts were placed into the payload as shown in Figure 49. The BALLUTE riser was attached to the intermediate riser with a connector link (MS 22002-4). The packaged BALLUTE then was inserted into the payload. The four legs of the static line were tied to the appropriate loops located on the deployment bag with a MIL-C-5040, Type-III web as shown in Figure 50.

The pickup line was attached to the quick release located under the helicopter. The free end of the static line was tied off to a lug located on the side of the hook. To prevent any entanglement of the static line and pickup line resulting from rotation of the payload during ascent, the two were taped together.

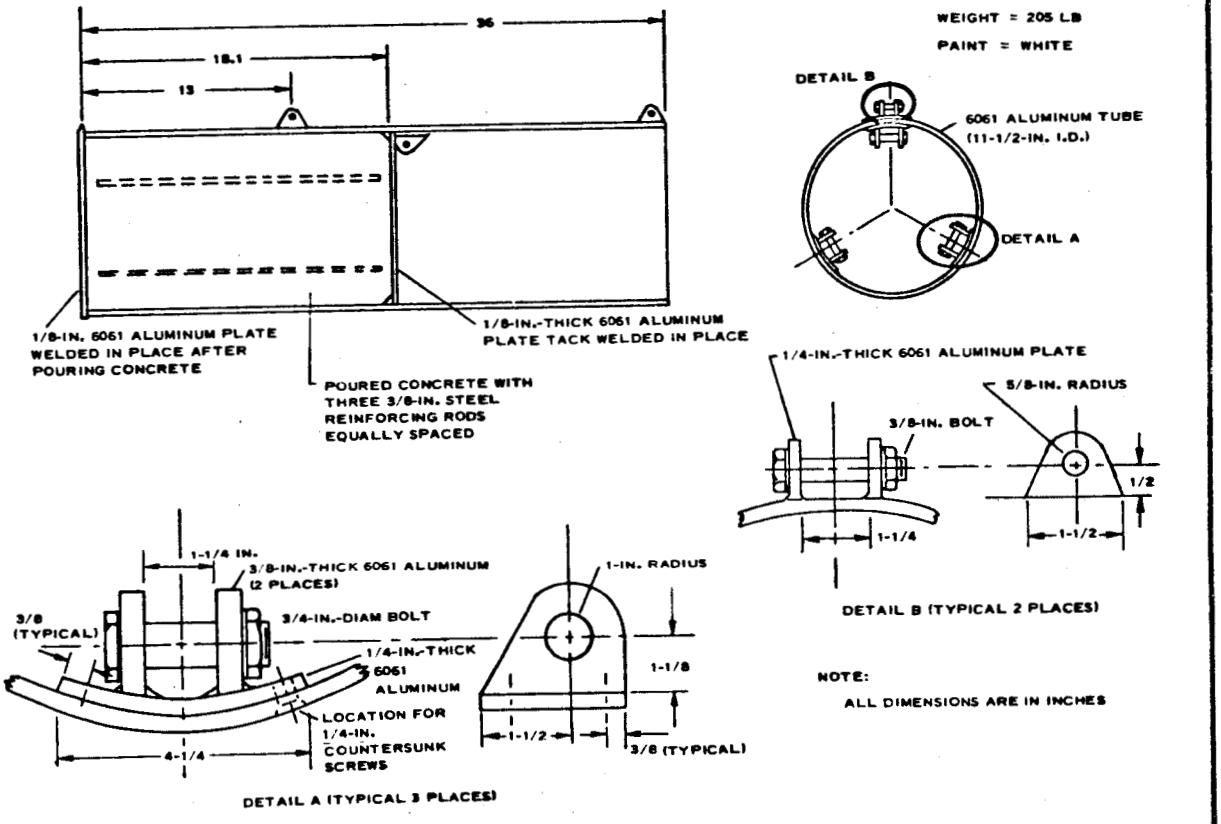

Figure 45 - Simulated PEPP Payload

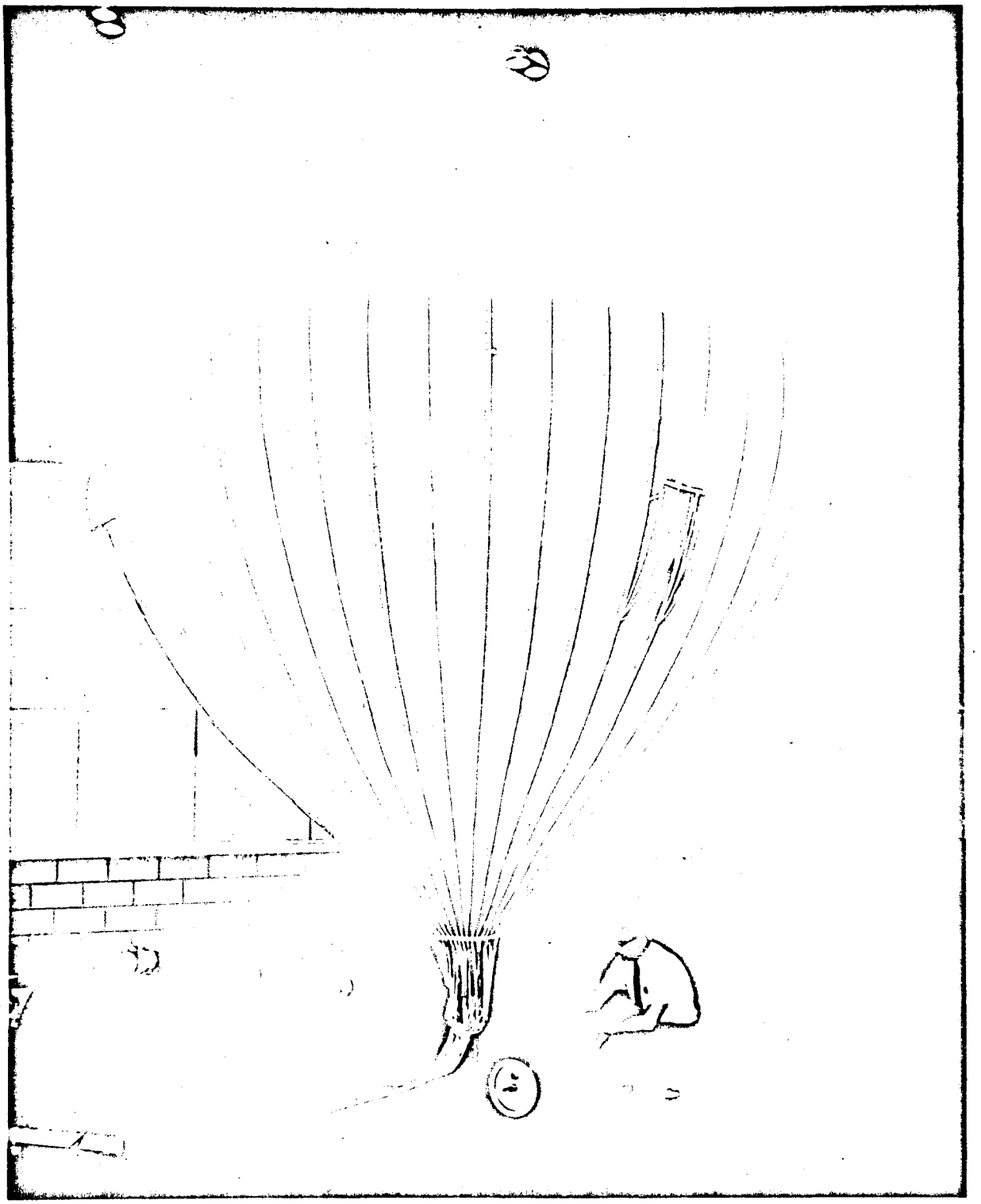

Figure 46 - 18-Ft-Diam BALLUTE

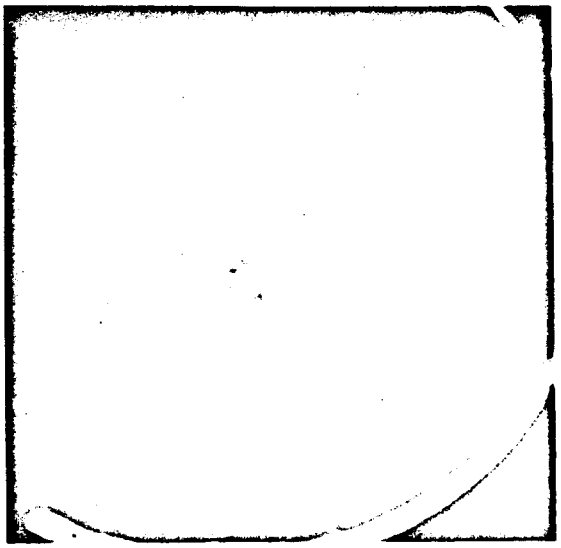

Figure 47 - Brackets inside Payload

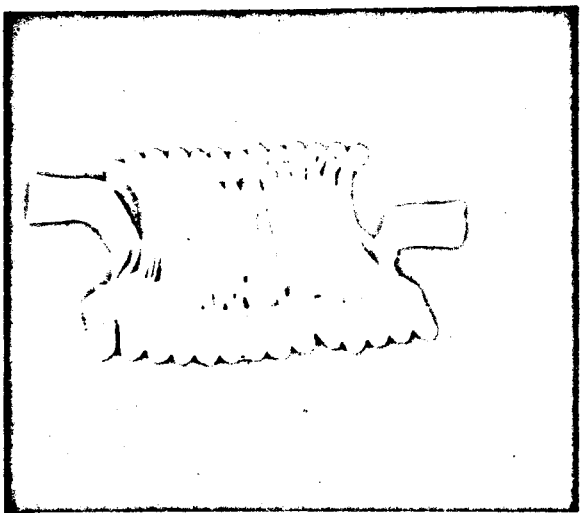

Figure 48 - Intermediate Riser (Folded)

Figure 49 - Placement of Riser and Bridle

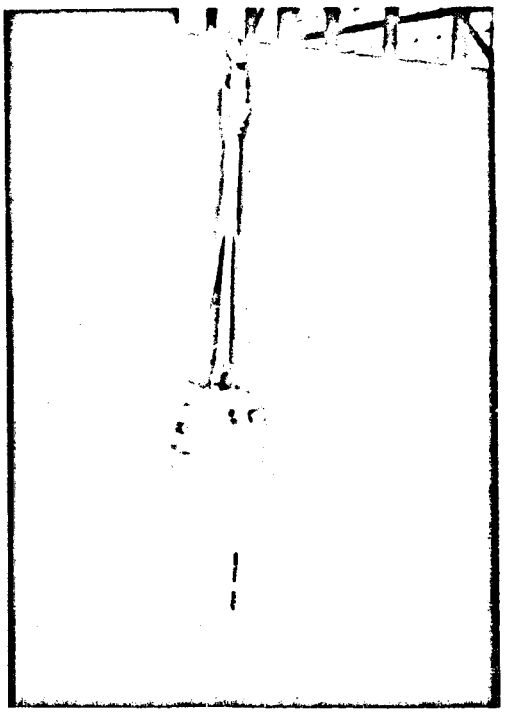

Figure 50 - Legs of Static Line

d. Test Procedure

The packaged BALLUTE and simulated payload was lifted to altitude with a helicopter to satisfy the test objectives. The payload/BALLUTE system was suspended on a nylon web from the quick-release hook located under the helicopter. The attachment point on the system was located to suspend the system at an approximate 16-deg inclination. Figure 51 shows the configuration during a pretest pickup. The extraction static line was attached to a lug located on the side of the quick release. An additional lightweight line was attached to the deployment bag and tied inside the helicopter; this line was used to pull the deployment bag back into the helicopter after deployment.

After attachment of the components to the helicopter, the helicopter ascended to 5000 ft and was positioned relative to the ground by radar vector. The pilot released the system at a verbal command from the ground.

e. Test Sequence

Upon release of the pickup line from the helicopter, the static line becomes taut and the tape to the pickup line breaks. The payload and BALLUTE

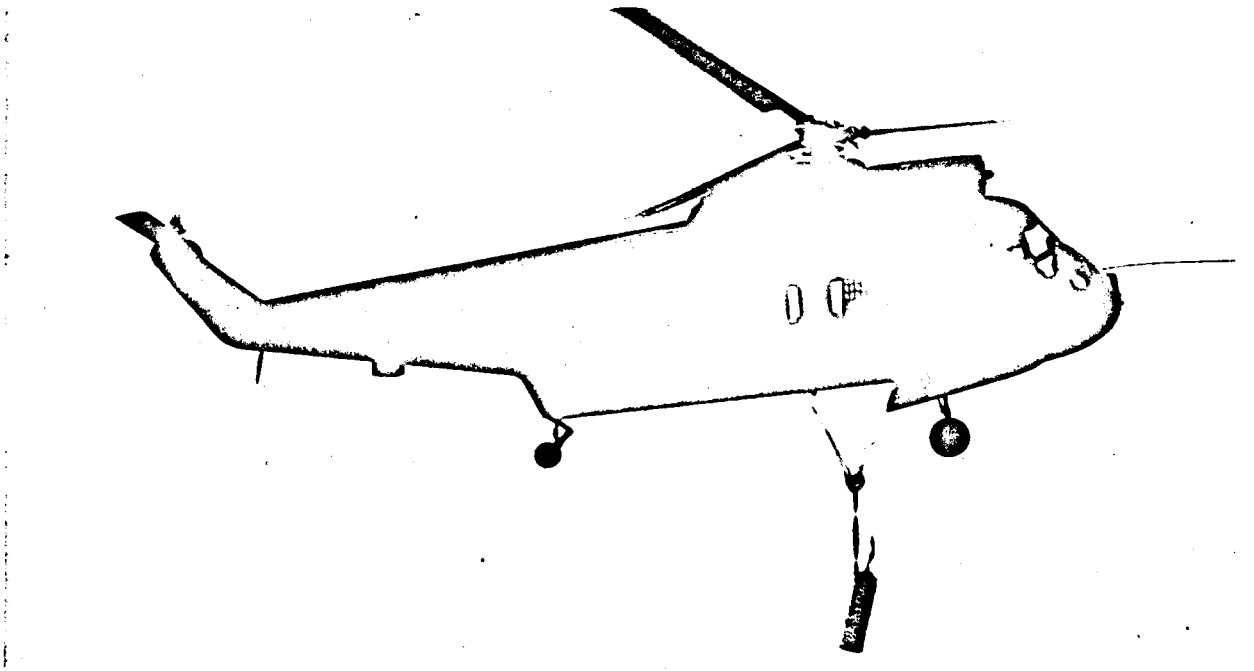

Figure 51 - Configuration of Payload/BALLUTE System during Pretest Pickup

system accelerate until the static line becomes taut (approximately 12 ft of freefall). Then the BALLUTE pack comes to rest and the payload continues accelerating. This acceleration continues until the three-leg bridle, intermediate riser, and BALLUTE riser become taut. When this occurs, two cutter knives attached to the riser sever the restraint that retains the BALLUTE in the bag.

The payload continues its descent and deploys the BALLUTE from the deployment bag. Once the BALLUTE is unfolded, the eight ram-air inlets open into the airstream and allow air to inflate the envelope and to its design shape. During the inflation process, the system is approaching its terminal velocity. When the BALLUTE is fully inflated, the terminal velocity is attained and the system descends to ground impact. The recovery site of the second drop is shown in Figure 52.

f. Test Results

The data obtained during the test performed on 26 July 1967 (LD 2106) and 27 July 1967 (LD 2107) were acquired with an FPS-16 skin tracking radar.

Figure 52 - Recovery Site of Second BALLUTE Drop Test

The radar data were analyzed by computer and the output digitized into the pertinent descent parameters. From these data, the apparent drag coefficient of the system was determined at the subsonic descent velocity. From the general equation for equilibrium descent conditions,

$$W = qC_D A = 1/2\,\rho V_D^2 C_D \pi R_B^2, \quad (114)$$

where

W = total system weight, lb,

ρ = air density, slugs/cu ft,

V_D = vertical descent velocity, fps,

C_D = apparent drag coefficient, and

R_B = total BALLUTE radius, ft.

For R_B = 9 feet, Equation 114 reduces to

$$W = 127\,\rho C_D V_D^2 \odot \quad (115)$$

For W = 247 lb (see Table XXI for component weights), Equation 115 becomes:

$$C_D = \frac{1.95}{V_D^2} \quad (116)$$

TABLE XXI - WEIGHT OF COMPONENTS

Item	Weight (lb)
BALLUTE	36.6
Riser	3.2
Bridle	1.2
Payload	206.0
Total	247.0

To solve Equation 116 for the drag coefficient, air density and descent velocity must be determined. From the equation of state for a perfect gas,

$$\rho = \frac{P}{RT}, \tag{117}$$

where

P = ambient pressure, psfa,

T = ambient temperature, Rankine,

R = gas constant for air, 1717 ft-lb/slug/Rankine

Thus, the air density at any point of the BALLUTE descent path may be determined. Table XXII shows the altitude, temperature, and pressure values recorded by the ESSA radiosonde at the BALLUTE drop times. From Equation 117, density can be determined for each of the "levels" shown in Table XXII. Plots of altitude versus air density for Tests LD 2106 and LD 2107 are shown in Figures 53 and 54, respectively. For comparison, a 1962 standard atmosphere is shown on each of these plots.

By definition, Reynolds number is equal to

$$Re = \frac{\rho V_D L}{\mu} = \frac{V_D L}{\nu}, \tag{118}$$

or

$$\frac{Re}{L} = \frac{V_D}{\nu}, \tag{119}$$

where

ρ = air density, slugs/cu ft,

V_D = velocity, fps,

L = characteristic length, ft, and

μ = viscosity, lb/sec/sq ft, and

$\nu = \rho/\mu$

= kinematic viscosity, sq ft/sec.

TABLE XXII - VALUES OF AMBIENT ATMOSPHERE

Test	Level	Altitude (KM)	Altitude (ft)	Temperature (F)	Air pressure (psfa)	Air density (slugs/cu ft)	Viscosity (lb/sec/sq ft)	Kinematic viscosity (sq ft/sec)
LD 2106	1	0.0	0.0	78.1	2117	0.002291	3.85×10^{-7}	1.680×10^{-4}
	2	0.385	1301.3	72.5	2029	0.002219	3.83×10^{-7}	1.726×10^{-4}
	3	0.760	2568.8	72.5	1940	0.002122	3.83×10^{-7}	1.805×10^{-4}
	4	2.28	7704.4	52.0	1624	0.001847	3.71×10^{-7}	2.009×10^{-4}
LD 2107	1	0.0	0.0	78.1	2121	0.002296	3.85×10^{-7}	1.677×10^{-4}
	2	0.28	908.0	74.5	2055	0.002239	3.84×10^{-7}	1.714×10^{-4}
	3	1.35	4428.0	62.2	1817	0.002026	3.77×10^{-7}	1.859×10^{-4}
	4	2.25	7380.0	53.6	1633	0.001851	3.72×10^{-7}	2.010×10^{-4}

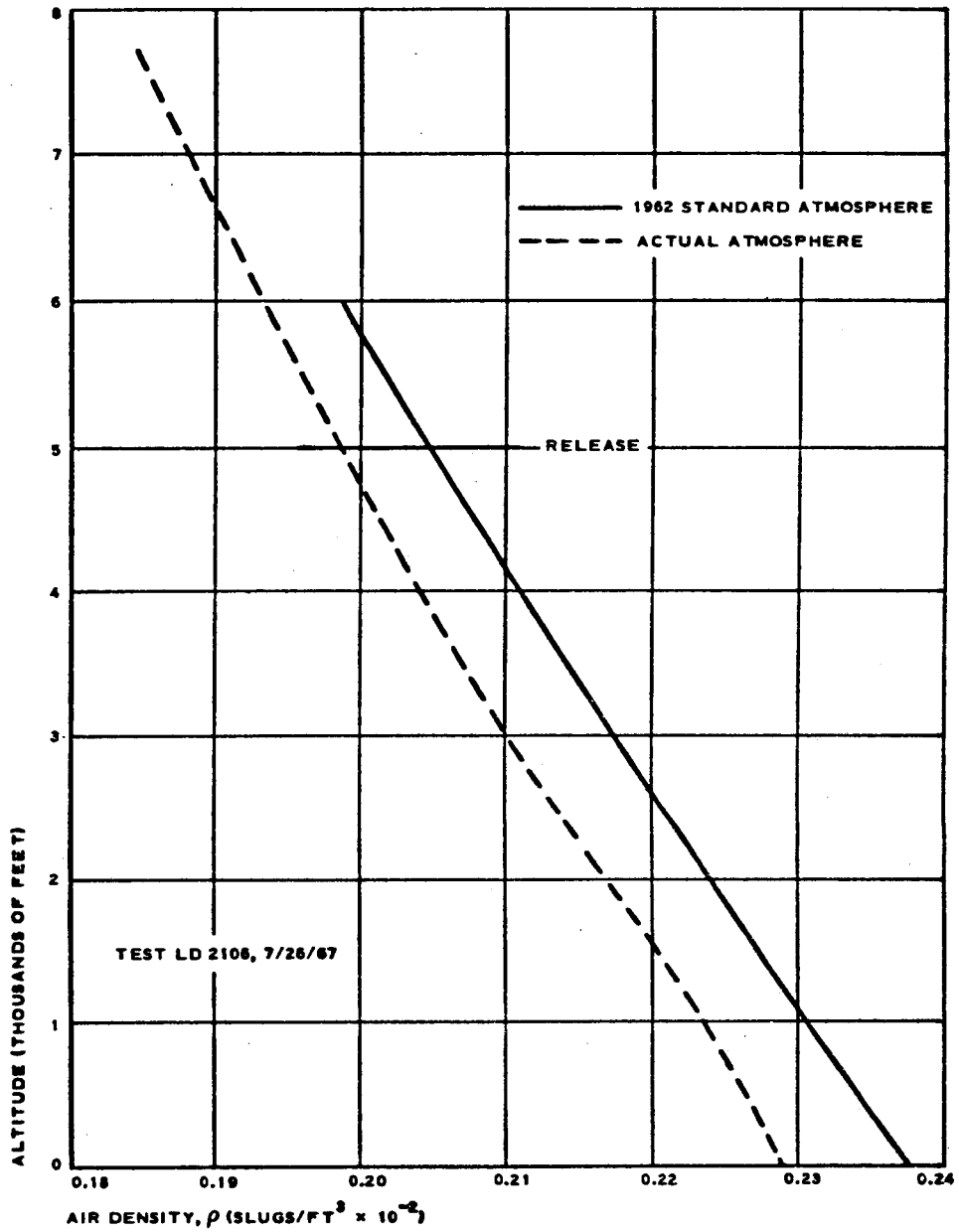

Figure 53 - Meteorological Conditions for Test LD 2106

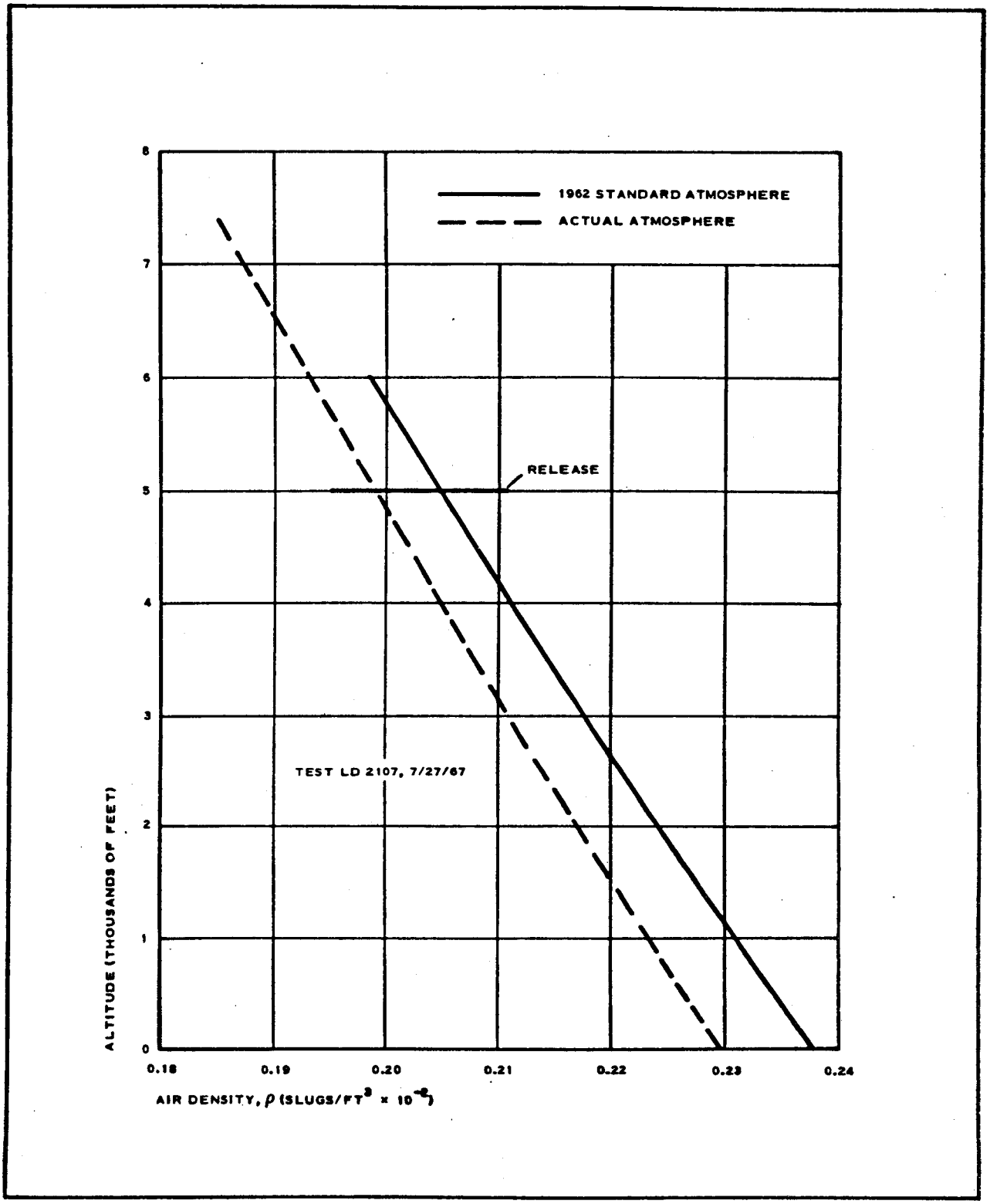

Figure 54 - Meteorological Conditions for Test LD 2107

Values for μ were obtained at each of the temperatures indicated and values for kinematic viscosity, ν, were calculated. Presented in Figure 55 is a plot of altitude versus kinematic viscosity for the two tests.

To solve Equation 116 for C_D, the values of V_D had to be determined. The FPS-16 tracking radar data exhibited certain inconsistencies in vertical velocity display. This shortcoming probably was attributable to poor tracking resolution caused by BALLUTE low descent velocity. The average velocities between selected descent altitudes had to be used to obtain a consistent V_D. A plot of altitude versus time during descent is shown in Figure 56. From this, steady-state descent velocities were shown to exist below 4000 ft (the first 1000 ft being consumed by deployment and inflation of the BALLUTE) and average V_D values were calculated. Table XXIII shows descent altitudes and times from helicopter BALLUTE release. The altitude increment, ΔA_N, was obtained by subtracting the N + 1 altitudes from the N altitudes. The values shown for density, ρ, are those corresponding to the average altitude during the increment that is: $A_{mean} = A_{(N)} + A_{(N+1)}/2$ and are taken from Figure 52 for Test LD 2106 and from Figure 53 for Test LD 2107.

Since velocity and density were known, the drag coefficient, C_D, was calculated for each of the altitude increments. Figure 57 shows the values for C_D versus descent velocity, V_D, for Tests LD 2106 and LD 2107. The Reynolds number was calculated using Equation 119 to obtain the Reynolds number per foot for each altitude's increment (see Figure 58).

A point-mass trajectory analysis for the expected flight profile (Mach 3.0, q = 23 psf, and γ = 77 deg) using a predicted drag coefficient produced a minimum terminal velocity of 47.35 fps. Under a zero wind condition, the range was approximately 21,000 ft. The difference between the predicted terminal velocity and those experienced in the drop tests can be influenced by the following factors:

1. Dynamic lift
2. Increased effective drag area caused by coning
3. Scale factors
4. Reynolds number effect

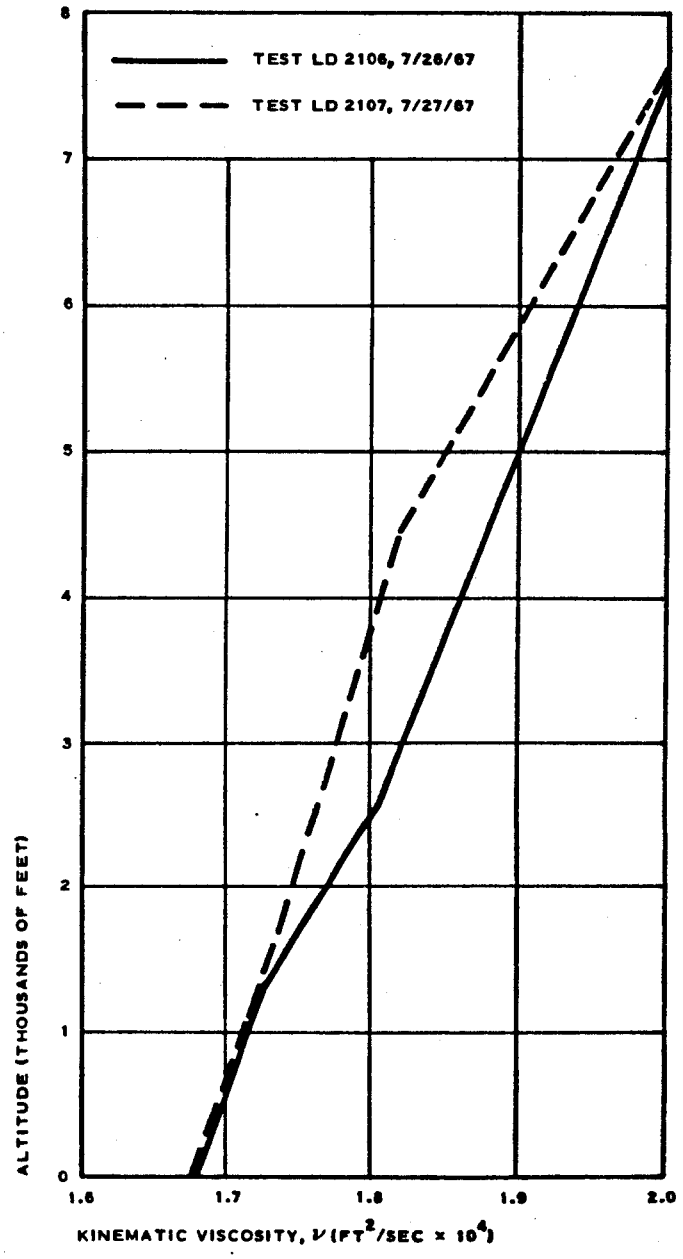

Figure 55 - Kinematic Viscosity versus Altitude

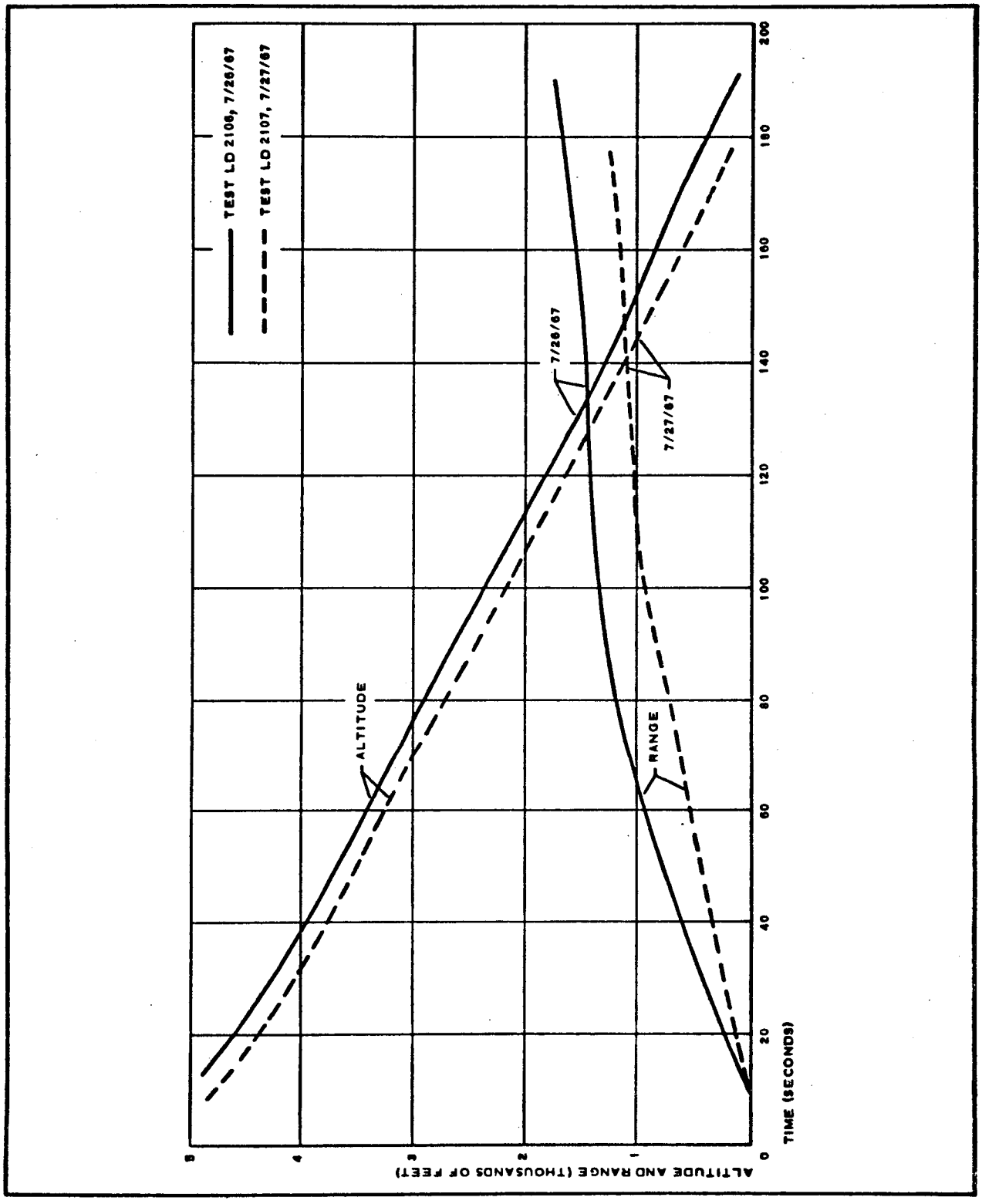

Figure 56 - BALLUTE Drop Test Flight Profile

TABLE XXIII - DESCENT HISTORY

Test and Level, N	Altitude, A_N (ft)	Total time,* t_N (sec)	$\Delta A_N = A_N - A_{(N+1)}$	$\Delta t_N = t_{(N+1)} - t_N$	$V_{D_N} = \frac{\Delta A_N}{\Delta t_N}$ (fps)	$V_{D_N}^2$ (ft^2/sec^2)	Air density,+ (slug/cu ft)	$V_{D_N}^2$ mean	Drag coefficient,‡ $C_D = \frac{1.95}{V_D^2 \text{ mean}}$	Kinematic viscosity,+ mean (ft^2/sec)	$Re/ft = \frac{V_D}{\text{mean}}$
LD 2106											
1	3500	57.33	500	18.80	26.60	707	0.002085	1.474	1.32	1.833×10^{-4}	1.451×10^5
2	3000	76.13	500	18.80	26.60	707	0.002117	1.497	1.30	1.812×10^{-4}	1.468×10^5
3	2500	94.93	500	18.23	27.40	751	0.002151	1.615	1.21	1.785×10^{-4}	1.535×10^5
4	2000	113.16	500	18.64	26.80	718	0.002183	1.567	1.25	1.755×10^{-4}	1.527×10
5	1500	131.80	500	20.65	24.20	586	0.002222	1.302	1.50	1.727×10^{-4}	1.401×10^5
6	1000	152.45	500	22.45	22.25	505	0.002253	1.138	1.71	1.708×10^{-4}	1.303×10^5
7	500	174.90	200	8.40	23.80	566	0.002272	1.286	1.52	1.692×10^{-4}	1.407×10^5
8	300	183.30	. . .	. . .	. . .	. . .	. . .	. . .	. . .	. . .	. . .
LD 2107											
1	3500	50.70	500	19.26	26.00	676	0.002095	1.416	1.38	1.785×10^{-4}	1.457×10^5
2	3000	69.96	500	18.04	27.70	767	0.002125	1.630	1.20	1.770×10^{-4}	1.565×10^5
3	2500	88.00	500	19.03	26.25	689	0.002156	1.499	1.30	1.755×10^{-4}	1.496×10^5
4	2000	107.03	500	18.50	27.05	732	0.002186	1.600	1.22	1.740×10^{-4}	1.555×10^5
5	1500	125.53	500	19.27	25.95	673	0.002217	1.492	1.31	1.727×10^{-4}	1.503×10^5
6	1000	144.80	500	19.10	26.20	686	0.002250	1.544	1.26	1.708×10^{-4}	1.533×10^5
7	500	163.90	200	7.76	25.80	665	0.002270	1.510	1.29	1.692×10^{-4}	1.525×10^5
8	300	171.66	. . .	. . .	. . .	. . .	. . .	. . .	. . .	. . .	. . .

*Times and altitudes taken directly from Test LD 2106 printout.

+The values for density and kinematic viscosity are taken at the mean altitude during the increment, i.e., $\frac{A_N + A_{(N+1)}}{2} = A_{mean}$ from Figures 53 and 54

‡Drag coefficient is based on projected area of an 18-ft-diam BALLUTE (254 sq ft).

111

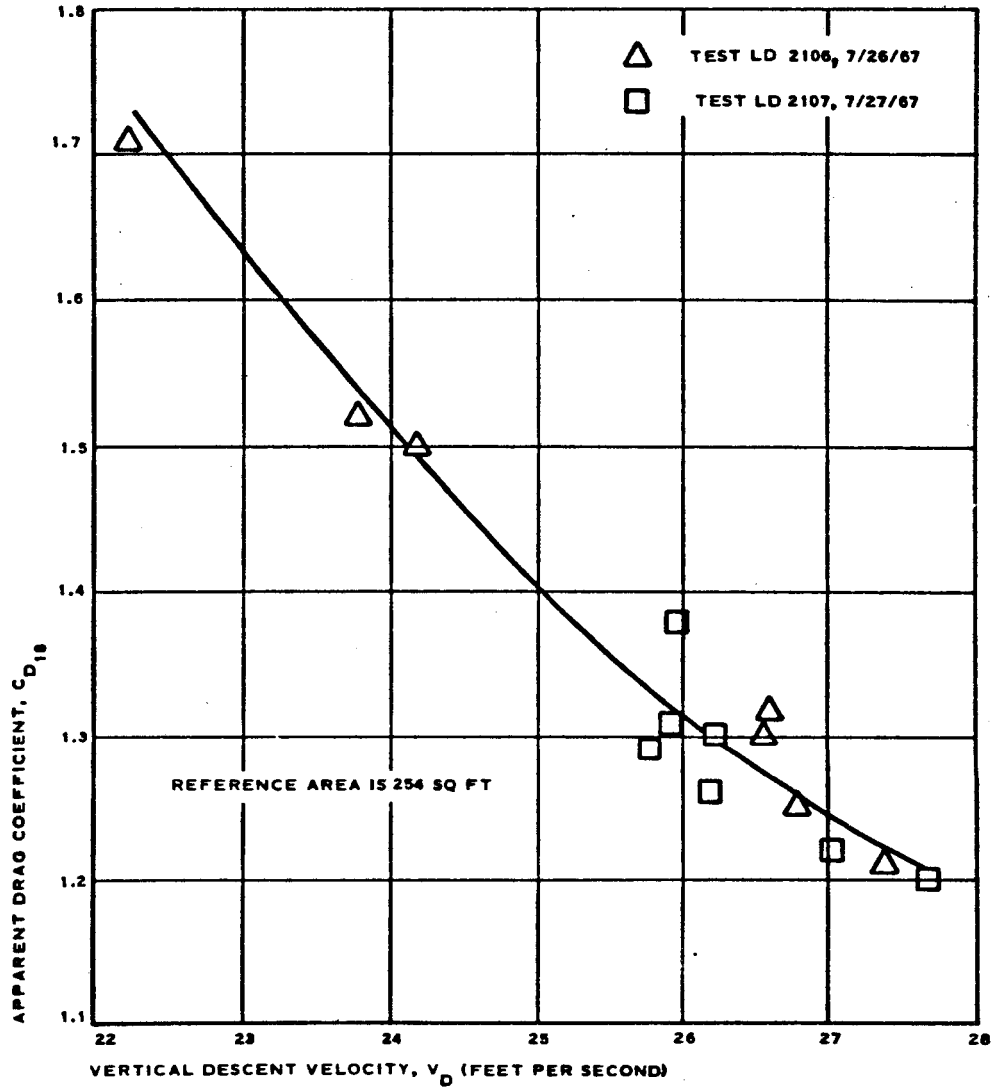

Figure 57 - Experimental Drag Coefficient versus Velocity

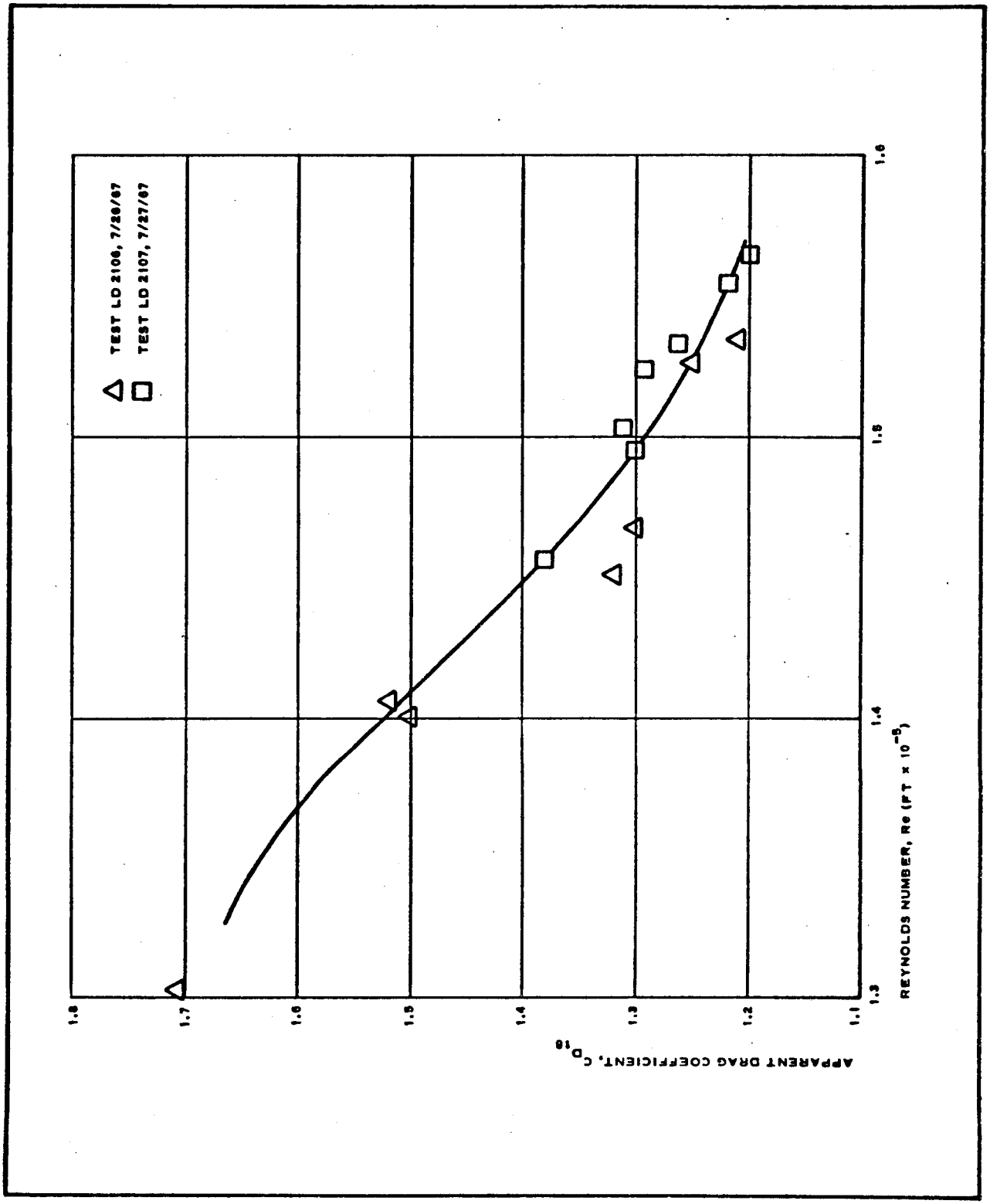

Figure 58 - Experimental Drag Coefficient versus Reynolds Number

5. Static lift or buoyancy
6. Lack of proper flow separation at the burble fence

Of these factors, the Reynolds number effect and static lift may be considered to be negligible. The remaining factors appear to contribute to the apparent high drag coefficient, but their individual contribution is difficult to establish. Motion picture analysis indicated a coning included angle in excess of 45 deg, which places the BALLUTE at a constantly varying angle of attack to produce some dynamic lift. This factor alone will not account for the increased apparent drag coefficient.

Since previous flight tests have shown the trailing BALLUTE to be a stable decelerator, the dynamic parameters that produced or permitted this coning action should be determined. One contributing factor was the physical attachment of the payload assembly to the drop test helicopter. The 16-deg slinging angle would, upon payload release, produce an initial perturbation and this was evident in the motion picture films. As the payload accelerated from zero velocity to terminal velocity, the drag forces increased less rapidly than they would during high-velocity deployment and the damping effect was considerably lower, resulting in prolonged coning prior to stabilization.

Another contributing factor was the low initial velocity at BALLUTE deployment. In actual rocket-launched high-velocity deployment, the burble fence will induce some flow separation and enhance system aerodynamic stability. During low velocity deployment, the velocity required to induce flow separation may not be attained as the low momentum of the system is incapable of providing the required energy. More simply, the higher drag and energy dissipation rate encountered in high-speed deployment and flight will increase the damping effects on the system and provide greater system stability. The coning action produces a larger effective drag area normal to the relative winds and this, when used with the nominal BALLUTE drag area, produces an excessively high apparent drag coefficient. Scale factors, especially in the burble fence radius of curvature, will tend to reduce flow separation at these low drop-test velocities. It is even reasonable to surmise that the flow may be attached well toward the center of the BALLUTE trailing face. This condition will not only permit coning, but actually induce such an instability.

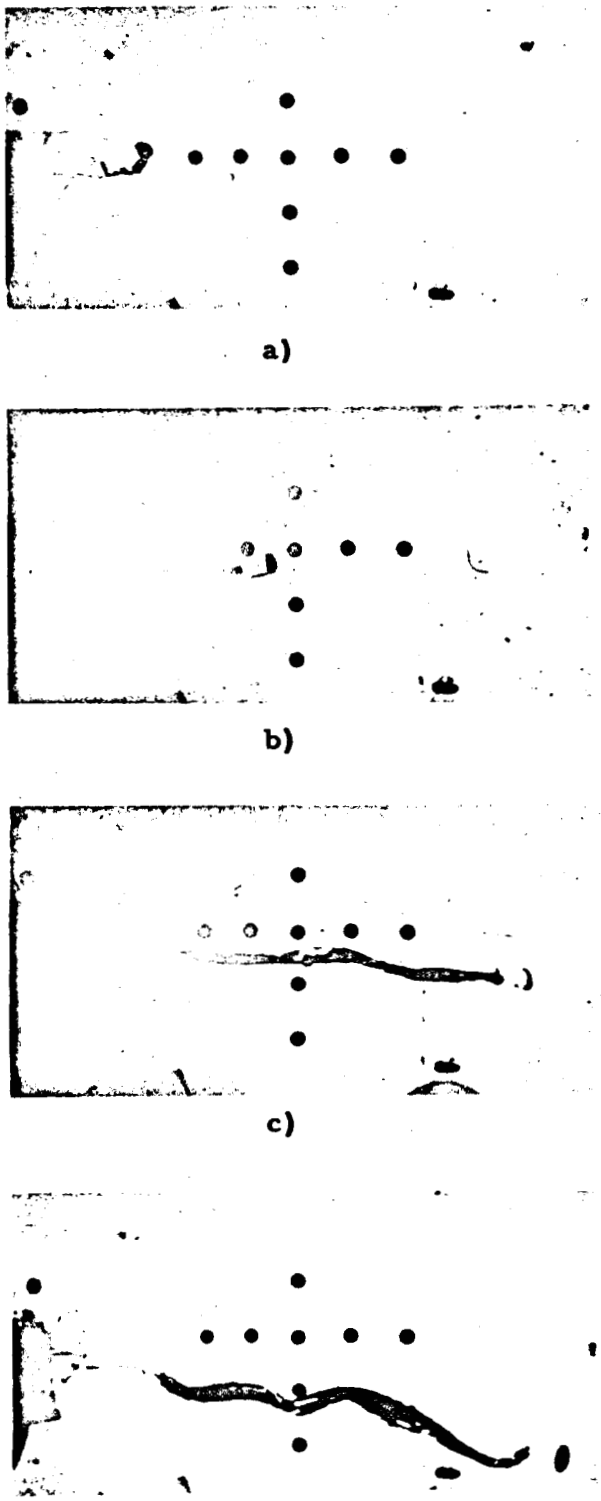

a)

b)

c)

d)

Figure 59 - Side View of Test (Without Inflation Aid, Atmospheric Pressure)

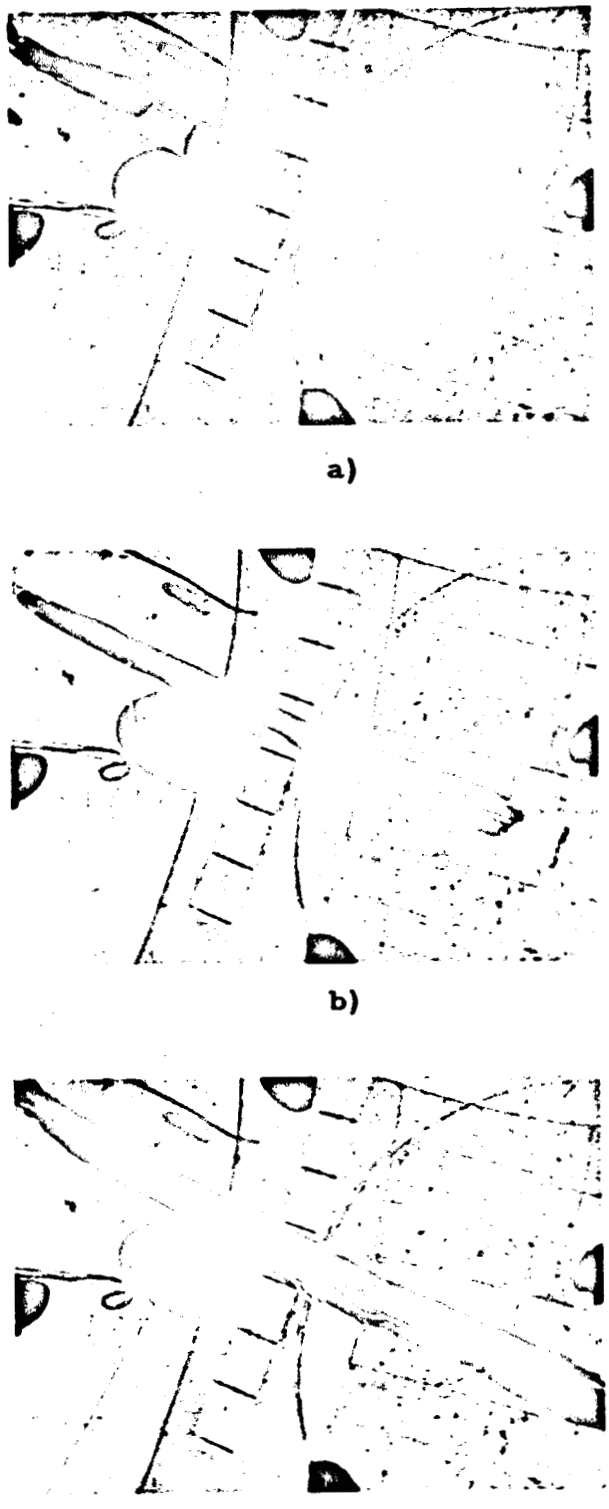

a)

b)

c)

Figure 60 - Top View of Test (Without Inflation Aid, Atmospheric Pressure)

a)

b)

Figure 61 - Side View (With Inflatation Aid, Altitude Pressure)

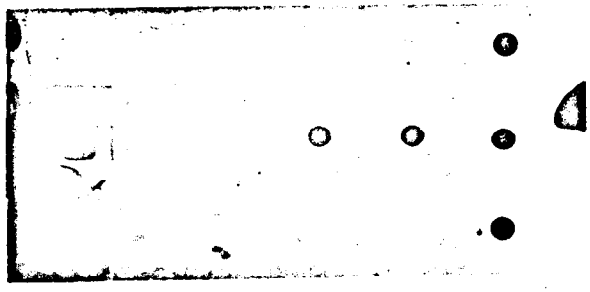

a)

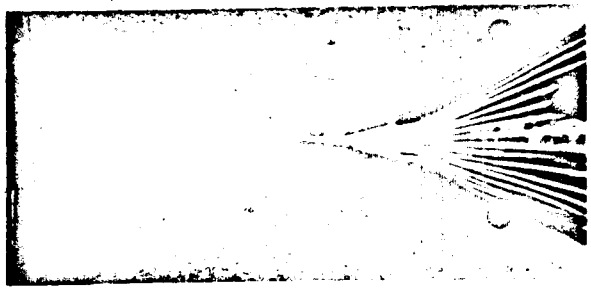

b)

Figure 62 - Enlarged Side View (With Inflation Aid, Altitude Pressure)

a)

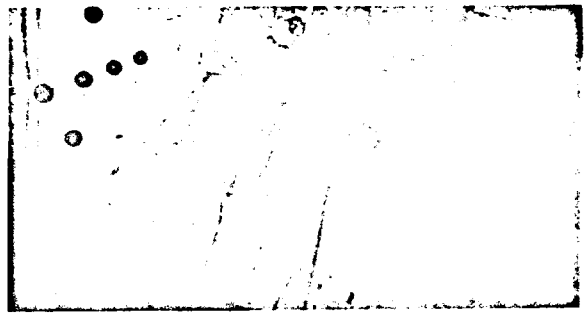

b)

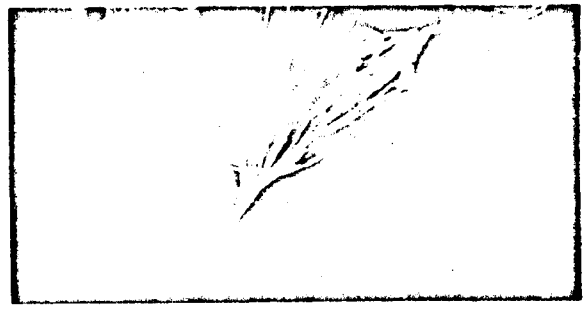

c)

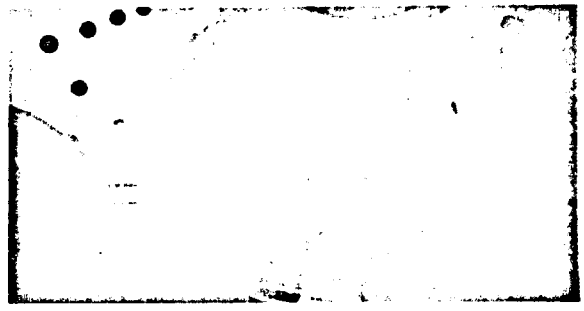

d)

Figure 63 - Top View (With Inflation Aid, Altitude Pressure)

a)

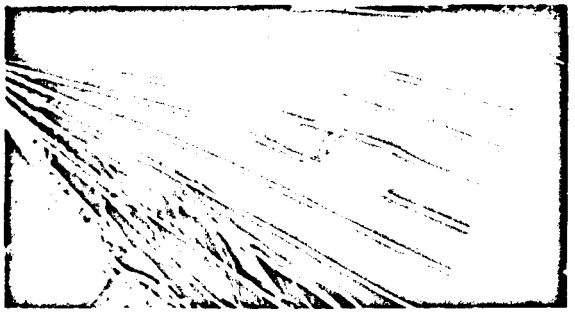

b)

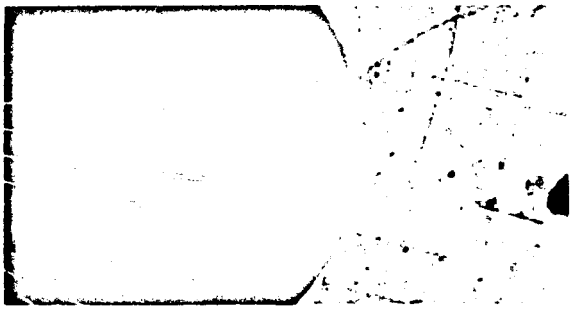

c)

d)

Figure 64 - Enlarged Top View With Inflation Aid, Altitude Pressure)

deployment bag was burned again at the same position, but no damage to the BALLUTE was observed. Post-fire chamber pressure increased to 5.346 psfa (approximately 134,000 ft, MSL). The BALLUTE was retained by NASA for proposed full-scale wind tunnel testing.

LIST OF REFERENCES

1. Jaremenko, I. M.: "BALLUTE Characteristics in the 0.1 to 10 Mach Number Speed Regime," J. Spacecraft and Rockets, August 1967; Vol 4, No. 8.

2. Nebiker, F. R.; et al.: Aerodynamic Deployable Decelerator Performance Evaluation Program. AFFDL-TR-65-27. Wright-Patterson AFB, Ohio, Air Force Flight Dynamics Laboratory. August 1965.

3. Jaremenko, I. M.: Wakes, Their Structure and Influence upon Aerodynamic Decelerators. CR-748, NASA, April 1967.

4. Dennard, J. S.; and Nelson, W. J.: Preliminary Investigation of the Effects of Inlet Assymmetry on the Performance of Converging-Diconverging Diffusers at Transonic Speeds. RM L52J20, NACA, November, 1952.

5. Weske, J. R.: Experimental Investigation of Velocity Distribution Downstream of Single-Duct Bends. TN-1471, NACA, January 1948.

6. Houtz, N. E.: Optimization of Inflatable Drag Devices by Isotensoid Design. AIAA paper 64-437 presented at 1st AIAA Annual Meeting, Washington, D. C., June 29-July 2, 1964.

7. Nissel, R. E.: Strength to Weight Values for Nomex Cloth and Webbing at Ambient and Elevated Temperatures. Aero-Mechanical Research and Development Department Memorandum, ARD 10,574. Akron, Ohio, Goodyear Aerospace Corporation, 24 April 1967.

8. Timoshenko, S.; and Woinowsky-Krieger, S.: Theory of Plates and Shells. 2nd ed. New York, McGraw-Hill Book Co., Inc., 1959.

9. Zeiberg, S. L.: "Transition Correlations for Hypersonic Wakes," AIAA Journal, March 1964; Vol 2, No. 3, pp 564-565.

10. GER-13367: BALLUTE Packing Procedure. Akron, Ohio, Goodyear Aerospace Corporation. 21 August 1967.

APPENDIX A - DERIVATION OF AREA AND VOLUME

The surface area and the volume of the basic BALLUTE are given by, respectively:

$$A_{fB} = \text{area of sphere} + 8.5 \text{ percent for gore lobes}$$

$$= 4\pi R^2 + 0.085\,(4\pi R^2)$$

$$= 4.35\pi R^2 \qquad \text{(A-1)}$$

and

$$V_B = \text{volume of sphere} + 16.6 \text{ percent for gore volume}$$

$$= \frac{4}{3}\pi R^2 + 0.166\,\frac{4}{3}\pi R^3$$

$$= 1.166\,\frac{4}{3}\pi R^3$$

$$= \frac{14}{9}\pi R^3 . \qquad \text{(A-2)}$$

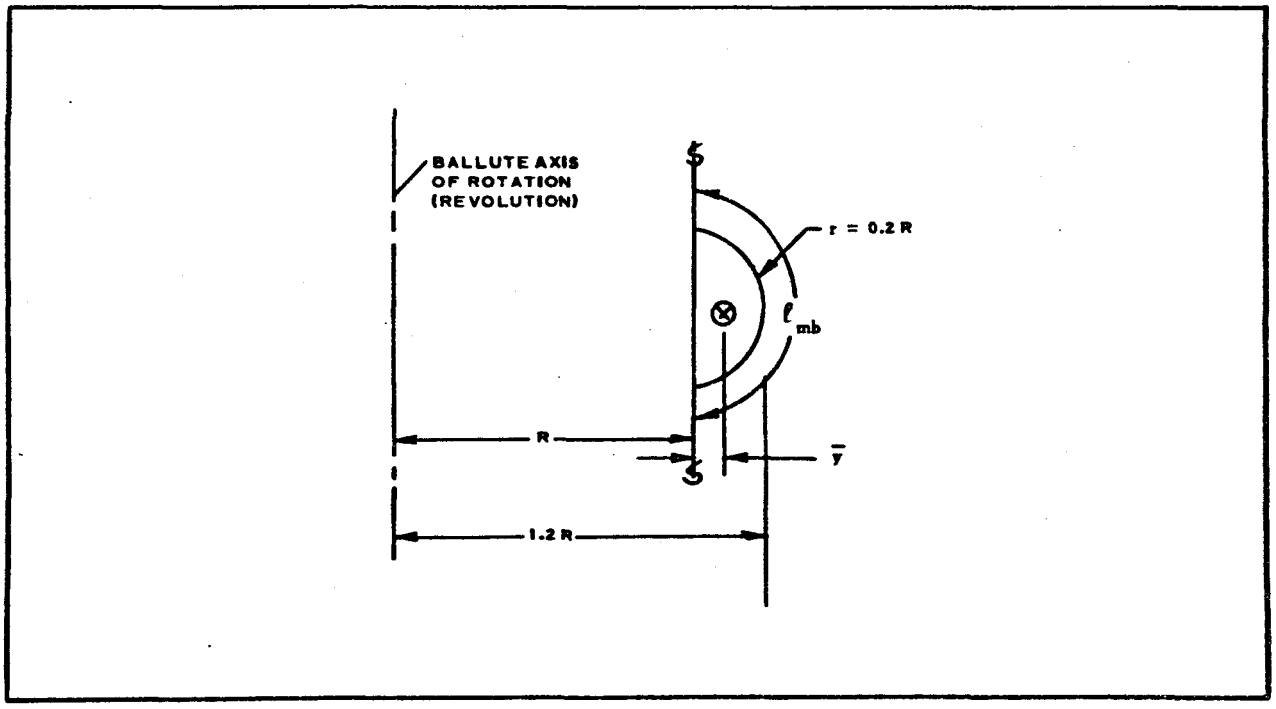

Figure A-1 - Cross Section of Burble Fence

The surface area of the 10-percent burble fence is calculated below. As shown in Figure A-1, the centroid and arc lengths are given by, respectively:

$$\bar{y} = \frac{2r}{\pi} = \frac{0.4R}{\pi} \tag{A-3}$$

and

$$\ell\, m_b = \pi r = 0.2\pi R. \tag{A-4}$$

Therefore, the surface area of the burble fence at the equator is given by:

$$A_{fb} = 2\pi R\left(1 + \frac{0.4}{\pi}\right)(0.2\pi R)$$

$$= 2(1.1271)(0.2)\pi\pi R^2$$

$$= 1.42\,\pi R^2 . \tag{A-5}$$

If the burble fence is aft of the equator (defined by θ_b), the surface area becomes:

$$A_{fb} = 1.42\pi R^2 \cos\theta_b. \tag{A-6}$$

For θ_b = 15 deg,

$$A_{fb} = (1.42)(0.965)\pi R^2$$

$$= 1.37\pi R^2. \tag{A-7}$$

The surface area of the burble fence divided by the surface area of the BALLUTE is

$$\frac{A_{fb}}{A_{fB}} = \frac{1.37}{4.35}$$

$$= 31.5 \text{ percent.} \tag{A-8}$$

Similarly, the volume of the burble fence is given by the following equations:

$$\bar{y} = \frac{4r}{3\pi}$$

$$= \frac{4}{3\pi}(0.2R)$$

$$= \frac{0.8R}{3\pi} , \tag{A-9}$$

$$V_b = 2\pi R\left(1 + \frac{0.8}{3\pi}\right)\frac{\pi}{2}(0.2R)^2$$

$$= 0.1364\pi R^3 \text{ (fence at equator)}, \quad \text{(A-10)}$$

or

$$V_b = 0.1364\pi R^3 \cos\theta_b \text{ (fence at } \theta_b); \quad \text{(A-11)}$$

for $\theta_b = 15$ deg,

$$V_b = 0.132\pi R^3. \quad \text{(A-12)}$$

The volume of the burble fence divided by that of the BALLUTE is:

$$\frac{V_b}{V_B} = \frac{0.132}{\frac{14}{9}}$$

$$= 8.46 \text{ percent} \quad \text{(A-13)}$$

In the basic BALLUTE, the length of the meridians and the area of the meridional seams are given by, respectively:

$$\ell_m = 3.48\, n_g R \quad \text{(A-14)}$$

and

$$A_{fg_m} = m w_m \ell_m$$

$$= 3.48\, n_g R\, m w_m. \quad \text{(A-15)}$$

See Figure A-2 for an example of m and w_m. The determination of the length of the BALLUTE cross-splice seams is based upon Equations A-16 through A-19, which are derived from Figures A-3 and A-4:

$$B_j = 1.085\,\frac{\pi X}{n_g} + m w_m \quad \text{(A-16)}$$

$$C_j = jA\sqrt{2\phi_j} \quad \text{(A-17)}$$

$$X_j = R' \sin\phi_j \quad \text{(A-18)}$$

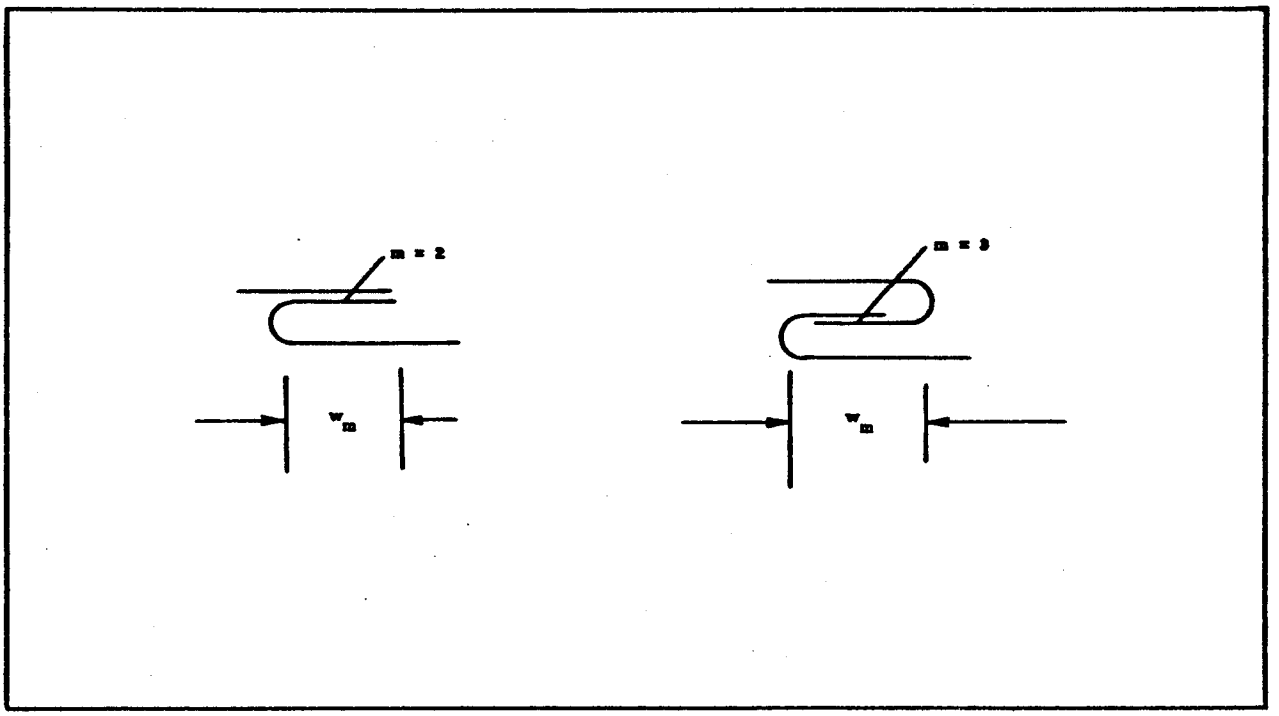

Figure A-2 - Determination of m

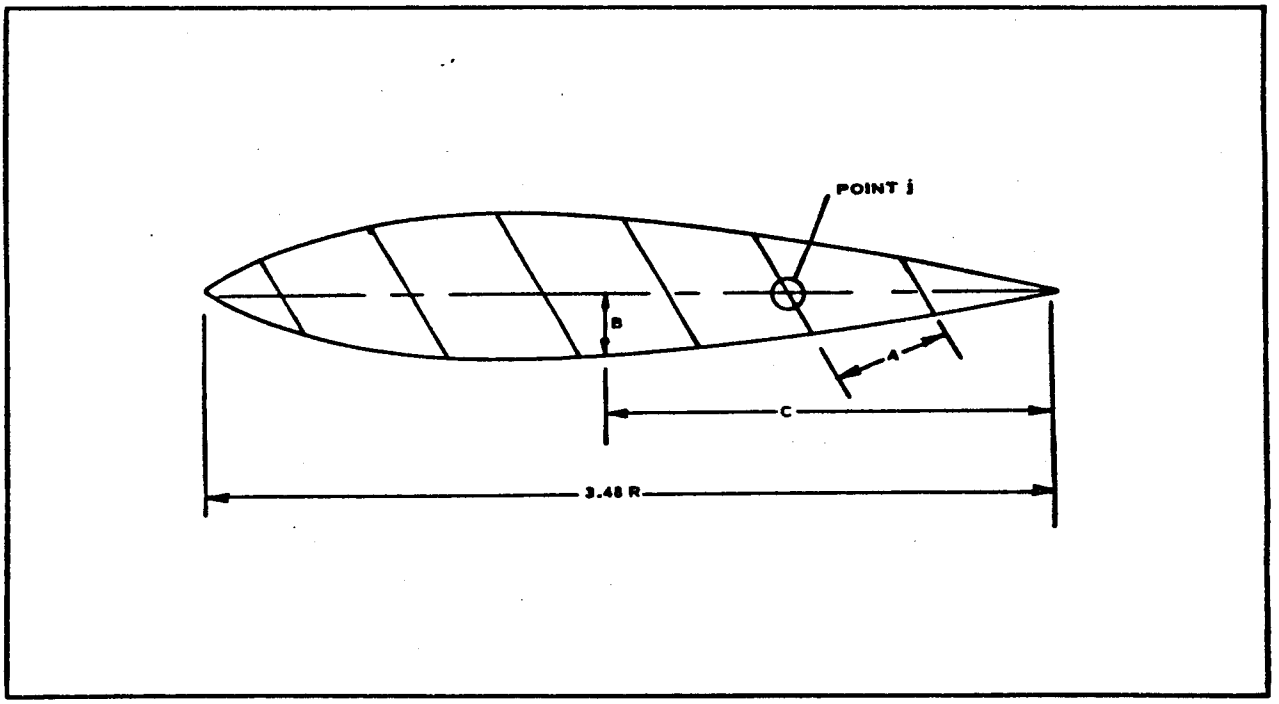

Figure A-3 - Determination of Reference Point j

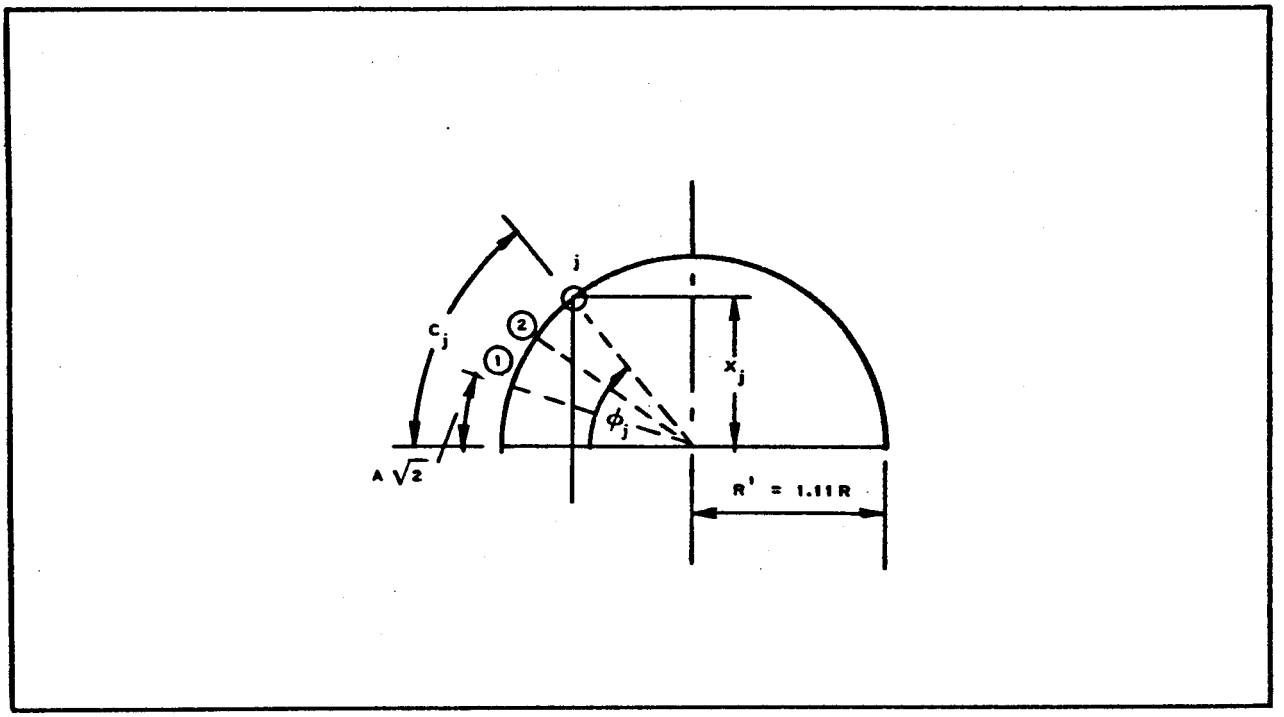

Figure A-4 - Determination of X_j

$$j_o = \frac{3.48R}{A\sqrt{2}} \qquad \text{(A-19)}$$

For the problem at hand, the values of R = 90 in., and A = 42 in. are substituted into Equations A-17 through A-19 to yield:

$$j_o = \frac{(3.48)(90)}{42\sqrt{2}} = \frac{313.5}{59.5} = 5.25 \text{ (use } j_o = 5) \qquad \text{(A-20)}$$

and

$$\phi_1 = \frac{A\sqrt{2}}{1.11R} = \frac{59.5}{100} = 0.595 \text{ rad or } 34 \text{ deg}. \qquad \text{(A-21)}$$

The sum of the X_j values is 334.1 in. (see Table A-I).

The total length of the bias seams is given by:

$$\ell_s = 2n_g\sqrt{2} \sum_{1}^{j_o} B_j = 2n_g\sqrt{2}\left(j_o mw_m + \frac{1.085\pi}{n_g} \sum_{1}^{j_o} X_j\right). \qquad \text{(A-22)}$$

TABLE A-I - DERIVATION OF X_j VALUES

Parameters	Values of j				
	1	2	3	4	5
C_j (in.)	59.5	119.0	178.5	238.0	297.5
θ_j (deg)	34.0	68.0	102.0	136.0	170.0
X_j (in.)	56.7	92.7	97.8	69.5	17.4

For this problem, the values R = 7.5 ft or 90 in., m = 2, A = 42 in., w_m = 1/2 in., j_o = 5, and n_g = 16 are substituted into Equation A-22 to yield:

$$\ell_s = (2)(16)\sqrt{2}\left[(5)(2)\left(\frac{1}{2}\right) + \frac{1.085\pi}{16}(334.1)\right]$$

$$= 45.3(5 + 71.3)$$

$$= 3490 \text{ in.}$$

$$= 290 \text{ ft .} \qquad \text{(A-23)}$$

The enclosed volume of the BALLUTE is:

$$V_B = \frac{14}{9}\pi R^3$$

$$= 1.55\pi R^3 , \qquad \text{(A-24)}$$

and of the burble fence,

$$V_b = 0.132\pi R^3 . \qquad \text{(A-25)}$$

APPENDIX B - MOMENT OF INERTIA AND WEIGHT ANALYSIS

The calculated mass moments of inertia for the inflated BALLUTE in roll, pitch, and yaw are shown on the inertia calculation sheet (Table B-I). Figure B-1 shows the axial station breakdown used for determination of center of gravity and mass moments of inertia using similarity to conventional geometric bodies. The weight total is based on the maximum fabric weight attainable using the maximum gage and coating tolerances.

The center of gravity of the BALLUTE in the "strung-out" condition was determined by test, using the conventional balance method. The cg is 20 ft, 5-1/4 in. aft of the main riser attachment fitting bolthole.

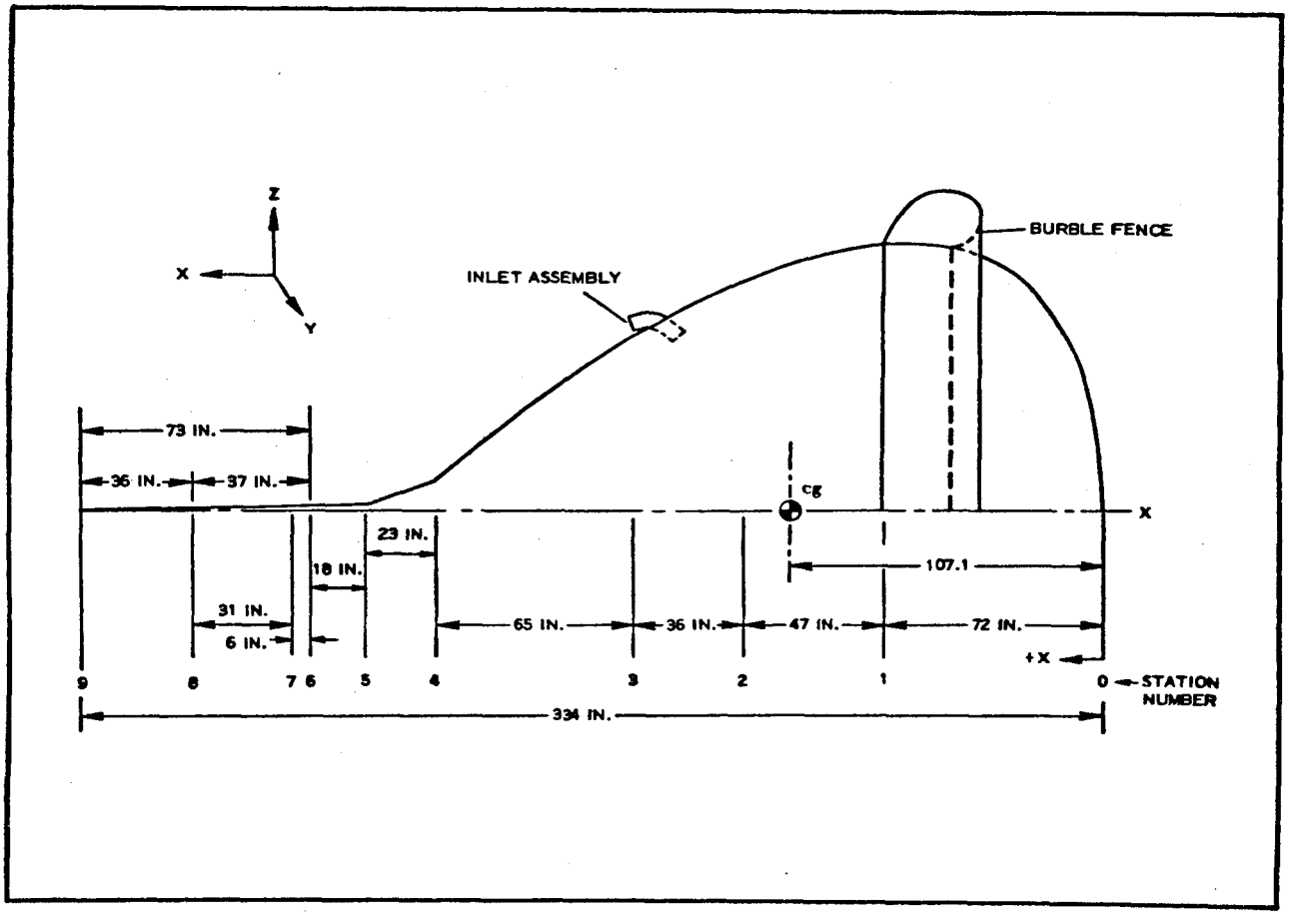

Figure B-1 - BALLUTE Dimensional Diagram

TABLE B-I - INERTIA CALCULATIONS

Station	Weight (lb)	X (in.)	Y (in.)	Z (in.)	W X (in.-lb)	W Y (in.-lb)	W Z (in.-lb)	W X^2 (lb-in.^{2})	W Y^2 (lb-in.^{2})	W Z^2 (lb-in.^{2})	Roll I_{ox} (lb-in.^{2})	Pitch I_{oy} (lb-in.^{2})	Yaw I_{oz} (lb-in.^{2})
8 to 7	0.452	282.0	0	0	128.0	0	0	35,945	0	0	Neg	43	43
9 to 8	0.525	316.0	0	0	166.0	0	0	52,424	0	0	Neg	57	57
7 to 6	0.242	263.5	0	0	64.0	0	0	16,803	0	0	Neg	. . .	. . .
6 to 5	0.465	250.5	0	0	116.5	0	0	29,178	0	0	2	13	13
5 to 4	1.395	233.0	0	0	325.0	0	0	75,733	0	0	51	81	81
4 to 3 (Fabric)	2.875	178.7	0	0	513.8	0	0	91,809	0	0	4,737	7,895	7,895
4 to 3 (Webs)	4.262	187.25	0	0	798.1	0	0	149,439	0	0	7,014		
3 to 2 (Fabric)	3.316	135.95	0	0	450.8	0	0	61,286	0	0	16,332	14,402	14,402
3 to 2 (Web)	2.232	137.0	0	0	305.8	0	0	41,892	0	0	10,993		
2 to 1 (Fabric	4.620	95.01	0	0	438.9	0	0	41,705	0	0	34,822	27,600	27,600
2 to 1 (Web)	2.510	95.5	0	0	239.7	0	0	22,891	0	0	18,919		
1 to 0 (Fabric)	6.228	30.5	0	0	189.9	0	0	5,793	0	0	35,143	38,000	38,000
1 to 0 (Web)	6.913	37.0	0	0	255.8	0	0	9,464	0	0	39,011		
Inlet assy. (8) 0.592 lb each	4.736	148.5	0	0	703.3	0	0	104,439	0	0	37,200	18,600	18,600
Burble fence	5.940	52.0	0	0	308.9	0	0	16,062	0	0	60,078	30,500	30,500
Totals	46.71	107.1			5004.5			754,863			264,302	137,191	137,191
W $\bar{X}^2$								535,982					
ΣWX^2								218,881				218,881	218,881
Moment of inertia about cg											264,302	356,072	356.072

APPENDIX C - DERIVATION OF EQUATIONS FOR THE ESTIMATION OF THE BURBLE FENCE DEFLECTION

The following nine equations may be established from the geometry and static equilibrium in Figure C-1:

$$F_1 \sin\omega_1 = F_2 \sin\omega_2 \tag{C-1}$$

$$F_1 \cos\omega_1 = F_2 \cos\omega_2 + P, \tag{C-2}$$

$$F_1 = pR_1, \tag{C-3}$$

$$F_2 = pR_2, \tag{C-4}$$

$$(\pi - \alpha_1) R_1 = (\pi - \alpha_o) R_o, \tag{C-5}$$

$$(\pi - \alpha_2) R_2 = (\pi - \alpha_o) R_o, \tag{C-6}$$

$$R_1 \sin(\alpha_1 - \omega_1) - R_1 \sin\omega_1 = R_o \sin\alpha_o + \Delta, \tag{C-7}$$

$$R_2 \sin(\alpha_2 + \omega_2) + R_2 \sin\omega_2 = R_o \sin\alpha_o - \Delta, \text{ and} \tag{C-8}$$

$$R_1 \cos(\alpha_1 - \omega_1) + R_1 \cos\omega_1 = R_2 \cos(\alpha_2 + \omega_2) + R_2 \cos\omega_2. \tag{C-9}$$

From Equation C-1,

$$F_2 = \frac{\sin\omega_1}{\sin\omega_2} F_1 .$$

By substituting into Equation C-2, the following is obtained:

$$P \sin\omega_2 = F_1(\sin\omega_2 \cos\omega_1 - \sin\omega_1 \cos\omega_2) = F_1 \sin(\omega_2 - \omega_1).$$

Also, from Equations C-3 through C-6,

$$R_1 = \frac{P}{p} \frac{\sin\omega_2}{\sin(\omega_2 - \omega_1)} - \frac{\pi - \alpha_o}{\pi - \alpha_1} R_o \tag{C-10}$$

and

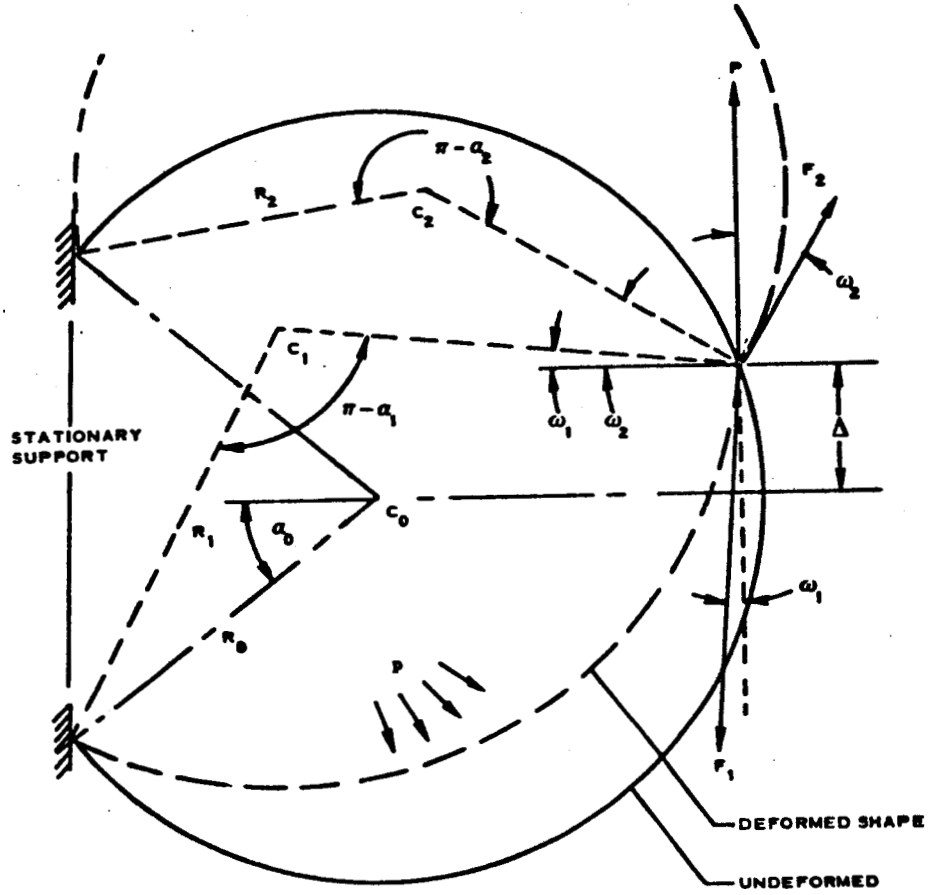

Figure C-1 - Deflection of Burble Fence

$$R_2 = \frac{P}{p} \frac{\sin \omega_1}{\sin (\omega_2 - \omega_1)} = \frac{\pi - \alpha_o}{\pi - \alpha_2} R_o \qquad \text{(C-11)}$$

By adding Equations C-7 and C-8,

$$R_1 \left[\sin (\alpha_1 - \omega_1) - \sin \omega_1 \right] + R_2 \left[\sin (\alpha_2 + \omega_2) + \sin \omega_2 \right] = 2R_o \sin \alpha_o. \qquad \text{(C-12)}$$

Let

$$X = \frac{R_o}{R_1} \qquad \text{(C-13)}$$

and

$$Y = \frac{R_o}{R_2}. \qquad \text{(C-14)}$$

Then, $X/Y = R_2/R_1$; therefore,

$$\sin \omega_1 = \frac{X}{Y} \sin \omega_2. \qquad \text{(C-15)}$$

By solving Equations C-10 and C-11 for α_1 and α_2 in degrees,

$$\alpha_1 = 180 + (\alpha_o - 180) X, \qquad \text{(C-17)}$$

and

$$\alpha_2 = 180 + (\alpha_o - 180) Y, \qquad \text{(C-18)}$$

Working with Equation C-9,

$$\cos (\alpha_1 - \omega_1) + \cos \omega_1 - \frac{X}{Y} \left[\cos (\alpha_2 + \omega_2) + \cos \omega_2 \right] = 0$$

or

$$\sin \alpha_1 \sin \omega_1 + (1 + \cos \alpha_1) \cos \omega_1 + \frac{X}{Y} \left[\sin \alpha_2 \sin \omega_2 - (1 + \cos \alpha_2) \cos \omega_2 \right] = 0. \qquad \text{(C-19)}$$

Similarly, from Equation C-12:

$$\sin \alpha_1 \cos \omega_1 - (1 + \cos \alpha_1) \sin \omega_1 + \frac{X}{Y} \left[\sin \alpha_2 \cos \omega_2 + (1 + \cos \alpha_2) \sin \omega_2 \right] = 2X \sin \alpha_o. \qquad \text{(C-20)}$$

ABSTRACT

The Supersonic Planetary Entry Decelerator Program 18-foot ballute design is analyzed with respect to aerodynamic, structural, and thermal requirements. Also included are results from both in-plant and development testing.